Dissertation

submitted to the

Department of Physics
Astronomy Division
University of Oulu
Oulu, Finland

Combined Faculties of the
Natural Sciences and Mathematics
Ruperto-Carola-University
Heidelberg, Germany

for the degree of

Doctor of Natural Sciences

Put forward by

Joachim Janz

born in: Heidelberg, Germany

Public defense: January 25, 2013

in Oulu, Finland

THE PUZZLING NATURE OF DWARF-SIZED GAS POOR DISK GALAXIES

Preliminary examiners:	Pekka Heinämäki Helmut Jerjen
Opponent:	Laura Ferrarese

ADVISORS:
Dr. Eija Laurikainen
Dr. Thorsten Lisker
Prof. Heikki Salo

Oulu, 2012

ABSTRACT

Early-type dwarf galaxies were originally described as elliptical feature-less galaxies. However, later disk signatures were revealed in some of them. In fact, it is still disputed whether they follow photometric scaling relations similar to giant elliptical galaxies or whether they are rather formed in transformations of late-type galaxies induced by the galaxy cluster environment. The early-type dwarf galaxies are the most abundant galaxy type in clusters, and their low-mass make them susceptible to processes that let galaxies evolve. Therefore, they are well-suited as probes of galaxy evolution.

In this thesis we explore possible relationships and evolutionary links of early-type dwarfs to other galaxy types. We observed a sample of 121 galaxies and obtained deep near-infrared images. For analyzing the morphology of these galaxies, we apply two-dimensional multicomponent fitting to the data. This is done for the first time for a large sample of early-type dwarfs. A large fraction of the galaxies is shown to have complex multicomponent structures.

The photometric parameters of the inner and outer components of the dwarfs are compared to bulge and disk components of other galaxy types from studies using a similar decomposition approach. The parameters of the bulges and disks form rather tight relations of size as a function of galaxy brightness. The inner and outer components of the dwarfs are offset from the extrapolations of these scaling relations, and we conclude that their nature is different. Complementary N-body simulations illustrate that the inner and outer components of the dwarfs may indeed have been formed from the disks of late-type galaxies that are harassed by the cluster environment. The multiple structure components may also explain our finding that the early-type dwarf galaxies show subtle deviations from common scaling relations with bright elliptical galaxies, i.e. the relation of size versus galaxy brightness. The dwarfs and giants would be expected to follow jointly one such relation, based on the observed, continuos variation of the light profiles, if all the galaxies followed simple one-component profiles.

Altogether our results indicate that many of the early-type dwarf galaxies may be disk galaxies. This view is supported by the fact that their sizes and galaxy brightnesses place the early-type dwarfs close to the extrapolation of the scaling relation of these parameters of disks in bright galaxies, but offset from that of the bulges. A possible explanation for early-type dwarfs beings disks is that they have been transformed from late-type disk galaxies by the cluster environment.

Furthermore, we demonstrate that processes that may be responsible for such transformations are also viable options for: *(i)* explaining that the slowly moving nucleated early-type dwarfs in the cluster center are round, while the fast moving are flat, *(ii)* making blue-compact dwarfs to evolve into early-type dwarfs, and *(iii)* forming ultra-compact dwarfs by disruption of nucleated early-type dwarfs.

TIIVISTELMÄ

Varhaisen tyypin kääpiögalakseja on alunperin pidetty elliptisinä piirteettöminä galakseina. Myöhemmin on kuitenkin osoittautunut, että jotkut niistä sisältävät kiekkomaisia rakenteita. On edelleenkin epäselvää seuraavatko ne jättiläisellipsigalaksien tapaan fotometrisiä skaalarelaatioita, vai ovatko ne pikeminkin muodostuneet myöhäisen tyypin galakseista galaksijoukoissa tapahtuneiden vuorovaikutusten seurauksena. Varhaisen tyypin kääpiögalaksit ovat runsaslukuisin tyyppi galaksijoukoissa, ja niiden pieni massa tekee niistä erityisen alttiita muutoksille ja näi nollen myös galaksien kehittymiselle. Kääpiögalaksit ovatkin erittäin sopivia kohteita tutkittaessa galaksien kehitystä.

Tässä väitöskirjassa tutkitaan varhaisen tyypin kääpiögalaksien mahdollista kehityksellistä yhteyttä muun tyyppisiin galakseihin. Työtä varten valitsimme 121:n galaksin otoksen, jolle otettiin syviä kuvia lähi-infrapunassa. Analysoitaessa niiden morfologiaa sovelsimme 2-dimensionaalista menetelmää, jossa analyyttisia funktiota sovitettiin useisiin eri rakennekomponentteihin. Kyseessä on itse asiassa ensimmäinen kerta, kun monikomponenttimenetelmää on sovellettu suurelle joukolle kääpiögalakseja. Osoitamme, että suurin osa kääpiögalakseista on monimutkaisia systeemejä, joilla on useita fysikaalisia rakennekomponentteja.

Kääpiögalaksien sisä- ja ulko-osien fotometrisiä parametrejä verrataan muiden galaksityyppien (kirkkaat galaksit) keskuspullistumien ja kiekkojen fotometrisiin parametreihin töissä, joissa on aiemmin käytetty samaa monikomponenttien sovitusmenetelmää. Kirkkailla galakseilla sekä keskuspullistumilla että kiekoilla on selkeä korrelaatio galaksin koon ja kirkkauden välillä. Extrapoloitaessa kyseiset relaatiot kääpiögalaksien alueelle, sekä niiden sisä- että ulko-komponentit poikkeavat kyseisistä relaatioista, minkä katsotaan osoittavan, että ne ovat myös luonteeltaan erilaisia. N-kappaleen simulaatiot myös osoittavat, että kääpiögalaksien sisä- ja ulko-komponentit ovat todellakin voineet syntyä myöhäisen tyypin galakseista, ns. 'harassment'-prosessissa galaksijoukon sisällä. Löytämämme monikomponenttirakenteet voivat olla myös selitys sille, miksi kääpiögalaksit hieman poikkeavat kirkkaille ellipsigalakseille löydetyistä skaalarelaatioista, kuten galaksin koko suhteessa sen kirkkausprofiiliin. Mikäli kaikki varhaisen tyypin

galaksit omaisivat vain yhden komponentin, kääpiö- ja jättiläisgalaksien olettaisi hyppäyksettä noudattavan kyseistä relaatiota, ottaen huomioon, että niiden kirkkausprofiilit muuttuvat tasaisesti galaksin kirkkauden/koon myötä.

Kaiken kaikkiaan tuloksemme viittaavat siihen, että monet varhaisen tyypin kääpiögalakseista saattavat olla kiekkogalakseja. Tätä käsitystä tukee myös se, että galaksin koon ja kokonaiskirkkauden perusteella kääpiögalaksit sijoittuvat lähelle samaa relaatiota kuin kirkkaiden galaksien kiekot (extrapoloitaessa relaatio kääpiögalaksien alueelle), mutta selvästi poikkeavat vastaavasta relaatiosta galaksien keskuspullistumille. Mahdollinen selitys sille, miksi varhaisissa kääpiögalakseissa on kiekkoja on, että ne ovat muodostuneet myöhäisen tyypin kiekkogalakseista ympäristön vaikutuksesta. Olemme lisäksi osoittaneet, että samat prosessit, joita tarvitaan tekemään myöhäisen tyypin spiraaligalaksista varhaisen tyypin kääpiögalaksi, voivat olla selityksenä myös seuraaville havainnoille: (i) lähellä joukon keskustaa hitaasti liikkuvat ytimelliset varhaisen tyypin kääpiögalaksit ovat pyöreitä, kun taas nopeasti liikkuvat ovat litteitä, (ii) siniset kompaktit kääpiögalaksit muuttuvat varhaisen tyypin kääpiögalakseiksi, (iii) ytimelliset varhaisen tyypin kääpiögalaksit menettävät identiteettinsä ja niistä syntyy ultrakompakteja kääpiösysteemejä.

ZUSAMMENFASSUNG

Zwerggalaxien frühen Typs wurden ursprünglich als elliptische Galaxien ohne herausstechende Merkmale beschrieben. Später wurden jedoch Anzeichen für Scheiben entdeckt. In der Tat wird noch heute darüber gestritten, ob sie ähnlichen Skalierungsrelationen folgen wie die großen elliptischen Galaxien, oder ob sie eher aus Galaxien späten Typs durch Transformation ausgelöst durch die Galaxienhaufenumgebung entstanden sind. Die Zwerggalaxien frühen Typs sind der häufigste Galaxientyp in Haufen, und ihre geringe Masse macht sie für Prozesse anfällig, die die Galaxien verändern. Damit sind sie als Testobjekte für das Studium von Galaxienentwicklung gut geeignet.

In dieser Doktorarbeit erforschen wir mögliche Verwandtschaften und entwicklungstechnische Verbindungen zwischen den Zwerggalaxien frühen Typs und anderen Galaxientypen. Wir haben eine Auswahl von 121 Galaxien beobachtet und tiefe nah-infrarot Bilder aufgenommen. Um die Morphologie dieser Galaxien zu analysieren, modellieren wir die Daten mit zweidimensionalen Mehrkomponenten-Fits. Das ist das erste Mal, dass diese Technik für eine große Auswahl an Zwerggalaxien frühen Typs angewandt wird. Es wird gezeigt, dass ein großer Teil der Galaxien komplexe Mehrkomponenten-Strukturen hat.

Die photometrischen Parameter der inneren und äußeren Komponenten der Zwerggalaxien werden mit den zentralen Verdickungs- und Scheibenkomponenten anderer Galaxientypen aus Studien, die mit ähnlichen Dekompositionsmethoden durchgeführt wurden, verglichen. Die Parameter der Verdickungen und Scheiben formen relativ strenge Relationen der Größe als Funktion der Galaxienhelligkeit. Die inneren und äußeren Komponenten der Zwerggalaxien sind im Vergleich zu den Extrapolationen dieser Skalierungsrelationen verschoben, und wir folgern, dass sie anderer Natur sind. Ergänzende N-Körper Simulationen illustrieren, dass die inneren und äußeren Komponenten der Zwerggalaxien in der Tat als Teile der Scheiben von Galaxien späten Typs durch die Einflüsse der Haufenumgebung geformt sein können. Die mehrfachen Strukturkomponenten könnten auch unser Ergebnis erklären, dass die Zwerggalaxien frühen Typs geringe Abweichungen von gemeinsamen Skalierungsrelationen mit den hellen elliptischen Galaxien, wie zum Beispiel in der Relation zwischen Größe und Galaxienhelligkeit, zeigen. Die Zwerg- und großen Galaxien sollten aufgrund der beobachteten kontinuierlichen Veränderung der Lichtprofilformen einer solchen Relation gemeinsam folgen, falls alle Galaxien einfache Einkomponenten-Profile hätten.

Insgesamt deuten unsere Resultate an, dass viele der Zwerggalaxien frühen Typs Scheibengalaxien sein könnten. Diese Ansicht wird unterstützt durch die Tatsache, dass die Größen und Helligkeiten der Zwerggalaxien frühen Typs nahe der Extrapolation der Scheiben in hellen Galaxien, nicht aber nahe der Extrapolation der Verdickungen liegen. Eine mögliche Erklärung für die Zwerggalaxien frühen Typs als Scheibengalaxien ist, dass sie durch die Haufenumgebung transformierte Scheibengalaxien späten Typs sind. Außerdem demonstrieren wir, dass die Prozesse, die für eine solche Umwandlung verantwortlich sein könnten, auch brauchbare Möglichkeiten sind, um *(i)* die Abhängigkeit der Form von Zwerggalaxien frühen Typs im Haufenzentrum von ihrer Geschwindigkeit zu erklären, *(ii)* um die blauen kompakten Zwerggalaxien sich in Zwerggalaxien frühen Typs entwickeln zu lassen, und *(iii)* um die ultra-kompakten Zwerggalaxien durch Auseinanderreißen von Zwerggalaxien frühen Typs mit Kern zu formen.

ORIGINAL PAPERS

I Janz & Lisker 2009, AN, 330, 948:
A continuum of structure and stellar content from Virgo cluster early-type dwarfs to giants?

II Janz & Lisker 2009, ApJ, 696, L102:
On the Color-Magnitude Relation of Early-Type Galaxies

III Lisker, Janz, et al. 2009, ApJ, 706, L124:
The First Generation of Virgo Cluster Dwarf Elliptical Galaxies?[1]

IV Paudel, Lisker, Janz 2010, ApJ, 724, L64:
Nuclei of Early-type Dwarf Galaxies: Are They Progenitors of Ultracompact Dwarf Galaxies?[2]

V Janz et al. 2012, ApJ, 745, L24:
Dissecting Early-type Dwarf Galaxies into Their Multiple Components

VI Janz et al. 2012, ApJ, (submitted):
A Near-infrared Census of the Multi-component Stellar Structure of Early-type Dwarf Galaxies in the Virgo Cluster

VII Meyer, Lisker, Janz, et al. 2012, A&A, (submitted):
What will blue compact dwarf galaxies evolve into?[3]

VIII Lisker, Weinmann, Janz, et al. 2012, (manuscript):
Dwarf galaxy populations in present-day galaxy clusters - II. The infall history of early-type and late-type dwarfs[4]

Remarks and own contributions to co-author papers

[1]My most significant contribution to the paper was to compare the observed shapes and line-of-sight velocities to a three-dimensional analysis of the kinematics of galaxies inside model clusters, a major step in the interpretation of the results. Furthermore, I assisted in the data analysis and contributed to the presentation of the results.

[2]For parts of the sample in this paper, I planned and carried out the observations jointly with S. Paudel and T. Lisker; the observing programme was granted based on a proposal (085.B-0971), of which I was co-investigator. Also, I participated in writing the article.

[3]For this paper I provided the comparison sample of early-type galaxies, discussed the interpretation of the results with H. T. Meyer and T. Lisker, and actively contributed to the publication of the paper.

[4]I provided the early-type galaxies to the observational comparison sample of the Virgo cluster and discussed the interpretation of the model comparisons with T. Lisker and S. M. Weinmann, and contributed to the analysis and presentation of the results.

Refereed publications that are not part of this thesis

i Janz & Lisker 2008, ApJ, 689, L25:
The Sizes of Early-Type Galaxies

ii Weinmann et al. 2011, MNRAS, 416, 1197:
Dwarf galaxy populations in present-day galaxy clusters - I. Abundances and red fractions

iii Graham et al. 2012, ApJ, 750, 121:
LEDA 074886: A Remarkable Rectangular-looking Galaxy

ACKNOWLEDGMENTS

I would like to express my gratitude to Eija Laurikainen, Thorsten Lisker, and Heikki Salo for their openness to this german-finnish adventure and the related support, as well as for many discussions and countless advice, scientific and otherwise.

Furthermore, I want to thank Pekka Heinämäki and Helmut Jerjen for reading this thesis and providing valuable comments, and all my collaborators for their contributions to this research.

Support from various sources made this thesis and the related travels to observing runs and conferences financially possibly. The longest time my PhD project was supported by the Gottfried Daimler- and Karl Benz foundation. Unfortunately, the foundation decided to end the program for international PhD projects. In smaller shares, but equally important, the funding came from the German Research Foundation, the Academy of Finland, and from the University of Oulu.

In this thesis I make use of data from a number of observatories and publicly available catalogs and databases. For both opportunities I am truly grateful. The official acknowledgements can be found in the back of the thesis.

CONTENTS

Part I

INTRODUCTION

1.1 EARLY-TYPE DWARF GALAXIES

This thesis is about red low-mass galaxies in the Virgo cluster. Such a characterization of the topic is obviously inexact, but with the simplicity comes one advantage: it is descriptive and independent of naming conventions.

Low-mass lacks a precise definition and is not a direct observable. Often the term *dwarf* galaxy is used, instead. How is a dwarf galaxy different from a *normal* galaxy? The word suggests that it is smaller. However, in astronomical terms most often a limit in galaxy brightness is used for the separation. The dividing line is usually taken somewhere between $M_B \sim -18$ mag (e.g. Boselli et al., 2008) and $M_B \sim -16$ mag (e.g. Ferguson & Binggeli, 1994). The large span of choices reflects the fact that it is even disputed whether or not the dwarf galaxies are really different from the brighter galaxies.

There is a large variety of different dwarf galaxy types (Fig. 1.1) and even more diversity in the names for these types. As Tolstoy et al. (2009) state: "The taxonomy of dwarf galaxies typically opens a Pandora's box." For example, Grebel (2001) lists: dwarf spirals (S0, Sa, Sb, Sc, and Sd), Magellanic irregulars (Sm, Sdm), Blue Compact Dwarf galaxies (BCDs), dwarf irregulars (dIrr), dwarf ellipticals (dE), dwarf spheroidal galaxies (dSph), and tidal dwarf galaxies. Tolstoy et al. (2009) cover in addition Ultra-Compact Dwarf galaxies (UCDs) and ultra-faint dwarfs (uFd). The galaxies in focus in our study are *red*, which excludes spirals, Sm, Sdm, BCDs, and dIrr. With our data sources and the interest in detailed morphologies of galaxies we are restricted to dEs. The other red low-mass galaxies are too small and faint at the distance of the Virgo cluster ($d = 16.5$ Mpc, Mei et al. 2007; UCDs: $M_B \geqslant -13$ mag and compact, Drinkwater et al. 2000; dSphs: $M_V \geqslant -14$ mag, Grebel 2001; uFds even fainter, see Tolstoy et al. 2009).

Not only is there no exact definition, but also the name for the galaxy type we are interested in, is disputed. It is criticized that the name *dwarf elliptical* implies that they are small versions of elliptical galaxies, which may not be the case (e.g. Kormendy et al., 2009). Instead, the name *spheroidal (Sph)* is suggested. This choice is motivated by the idea that they are brighter versions of dwarf spheroidal galaxies (dSphs). However, the name also suggests that the galaxies have a three-dimensional spheroidal shape. The advantages and disadvantages of both names were already discussed by Binggeli (1994) and Kormendy & Bender (1994) (for a historical overview also see Sandage 2005, §7). Throughout this thesis we will adopt another possibility and refer to them as early-type dwarf galaxies, in order to emphasize their smooth light distributions without further implications of their physical nature.[1]

In the past, one of the reasons to separate the early-type dwarfs from elliptical galaxies was that they were believed to have exponential surface brightness profiles, while the bright ellipticals were thought to have steeper de Vaucouleurs profiles (Wirth & Gallagher, 1984). Sandage & Binggeli (1984) accounted for that to some extent by using surface brightness instead of total galaxy brightness as their main criterion in classifying dwarf

1 We use *early-type* as a morphological description detached from Hubble's original idea of an evolutionary link (Hubble, 1936) from the *early* to the *late* types in his classification scheme (Hubble, 1926).

FIGURE 1.1: Example galaxies of different morphological types in the Virgo cluster (the classification is given in the label, as well as the Virgo cluster catalog (VCC) number and the coordinate). In the *left* column late-type disk and dwarf galaxies are shown, in the *right* column intermediate mass lenticular and elliptical galaxies. Different early-type dwarfs are shown in the two columns in the *middle* (dS0 with disk signatures; dE(N) and dE(nN) with and without a nucleus; dE(bc) with a blue core, Lisker et al. 2006a). Images from Sloan Digital sky survey (SDSS), `http://skyserver.sdss.org/dr7/en/tools/chart/list.asp`.

and non-dwarf ellipticals. Later, it was shown that neither all the bright ellipticals have de Vaucouleurs profiles, nor do all the early-type dwarfs have exponential profiles. Instead, the profile shape varies continuously with the galaxy brightness (e.g. Jerjen & Binggeli, 1997; Binggeli & Jerjen, 1998). We use the VCC of Binggeli et al. (1985) as the galaxy census in the Virgo cluster and follow their classifications based on Sandage & Binggeli (1984). However, the question: "Are dwarf ellipticals genuine ellipticals?" (Jerjen & Binggeli, 1997) remains unanswered and is one of the themes in this thesis.

With a classification based on surface brightness, dwarf and non-dwarf galaxies overlap in total brightness, and distinct galaxy Luminosity Functions (LFs) for the two types have been found (e.g. Sandage et al., 1985; Jerjen & Tammann, 1997). The population of early-type dwarf galaxies is far from homogenous. Already Sandage & Binggeli (1984) list three different morphological flavors of early-type dwarfs: galaxies with a nucleus (dE,N), with disk signatures (dS0), and those having neither of them. Later, nuclei of all strengths were identified (Grant et al., 2005; Côté et al., 2006), spiral arms were discovered in some of the galaxies (e.g. Jerjen et al., 2000), and disk signatures were systematically searched for (Lisker et al., 2006b). Nearly round early-type dwarf galaxies exist, as well as flat ones, and also their clustering properties differ (Lisker et al., 2007). Likewise, their dynamical configurations range from rotating to pressure supported systems (Simien & Prugniel, 2002; Pedraz et al., 2002; Geha et al., 2003; van Zee et al., 2004; Chilingarian, 2009; Toloba et al., 2009, 2011). The stellar populations have a large variety of ages and metallicities (e.g. Michielsen et al., 2008; Paudel et al., 2010b), and some of the early-type dwarfs even have formed stars recently in their centers (Lisker et al., 2006a). The dynamical mass-to-light ratios (M/L) in the inner regions of bright early-type dwarfs may be consistent with the M/L derived from stellar population models, while in others Dark Matter (DM) is required to explain the observed M/L (Geha et al., 2003; Beasley et al., 2009; Penny et al., 2009; Toloba et al., 2012). At lower masses, dSphs are believed to be the most DM dominated galaxies (Strigari et al., 2008a,b).

Why is it worthwhile to study early-type dwarf galaxies? After this collection of variety in the early-type dwarf galaxy population it should be needless to say that their enigmatic nature makes them very interesting objects. Moreover, they are the most abundant galaxy type in galaxy clusters and perhaps even in the whole present day Universe (Baldry et al., 2012). For example, in the VCC about half of the galaxies are early-type dwarfs. Obviously, the nature of the galaxy population that outnumbers the others needs to be known in order to understand galaxy cluster evolution. However, even though the early-type dwarfs are so numerous, an exhaustive and definitive theoretical explanation of their origin has not yet been established. Furthermore, their low masses and shallow potential wells make the early-type dwarf galaxies more prone to many internal or external processes that drive galaxy evolution. This fact and their large number give them a key role in understanding galaxy evolution.

Any theory to explain the population of early-type dwarf galaxies needs to account for the following properties, as listed by Lisker (2009): they have a smooth light distribution and nearly ellipsoidal shape with large range of axial ratios, the shape of the surface brightness profile is overall determined by the galaxy brightness, they host little or no

remaining gas, and their stars are relatively old. The list could be continued with stellar population ages, metallicities, et cetera (see also Ferguson & Binggeli 1994, their Table 2). Do the early-type dwarfs constitute an old galaxy population in the cluster or have they recently been accreted to it? Are they more closely related to spiral or bright elliptical galaxies? By their appearance both options seem plausible (Fig. 1.2). On one hand, they are suggested to be the descendants of the original building blocks of structure formation in the Universe. On the other hand it is also possible that the cluster environment led to a transformation of late-type (spiral, irregular, and starbursting) galaxies into today's early-type dwarfs. Processes involved could be, for example, ram pressure stripping (Boselli et al., 2008) or harassment (Moore et al., 1996).

That no consistent picture for the dwarfs' origin has emerged has mainly the following reasons. Their low surface brightness makes them expensive to observe. Most of their aforementioned properties depend both on the galaxy brightness and the local galaxy density. As a result there are many interrelations, which are hard to disentangle. Furthermore, the proposed transformation processes are expected to inevitably be in action in the dense cluster environment, or as Kormendy & Bender (2012) put it: the problem is better described by the rhetoric question "How can you stop any of them from happening?" rather than "which of these [...] is correct?". The diversity of early-type dwarfs may also suggest that the answer to the question 'which process contributed how much to shaping a single galaxy' depends on the individual path of the galaxy through the cluster and its history of encounters with other galaxies. With large observational samples and comparisons to simulated clusters one can hope to statistically weight the influence of the different processes. However, cosmological simulations have only recently reached the resolution needed for studying low-mass DM halos that potentially host such galaxies (Boylan-Kolchin et al., 2009; Guo et al., 2011).

There are two possible ways to learn about galaxy evolution. The finite speed of light makes a telescope a time machine. The more distant a galaxy is, the longer is the look-back time. If galaxies are studied at different distances and if the populations can be assumed to have evolved from one to the other, different snapshots of their evolution can be studied. However, this approach is not viable for dwarf galaxies, since they can be studied only fairly close by. The other way to study galaxy evolution is to study in detail the present day galaxy population in the local Universe, which can be done in-depth. From such detailed studies a galaxy's history can be inferred.

In this thesis we pursue this second, archeological approach. All the studied galaxies are located in the nearby Virgo cluster. In spite of all the studied galaxies living in the local Universe, the time scales of some of the processes shaping their present-day appearance are so long that the galaxy cluster, and even the Universe, cannot be considered as static entities. Therefore, the next sections are devoted to sketching the current understanding of the Universe as a whole and introducing simulations used to study structure formation. Finally, the processes that may be important for the formation of the early-type dwarfs are summarized and the Virgo cluster is characterized in more detail.

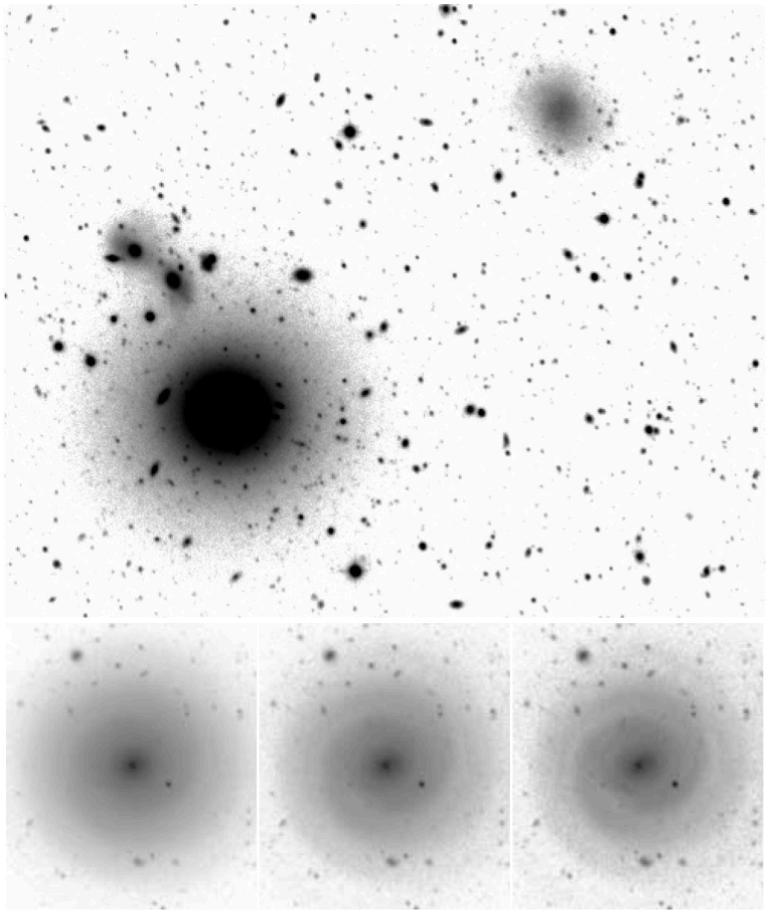

FIGURE 1.2: Deep ESO/2.2m wide-field imager (WFI) images taken with a *white* filter (Lisker, 2009). The Figure illustrates the enigmatic nature of early-type dwarf galaxies. In the *upper* panel VCC0856 is located in the lower left corner and VCC0839 can be found in the upper right corner. The field of view is $6' \times 5'$. The former galaxy looks in this images rather round and featureless, and significantly more massive than the faint galaxy. Nevertheless, both of them are classified as dE galaxies in the Virgo cluster catalog (VCC). The *lower* panels show a sequence of images of VCC0308. This galaxy is classified as dS0 in the VCC. The *left* image is the original image, while the others enhance the spiral structures by a factor of 2 and 3. This is achieved by subtracting the smooth light distribution from the image, multiplying the residual image with the amplification factor, and adding back the smooth light distribution. Even a moderate enhancement of the structure makes the galaxy resemble a bright spiral galaxy.

1.2 COSMOLOGY

The Universe is believed to have begun in the Big Bang 13.8 billion years ago (Komatsu et al., 2011; Jarosik et al., 2011) and to be expanding ever since. The concept of a beginning and a subsequent expansion of the Universe (Lemaître, 1927) gained observational evidence with Hubble's (1929) discovery that the larger distance a galaxy has, the faster its apparent recession velocity. Gamow (1946) predicted that the photons from the hot and dense early Universe should be observable as background radiation redshifted to microwave wavelengths. The discovery of this cosmic microwave background radiation (CMBR) (Penzias & Wilson, 1965) argued in favor of the Big Bang. Strong evidence for the theory was provided by the observations with the cosmic background explorer (COBE) satellite: the CMBR has a perfect blackbody spectrum with $T = 2.725$ K (Mather et al., 1990) and it has only extremely small anisotropies (10^{-5}, Smoot et al. 1992). Both findings are hard to explain without Big Bang, and this idea became the standard model of cosmology.

The theory to describe the Universe as a whole is general relativity (Einstein, 1916). Based on the assumptions that the Universe is homogenous and isotropic the Friedman-Lemaître-Robertson-Walker metric was derived (Robertson, 1935; Walker, 1935), and the Friedman equations were found from Einstein's field equations (Friedman, 1922). These equations, together with the equation of state, describe how of the Universe expands, and how this expansion depends on the energy densities and the equation of state parameters of the constituents of the Universe. For example, the Friedman equations describe how the gravitational pull of matter slows down the expansion. Also, solutions can be found how the energy densities of the constituents drop with time during the expansion. At the beginning, the Universe was smaller, hotter, and denser. During the first fraction of a second (to about 10^{-34}s) the energy density was so high that all known concepts of physics break down. The understanding of this period is limited. However, two mechanisms can be indirectly inferred: inflation and baryogenesis.

The horizon problem, maybe first discussed by Misner (1969), questions how the CMBR can be so isotropic, since patches in opposite directions on the sky should not be in causal contact. Furthermore, from properties of the CMBR it can be measured that the Universe is very close to have a flat geometry (see below). General relativity implies that the geometry should depart more and more from being flat with the expansion, if it was not exactly flat in the beginning. In order to explain the observed present-day flatness, the Universe had to be extremely flat at the beginning, which is a *fine-tuning* problem (Dicke & Peebles, 1979; Hawking, 1974). Both problems disappear, if the Universe is assumed to expand exponentially in an early period dubbed *inflation* (Guth, 1981). The fast growth drove causally connected regions apart to the apparently disconnected regions with the same CMBR temperature observed today, and naturally drove the Universe close to a flat geometry.

At the beginning, when the energy density was high, all sorts of (also unknown) pairs of particle and anti-particle were spontaneously created and annihilated. Since we observe matter today, the symmetry between matter and anti-matter must have been broken. We

can conclude from the ratio of baryons and photons, which is known from the Big Bang nucleosynthesis and CMBR properties (see below), that there was an excess of $\sim 1/10^9$ of quarks compared to anti-quarks. The surviving quarks formed baryons. The whole process is called baryogenesis (see Dine & Kusenko, 2003, for a review).

As the Universe expanded further, temperature and density decreased. Our understanding of the following evolution at smaller energy densities is more profound. The rates of weak interactions determined the ratio of neutrons and protons ($n_n/n_p \sim 1/10$). They started to form atomic nuclei. As long as the energy was high enough, nuclear fusion built the first nuclei of elements other than hydrogen. Big Bang nucleosynthesis explains the abundances of the primordial light elements: H, D, ^{3}He, ^{4}He, traces of ^{7}Li, and some amounts of the unstable ^{3}H, ^{7}Be, ^{8}Be (Alpher et al. 1948; for a complete analytical derivation see Mukhanov 2004; for a recent review see Pospelov & Pradler 2010; and for a discussion of problems with the ^{7}Li abundance see Fields 2011).

At recombination the electrons combined with the atomic nuclei to form neutral atoms. Photons could then travel long ways without interactions, and the Universe became transparent. Today we observe the CMBR as the last scattering surface of these photons. During inflation, Heisenberg's uncertainty principle led to quantum fluctuations and these perturbations were blown up to macroscopic scales. The resulting fluctuations are assumed to be Gaussian, scale-invariant, and adiabatic,[2] which is consistent with CMBR observations (Tegmark, 1996). The density fluctuations started to oscillate due to the competing forces of gravity and pressure. The sizes of regions that went through full oscillation cycles set characteristic scales (baryon acoustic oscillations). The angular power spectrum of the CMBR anisotropies measures the apparent sizes of these scales today and is very sensitive to the cosmological parameters (see Hu & Dodelson 2002 for a review). Therefore, the measurements of the CMBR temperature fluctuations allow to put precise constraints to the cosmological parameters (e.g. Spergel et al. 2003 with the Wilkinson Microwave Anisotropy Probe, WMAP, Bennett et al. 2003; soon the results of the Planck mission will become available, Planck Collaboration et al. 2011, including measurements of the CMBR polarization).

The location of the first peak of the CMBR power spectrum, at approximately 1°, indicates that the Universe is flat. The location of the next peak measures its matter content. Since it is less than required to make the Universe flat, it can be concluded that the Universe has to be filled with something additional, which is called *dark energy*. The ratio of the powers in the first and third peaks determines the fraction of baryonic matter. Komatsu et al. (2011) list that the baryonic matter makes up 4.51% of today's Universe, about a quarter, 22.6% is DM, and most of the Universe energy budget (72.9%) is hidden in the dark energy sector. DM is not yet directly detected, and the dark energy is nothing more than a parameter introduced to explain the Universe's flatness and the present-day acceleration of the expansion. The vacuum energy of the standard model of particle physics would in principle behave like dark energy. However, the amount of energy is wrong by a factor of 10^{120} (see Ishak 2007 for a review) – maybe the biggest mismatch in science. It

2 Adiabatic means here that matter and radiation are perturbed in the same manner. The total density varies, but the photon-to-baryon ratio is spatially invariant.

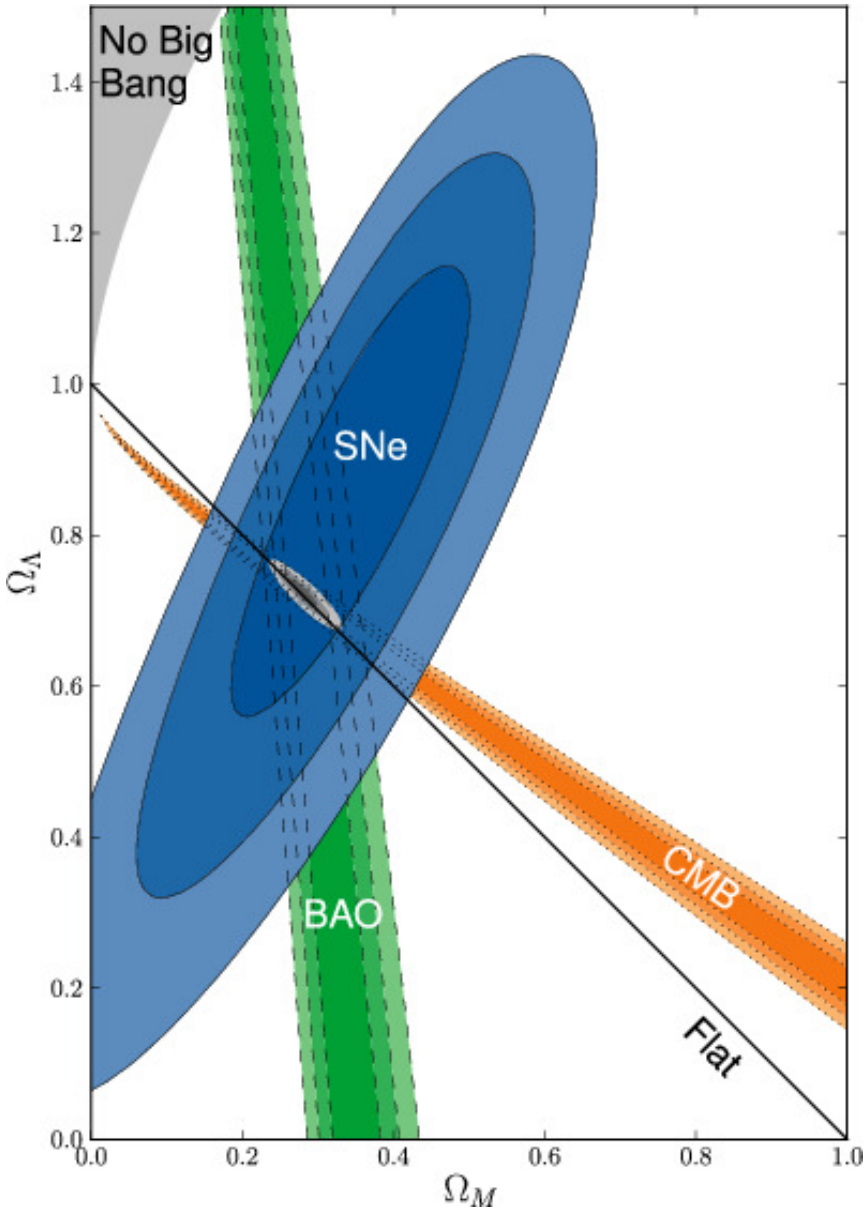

FIGURE 1.3: Constraints on the matter and dark energy density from different measurements (Cosmic microwave background - CMBR, Baryon acoustic oscillations - BAO, and Supernovae type Ia, SNe) as an example of how parameters of ΛCDM are constrained. Ω_Λ and Ω_M are the present-day energy densities of dark energy and matter in units of the critical density, which makes the Universe flat. The contours show 68.3%, 95.4%, and 99.7% confidence levels including systematic errors. Figure taken from Amanullah et al. (2010).

might be that the standard model is fundamentally wrong, although it is self-consistent. Nonetheless, the observations are well described and many measurements in addition to the CMBR measure independently cosmological parameters consistent with the CMBR results (Fig. 1.3).

In the 90s there was an age crisis, with the oldest objects measured to be older than the Universe according to the standard model, e.g. stars older than 15 Gyrs (Cowan et al., 1997, 1999) and globular clusters as old as 14.5 Gyrs (Chaboyer et al., 1996). Until now, the measured ages of the oldest objects converged to values that are consistent with the age of the Universe. A 13.2 Gyrs old star was discovered (Frebel et al., 2007). While this star cannot be the oldest, since it contains little amounts of metals[3], it suggests that the oldest stars had enough time to form after the Big Bang (for a review of stellar ages see Soderblom 2010). Also, the ages of globular cluster are consistent with the age of the Universe (see, e.g., Dotter et al. 2010, and Kalirai 2012 with inclusion of white dwarf dating), and the earliest galaxy was detected, at a distance corresponding to an age of the Universe of 480 Myrs (Bouwens et al., 2011).

The value for the Hubble constant H_0 from CMBR measurements is consistent with the directly measured value (e.g. Freedman et al. 2001, $H_0 = 72 \pm 8$ km/s/Mpc). Supernovae of type Ia have been used to measure the acceleration of the expansion rate of the universe at late times (Riess et al., 1998; Perlmutter et al., 1999). This is sensitive to the ratio of the densities of matter and dark energy, and gives a consistent result for the dark energy contribution to the energy budget of the Universe. The matter content is consistently determined with the baryon acoustic oscillations' imprint on the galaxy and galaxy cluster distributions (Eisenstein et al. 2005; Percival et al. 2010; for a general review of cosmological parameters from galaxy clusters see Voit 2005; Allen et al. 2011). Also for the DM, there are several other evidences on different scales that draw a consistent picture (see next section).

Therefore, the standard model can be at least used as a phenomenological description and framework for modeling structure formation.

1.3 STRUCTURE FORMATION AND GALAXY EVOLUTION

After recombination, matter decoupled from the photon field. Density perturbations started to grow under the influence of self-gravity, if the scale of the perturbation was larger than the Jeans length, or accordingly more massive than the Jeans mass (Jeans 1902; with expanding background the conditions were worked out by Gamow & Teller 1939 and Lifshitz 1946). The Jeans mass after recombination was $10^5 - 10^6 M_\odot$ (Doroshkevich et al., 1967; Peebles & Dicke, 1968), so that the least massive objects possible to form would have been globular clusters or supermassive first stars. However, Silk (1968) showed that the drag of the photons before recombination washed out perturbations smaller than $10^{12} - 10^{14} M_\odot$.

3 For a more metal-poor star see, e.g., Caffau et al. (2011).

As long as the density contrast was small, $\delta \ll 1$, the perturbations grew linearly, but once the contrast became large enough, $\delta \gtrsim 1$, non-linear evolution set in and it was ruled by gravitation and complicated gas dynamics. This evolution is nowadays studied in large cosmological computer simulations. However, some important results were already obtained with analytic approximations. Silk (1967) and Zel'dovich (1970, 1972) calculated the strength of the density fluctuations required for the formation of the large scale structure of galaxy clusters and galaxies observed today. The calculated amplitude (10^{-4}) was an order of magnitude larger than the CMBR anisotropies, which were discovered later. The solution to this problem in the standard model is the existence of DM. The DM does not interact via the electromagnetic interaction and, therefore, could form structures already when the baryons were still held in equilibrium with the photons. In that case atoms could then fall quickly into the pre-existing DM potential wells after recombination.

The DM also needs to be cold, i.e. when it decoupled it had to move with non-relativistic velocities. One candidate for a DM particle had been a massive neutrino, which would be hot DM. White et al. (1984) demonstrated that neutrinos as hot DM cannot reproduce the observed structures, since their relativistic movements wash out all structures on small scales. Also, Lin & Faber (1983) and Gerhard & Spergel (1992) excluded neutrinos as a DM candidate, based on the DM halos of dwarf galaxies ($M/L_V = 79$, 85 for Ursa Minor and Draco, from the dSph review Mateo 1998), and the limited phase space that would be available to the neutrinos due to Pauli's exclusion principle, and the restriction of the spatial extent of the DM due to the observed orbits of these dSphs around the Milky Way. Recently, the possibility of warm DM has been a topic of the research activities (e.g. de Vega & Sanchez, 2011; Parry et al., 2012; Lovell et al., 2012). This may be one way to solve the missing satellite problem (see below).

As DM plays an important role in cosmology and galaxy evolution, we want to list at this point further evidence for DM. On different scales DM is needed to explain the amount of matter that is found by dynamical arguments, in comparison to stars and gas that are detected by the light that they emit. In spiral galaxies the rotation curves are found to be flat (Bosma 1978; Rubin et al. 1980; even beyond their visible extent, when measured with H I), while they should drop at large radii, if only the luminous matter was present. In some early-type dwarfs evidence for dark matter is found (e.g. Beasley et al. 2009), while at lower galaxy masses the dSphs are the most DM-dominated galaxies (Strigari et al., 2008a,b). Also, on larger scales dark matter was found via the motions of satellite galaxies around spiral galaxies including the Milky Way (Ostriker et al., 1974; Einasto et al., 1974b,a), and via the motions of galaxies in galaxy clusters (Zwicky, 1933, 1937). Galaxy clusters have so large masses that they can act as gravitational lenses (predicted by Chwolson 1924; Einstein 1936; first strong lens discovered by Walsh et al. 1979). The light of background sources is deflected by the deep potential well of the cluster. Kaiser et al. (2000), Bacon et al. (2000), and Wittman et al. (2000) used this effect to deduce the masses of clusters and to measure the matter densities at different scales and times. They found them to be consistent with the standard model, including the large DM contribution (for a review of lensing and DM see Massey et al. 2010). The masses of galaxy clusters can also

be deduced from the temperature of the X-ray emitting gas, if it is in equilibrium with the cluster potential. The most direct evidence for DM is considered to be found in systems like the Bullet cluster (Clowe et al., 2004; Markevitch et al., 2004). After a collision of two galaxy clusters, the baryonic matter distribution, traced by the X-ray emission of the hot gas,[4] is clearly offset from the mass distribution modeled via the gravitational lensing of background galaxies.

So with the help of the DM, density fluctuations began to grow. First this process was linear, then the growth became non-linear and dense structures started to fall onto each other. Given the observed slope of the power spectrum, the primordial over-densities had to fragment to sub-clouds, as shown by Hoyle (1953) and Hunter (1962). First stars (Abel et al., 2002), galaxies (Bromm & Yoshida, 2011, for a review), and galaxy clusters started to form. Most probably, the massive galaxies did not form in a monolithic collapse (Eggen et al., 1962) and structures did not grow in a *top-down* fashion, Instead, the massive galaxies were built up by coalescence of smaller progenitors (Searle & Zinn, 1978) in a *bottom-up* fashion. Today's dwarf galaxies could be the descendants of these low-mass building blocks. However, they do not necessarily need to appear as the oldest galaxies: while the stars of massive galaxies formed early and on short time scales (manifested as an α-enhanced chemical composition), low-mass galaxies have had prolonged star formation on a low level (e.g. Juneau et al., 2005). This means that the stellar population of the oldest galaxies can appear younger than in massive, later assembled galaxies. This twist is called *down-sizing*.

Press & Schechter (1974) calculated the mass function of galaxies in this hierarchical merging scenario. The observed LFs of galaxies has been found to have a similar shape. Zel'dovich (1970) showed that large over-densities collapsed first along one direction to form sheets, and subsequently along the next dimension, thus providing an early prediction of filamentary structure. This non-linear regime of structure formation is best studied in large cosmological computer simulations. They demonstrated how the primordial fluctuations, which were seeded by quantum fluctuations and enlarged by inflation, evolved over the life-time of the Universe, and developed the large scale structures that we observe today (e.g. Bond et al., 1996). The baryon acoustic oscillations are echoed in the distributions of galaxies (Percival et al., 2010). Even a filament of DM, bridging two galaxy clusters as part of the cosmic web, has recently been discovered by its lensing signal (Dietrich et al., 2012).

Today, large N-body computer simulations like Millennium (Springel et al., 2005) and Millennium-II (Boylan-Kolchin et al., 2009) can track the evolution of DM in great detail (Fig. 1.4). They successfully reproduce the observed large scale structures like sheets and filaments, as well as voids of basically empty space in-between them (Geller & Huchra, 1989). The mass of a single particle in the latest simulations is small enough to resolve DM halos that are assumed to host galaxies with masses in the dwarf galaxy regime. However, these simulations do have one important simplification: they basically use only DM, i.e. particles that interact only via gravitation. Real galaxies with their baryons include complicated processes. The dynamic range that would be needed for simulations to include

4 The stars and galaxies do not follow the gas during the collision.

both the large scale structure formation, as well as baryonic physics within the galaxy, is too large even for the most powerful computers. In order to study galaxy formation and evolution, processes like gas cooling, star formation, or stellar evolution are included by rather simple analytic recipes in so called *semi-analytic models* (e.g. Guo et al. 2011).

Three potential problems of ΛCDM cosmological simulations are commonly discussed (also see Kroupa, 2012): *(i)* the missing satellite problem, i.e. an over-prediction of low-mass galaxies in the models (e.g. Klypin et al. 1999; Moore et al. 1999a; Kravtsov et al. 2004; Tollerud et al. 2008, also see the too large dwarf-to-giant ratios and the discussion in Paper ii). *(ii)* The cusp/core problem, i.e. DM simulations predict that the DM halos have a cuspy density profile, while observations suggest a core profile, with a flat inner profile, instead of a sharply rising one (see, e.g., de Blok, 2010, for a review). *(iii)* the problem of bulgeless galaxies[5], which are hard to explain with all the merging of halos and galaxies going on in the models (Kormendy et al., 2010). At least the first two problems or their solutions are thought to be related to baryonic physics and their inadequate modeling by the semi-Analytic Models (SAMs).[6]

Indeed, recent hydrodynamical simulations suggest that those problems can be solved by including more detailed baryonic physics.[7] However, it is hard to run such simulations in cosmological context with high resolution and a large box size. Also, subgrid physics, such as star formation, still need to be included as some recipes. Nevertheless, Ruiz et al. (2012) study with three-dimensional hydrodynamic simulations (not cosmological) the mass loss due to superNova (SN) feedback and its influence on the DM in dSphs. They conclude that these processes may prohibit star formation. The darker galaxies would lessen the problem of missing satellite galaxies. Furthermore, several papers suggest that the baryonic physics can make the DM halos (at least of dwarf galaxies) to have constant density cores (Governato et al., 2010; Oh et al., 2011; Governato et al., 2012; Teyssier et al., 2012), and can also make dwarf galaxies bulgeless (Governato et al., 2010).

1.4 ON THE LIVES OF LOW-MASS GALAXIES OR HOW EARLY-TYPE DWARFS MAY FORM

As described above, low-mass galaxies are expected to have formed as first galaxies. Many of them were the building blocks that merged to form more massive galaxies. Early-type dwarfs may be descendants of such building blocks.

5 In this context *bulgeless* means the absence of a merger-built bulge. *Pseudo-bulges* (Kormendy & Kennicutt, 2004; Graham, 2011, §4.3) form by secular processes and should be excluded when comparing the number of (merger-built) bulges in models and observations.

6 It is somewhat ironic and criticized by ΛCDM skeptics that baryons are blamed for the problems, while they are the only significant contribution to the energy budget of today's Universe that we really know.

7 In passing we note that we concluded in Paper ii that the too high dwarf-to-giant ratios in the SAM compared to the observations is probably due to an insufficient modeling of tidal disruption of dwarf galaxies.

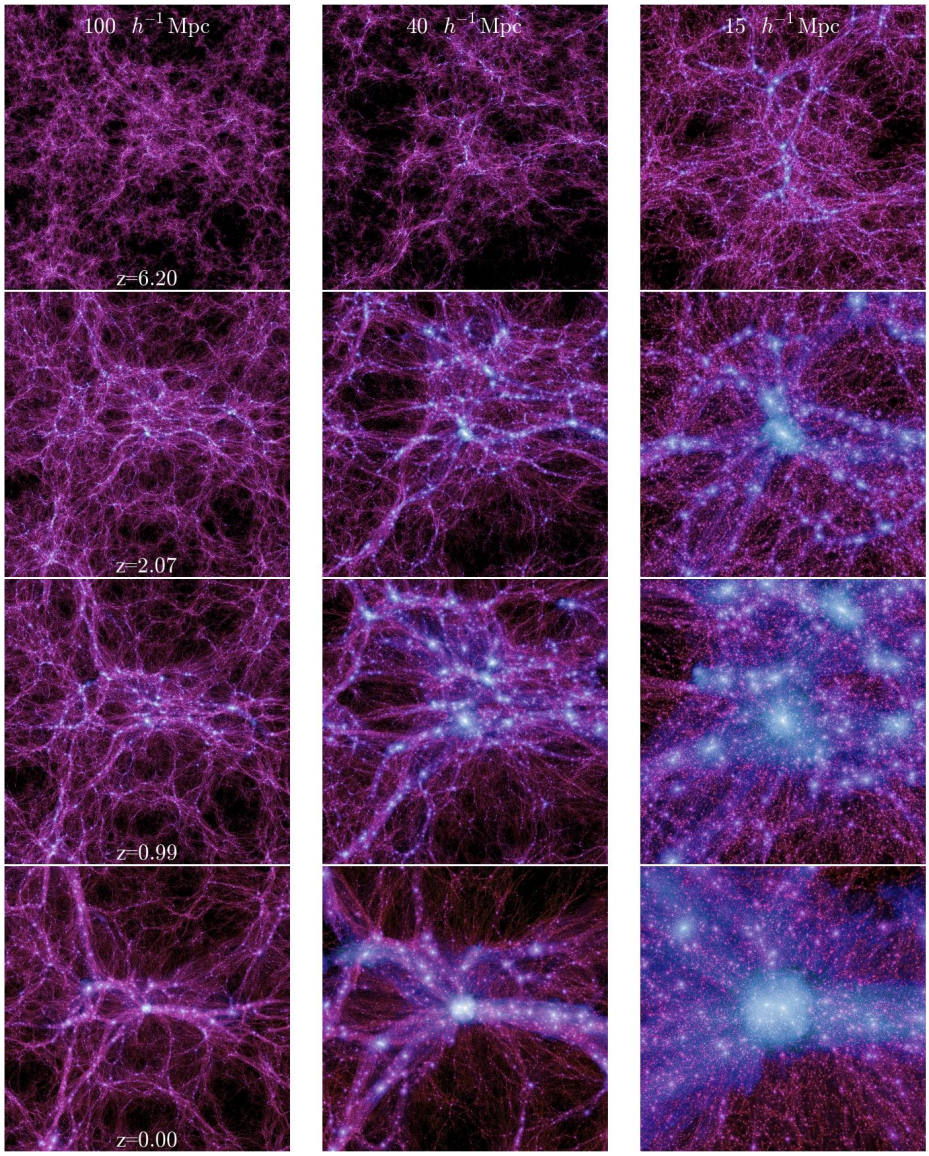

FIGURE 1.4: "This set of 12 images shows the growth of the most massive halo over cosmic time. The left column is 100 x 100 Mpc/h, the center column is 40 x 40 Mpc/h, and the right is 15 x 15 Mpc/h (in comoving units). From top to bottom, the regions are plotted at redshift 6, 2, 1, and 0." The Figure shows a Coma-like cluster forming in the Millennium-II simulation. Figure taken from Boylan-Kolchin et al. (2009).

Galaxy mergers

As such, the early-type dwarfs may be the results of small scale mergers themselves. Galaxy mergers are known to play an important role in the formation of elliptical galaxies, but might have played also their part in shaping low-mass galaxies. In the early-universe the density was higher, while the relative velocities were not as high as in today's clusters: their deep potential wells had not yet been built up. Therefore, mergers were much more frequent, since they effectively can only happen if the orbital energy is smaller than the mean internal energy (for spherical galaxies this implies $\langle v^2 \rangle > \sigma^2$, with the internal mean square velocity $\langle v^2 \rangle$ and the velocity dispersion σ of the group or cluster, see, e.g., Mo et al. 2010). Today, mergers are much more likely to happen in galaxy groups and than in clusters, where the relative velocities are too high. For in-falling galaxy groups in low-redshift clusters on the other hand, the merger frequencies may be enhanced (Moss, 2006). That mergers of low-mass galaxies still do occur was shown by the recent discovery of one such example (Martinez-Delgado et al., 2012).

The first three-dimensional self-consistent simulations of mergers of spheroidal galaxies showed that the density profile of the merger remnant resembles that of massive elliptical galaxies (White, 1978, 1979). Later, simulations with increasing resolution showed that also major mergers (i.e. both progenitors have similar mass) of two disk galaxies can create an elliptical galaxy (e.g. Hernquist, 1992; Barnes, 1988). Indeed, massive elliptical galaxies are assumed to form via major mergers (an idea originally suggested by Toomre & Toomre 1972). The actual outcome depends on the mass ratio, the morphological types of the progenitor, the gas mass fraction, and the orbital parameters. On the other hand, minor mergers may contribute to the build-up of spheroids (see, e.g., Kormendy & Kennicutt, 2004; Bournaud et al., 2007b; Naab et al., 2009), and may also heat the disks (e.g. Benson et al., 2004). With the apparent structural similarities, the idea that early-type dwarfs form in a similar manner as the bright ellipticals may be appealing. In principle, their lower surface brightness could be explained by less dense progenitors. However, in the cosmological context it would then be expected that the dwarfs are less concentrated in clusters than giant ellipticals (see, e.g., Mo et al. 2010), whereas observations indicate a similar clustering behavior for both types (Norberg et al., 2002). Also, only few examples, if any, of isolated early-type dwarfs are known (e.g. Wang et al., 2007).

Feedback

The term feedback is used in this context to describe the influence of Active Galactic Nuclei (AGN) and of SNe on the host galaxy. Both mechanisms are essential ingredients in semi-analytic Models (SAMs) of galaxy evolution for reproducing the observed galaxy Luminosity Functions (LFs) (Somerville & Primack, 1999; Croton et al., 2006; Kereš et al., 2009). While AGNs are found in massive galaxies, SN feedback is efficient in low-mass galaxies. They lower the number of galaxies, as compared to a hypothetical situation without feedback, at high and low masses, respectively, by regulating star formation. In low-mass galaxies the winds from superNovae (SNe) after a starburst can expel the gas and

possibly also heat the galaxy. The timescale for the responsible type II SN to explode is $\sim 10 - 100$ Myrs. Ferrara & Tolstoy (2000) calculated that a mass loss by outflow can occur in a galaxy less massive than $M \lesssim 10^9 M_\odot$, whereas dwarfs with $M \lesssim 5 \cdot 10^6 M_\odot$ can be completely blown out. In principle this diminishing capability to retain the baryons may explain why the least massive dwarfs have the highest mass-to-light ratios. Also, the observed mass-metallicity relation may be explained, since in less massive galaxies metals are lost in outflows, so that they cannot contribute to the chemical enrichment (Larson, 1974; Dekel & Silk, 1986; Vader, 1986; Yoshii & Arimoto, 1987; Dekel & Woo, 2003). The gas loss can also change the size of a galaxy by the stars reacting to the dynamic feedback due to the mass loss (Dekel & Silk, 1986; Yoshii & Arimoto, 1987). This is the explanation of how the size distribution of the early-type galaxies in Paper I is reproduced in the framework of the SAM of Nagashima et al. (2005).

It is observed that elliptical galaxies are abundant in massive galaxy clusters, while spiral galaxies are more frequent in low-density environments. This is known as the morphology-density relation (Dressler, 1980). The same trend is observed also for dwarf galaxies (e.g. Ferguson & Binggeli, 1994), and even for the different subclasses of early-type dwarfs. Namely, those with recent residual star formation in the centers and with disk signatures are less centrally concentrated than those without (Lisker et al., 2007). Also, early-type dwarfs in the field are rare. Furthermore, galaxy clusters at larger distances contain more blue galaxies (Butcher-Oemler effect, Butcher & Oemler 1978). Therefore, it is often assumed that cluster-specific processes play an important role for the formation of early-type (dwarf) galaxies (see Boselli & Gavazzi, 2006, for a review). If a star-forming, late-type galaxy is transformed into an early-type dwarf by the cluster environment, it has to lose its gas, cease the star-formation, and redden, and the galaxy needs to be dynamically heated. In the following we describe processes that are expected to act in the cluster environment, and that can contribute to such a transformation. We start with tidal interactions with other cluster members and the cluster potential, and continue with the interaction with the hot intra-cluster gas.

Harassment

In a cluster low-mass galaxies typically have high-speed encounters, since the velocity dispersion of the cluster is much larger than the velocities of the stars inside the low-mass galaxy. In this situation the impulse approximation is valid (see, e.g., Binney & Tremaine, 2011): the two galaxies pass by each other with nearly constant velocities, the stars inside the galaxies do not move much during the short duration of the encounter (with typical velocities inside a cluster only several Myrs) and the influence of the perturbation can be approximated just by a change of the velocities of the stars. This way the internal kinetic energy is increased. If for a star the gain in energy is large enough it can become unbound, resulting in a mass loss for the galaxy. The remaining stars will return to a new equilibrium after a few galaxy rotation periods. Moore et al. (1996, 1998) showed that the combination of repeated encounters with other cluster members and the influence of the

tidal field of the cluster potential can turn a disk galaxy into a spheroidal system during a few passages through the cluster (the cluster crossing time in the Virgo cluster is 1.7 Gyrs, Boselli & Gavazzi 2006). Moore et al. gave this process the name *harassment*. For early-type disk galaxies (Sa-Sb) harassment has less impact, since their dynamical time scales are shorter due to higher rotation velocities (Moore et al., 1999b). Mastropietro et al. (2005) traced the path of a late-type disk galaxy, i.e. a disk galaxy with a small bulge (in this particular case a pure disk galaxy), in a simulated ΛCDM cluster, in order to predict the influence of harassment in more detail. They found that in none of the simulated galaxies the disk was completely destroyed.[8] The most complete transformation to a spheroidal object occurred for galaxies that penetrated deep into the cluster center. The more a galaxy was transformed, the more substantial was its mass loss. However, harassment might have difficulties to explain the pressure supported early-type dwarfs. While Aguerri & González-García (2009) claimed that harassment can reproduce the kinematics of early-type dwarf galaxies reasonably well, placing them on the fundamental plane[9], Smith et al. (2010) showed that for an in-falling population the orbits that plunge deep into the cluster center are rare. They concluded that harassment is not efficient enough to explain the population of early-type dwarfs by the transformation of recently accreted late-type galaxies.

In Paper VI we find many early-type dwarf galaxies to have multiple structural components. With N-body *toy-model* simulations we illustrate that high-speed encounters can in principle lead to changes of the disk light profiles in such a manner that they appear as multiple components. In Paper ii we speculate that the discrepancy of the dwarf-to-giant ratio between the model and the observations may be due to an insufficient modeling of tidal disruption in the SAM of Guo et al. (2011).

Tidal stirring

If the relative velocities are smaller, e.g. if a dwarf galaxy revolves around a more massive galaxy, the tidal forces act in a different manner. The change of the tidal field along the orbit can shake up the dwarf galaxy repeatedly and dynamically heat it (Mayer et al., 2001a,b; Łokas et al., 2011). This process is only efficient with small relative velocities, e.g. for dwarf galaxies around a Milky Way sized halo, but not in a galaxy cluster like the Virgo cluster. In this sense tidal stirring is complementary to harassment. Mostly it is used to explain the formation of the dSph galaxies in the Local Group. However, if galaxies fall into the cluster in small groups, tidal effects might pre-process dwarf galaxies via tidal stirring before the group is accreted to the cluster.

8 Mastropietro et al. also concluded that a disk galaxy cannot be transformed into an UCD by harassment.

9 The fundamental plane is a tight relation between mean effective surface brightness, effective radius, and velocity dispersion for elliptical galaxies (Djorgovski & Davis, 1987; Dressler et al., 1987).

Ram pressure stripping

Galaxy clusters are filled with hot intra-cluster gas, which is observed in X-rays (e.g. Böhringer et al., 1994). If the ram pressure force of that gas, acting on the gas inside a galaxy, becomes larger than the restoring force of the gravitational potential, the gas can be swept out:

$$\rho_{ICM} v^2 > 2\pi G \Sigma_* \Sigma_{ISM} \,, \tag{1.1}$$

where ρ_{ICM} denotes the density of the intra-cluster gas, v the velocity of the galaxy, G the gravitational constant, and Σ_* and Σ_{ISM} are the surface densities of stars and the interstellar gas inside the galaxy, respectively (Gunn & Gott, 1972). Since the surface densities inside a galaxy are a function of radius, the ram pressure stripping will occur only up to a certain radial distance, for a given level of ram pressure. The ram pressure may confine the retained gas to a smaller region, which can enhance the star formation rate (Dressler & Gunn, 1983; Gavazzi et al., 1995). The stripped gas may also fall back later and form stars then (Vollmer et al., 2001). However, the gas can be completely stripped, if the galaxy moves through the cluster center.[10]

With a subsequent aging of the stellar population a dwarf irregular might turn into an early-type dwarf galaxy as suggested by Lin & Faber (1983). Ram pressure stripping has been used to explain such observations as the rotation and disk features of early-type dwarf galaxies as being inherited from the progenitor galaxies (e.g. van Zee et al. 2004, de Rijcke et al. 2010). This scenario provides also a natural explanation for the observed exponential light profiles in early-type dwarfs, and why their flattening distribution is similar to that of late-type galaxies (Ferguson & Sandage, 1989; Binggeli & Popescu, 1995). Boselli et al. (2008) conclude with multi-zone chemospectrophotometric models that star formation can be quenched on a short time scale (< 150 Myrs), and that the resulting ultraviolet and infrared colors match the observed colors of the early-type dwarfs. Furthermore, the transformation reproduces the observed early-type dwarf surface brightnesses and effective radii. Smith et al. (2012) demonstrated that the drag force of the stripped gas can lead to a dynamical heating of the stellar disk. Also, the multicomponent structures found in early-type dwarfs in Papers V and VI may be partly explained with ram pressure stripping of late-type galaxy progenitors. However, ram pressure stripping is not expected to form nuclei that are frequently found in early-type dwarfs (Binggeli et al., 1985). Also, the number of globular clusters (GCs) in a galaxy should not be affected by ram pressure stripping. Therefore, the specific frequency of GCs, i.e. the number of GCs normalized by the galaxy brightness, is expected to decrease only mildly due to a passive fading of the stellar population after the ram pressure event. This may be inconsistent with the observed high specific GC frequencies in the early-type dwarfs ($S_N > 5$, Durrell et al. 1996; Miller et al. 1998; Peng et al. 2006; while $S_N < 1$ for dIrr, Harris 1991).

10 Ram pressure stripping may in principle also take place in less dense environments via the gas surrounding a close companion (Lin & Faber, 1983).

In the Virgo cluster there is plenty of observational evidence for the ram pressure acting on the gas in spiral galaxies. When they fly through the hot intra-cluster gas their gas disks are perturbed and they start to develop gaseous tails, which can be seen in maps of the HI gas (i.e. van Gorkom, 2004).

Starvation or strangulation

In this scenario the ram pressure removes the gas that surrounds the galaxies (Larson et al., 1980; Balogh et al., 2000; Kroupa et al., 2010), instead of affecting the internal gas. With the lack of a gas reservoir the gas inside the galaxy is not replenished anymore and is eventually consumed by star formation. With no new stars forming the stellar population of the galaxy ages and the color reddens. The time scale of this process is much longer than in case of a complete gas removal (~6 Gyrs, Boselli et al. 2008), but it can also act in regions with less dense intra-cluster gas (e.g. Tonnesen et al., 2007). This mechanism and the direct removal of the internal gas by ram pressure stripping naturally explain the trends of the stellar population age and the HI deficiency with clustercentric distance (e.g. Chamaraux et al., 1980).

Tidal dwarfs

There is another, alternative formation scenario for early-type dwarfs that we want to mention briefly. Low-mass galaxies can form in the tidal tails of interacting (gas-rich) galaxies (Barnes & Hernquist, 1992; Bournaud & Duc, 2006). Okazaki & Taniguchi (2000) and Dabringhausen & Kroupa (2012) even suggested that a large fraction of the dwarf galaxies, including those with high masses, could form this way. However, tidal dwarf galaxies are not expected to contain any dark matter (but see discussion in Bournaud et al. 2007a). As an example Duc et al. (2007) analyzed VCC2062 and claim that it is an old tidal dwarf.

Many of the processes discussed above are illustrated with example galaxies in the Virgo cluster in Fig. 1.5. The figure is taken from Ferrarese et al. (2012, the NGVS) and the original figure caption reads (the letters labeling the panels were substituted with the appropriate numbers):

"Panels (1)-(3): a ram-pressure-stripping sequence of VCC630, VCC1690, and VCC1516, illustrating gas stripping before, during and after its peak intensity (as inferred from HI observations). Panel (4): VCC1632, a remnant of a gas-poor merger. Panel (5): VCC1249, a gas-rich dwarf being accreted by M49 and an example of a 'wet' accretion event. Panel (6): VCC355, an S0 galaxy with an extended star-forming ring, perhaps triggered by tidal interactions. Panel (7): VCC1673 and VCC1676, an interacting pair with tidally triggered star formation. Panel (8): VCC979, a possible post major merger Sa galaxy. Panel (9): VCC2062, a candidate tidal dwarf system. Panel (10): VCC1786, a possible binary dwarf system. Panel (11): VCC1199, a close companion of M49 that has likely undergone severe tidal stripping.

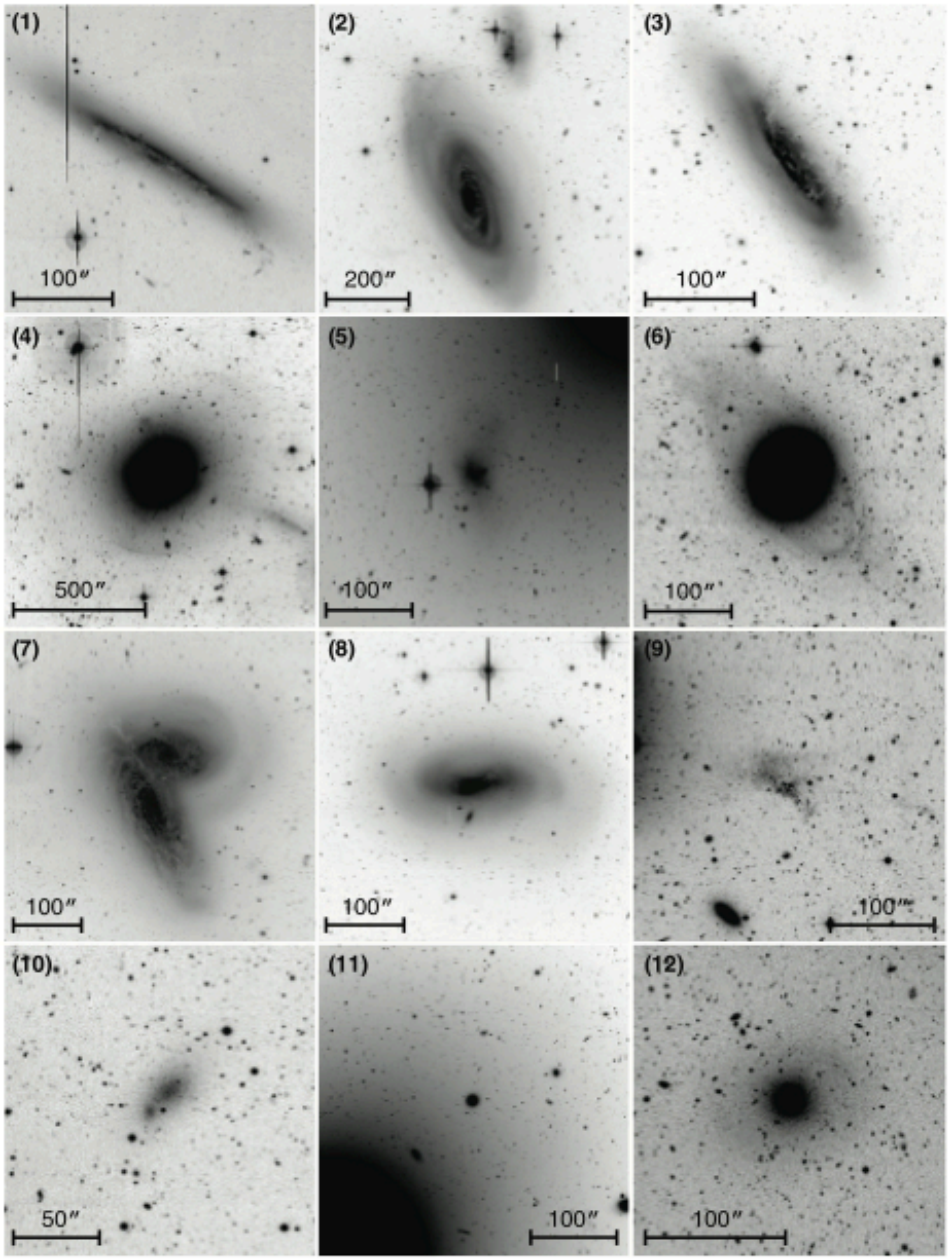

FIGURE 1.5: Galaxies in the Virgo Cluster illustrating the various processes (see text). Figure taken from Ferrarese et al. (2012)

Panel (12): VCC1681, a faint dwarf elliptical galaxy that shows faint spiral arms, possible evidence for the transformation by the tidal forces acting in the cluster environment. All images are in the g-band; the scale is as shown in each panel (100″corresponds to ~8 kpc at the distance of the Virgo cluster).” (Ferrarese et al., 2012)

1.5 THE VIRGO CLUSTER

The Virgo cluster is a galaxy cluster in the constellation of Virgo. It is the closest rich galaxy cluster to the Milky Way at a distance of 16 Mpc (Jerjen et al., 2004). Its proximity has given the cluster a prime role in studying galaxy clusters and their evolution, as well as for other studies. For example, studies of this cluster made it possible to avoid the Malmquist bias (Teerikorpi, 1984), which means that surveys with limited apparent magnitude favor intrinsically bright galaxies. The restriction of a survey to a cluster, and therefore approximately to one distance, allows to overcome this problem, since the apparent brightness limit corresponds to a limit in absolute galaxy brightness. With the observation of cepheids in M100 (Freedman et al., 1994; Ferrarese et al., 1996), the distance to the Virgo cluster was determined to be 16.1 Mpc. These variable stars have a known relation between their luminosity and the period of the variability (discovered by Leavitt & Pickering 1912; see, e.g., Feast 1999 for the use as a distance indicator). The distance measurement gave also a new value for the Hubble constant of 88 ± 24 km/s/Mpc, and was an important step on the cosmic distance ladder. Today, a larger number of distances to individual galaxies in the Virgo cluster are known. For spiral galaxies the cepheids offer precise measurements, but detailed observations with the Hubble space Telescope (HST) are required. It is not feasible to obtain distances to many individual galaxies this way. Therefore, the Tully-Fisher relation between absolute galaxy brightness and rotation velocity (Tully & Fisher, 1977) has been utilized to obtain the distances (Fukugita et al., 1993; Gavazzi et al., 1999). Elliptical galaxies do not host cepheids, since their stellar populations are too old for such short-lived stars. Neither do they follow the Tully-Fisher relation. However, high quality data allowed to determine distances to early-type galaxies with the surface brightness fluctuation method (Tonry et al., 2001; Jerjen et al., 2004; Mei et al., 2007), which works as follows. Early-type galaxies are characterized by a smooth distribution of the stars. The stars are discrete sources of different amounts of light. Seen with limited resolution at a large distance, they form a more or less smooth surface. The granularity can then be used to infer the distance of the galaxy.

The interest and the knowledge about the Virgo cluster increased dramatically with the series of “Studies of the Virgo cluster I-VI” by Binggeli, Sandage, Tamman, et al. (1984-1987). They carried out a 150 $\deg^2$ survey with photographic plates, and cataloged and classified the galaxies in the Virgo cluster. Their Virgo cluster catalog (VCC) is complete down to $m_B \sim 18$ mag, which corresponds to $M_B = -13.09$ mag assuming a distance modulus of $m - M = 31.09$ mag (Mei et al., 2007). In the subsequent papers they characterized the galaxies’ morphologies, analyzed the spatial and kinematical structures of the different galaxy subpopulations, and calculated the LFs of the various galaxy types. It is not exaggerated to say that these studies built up the foundation of our knowledge and

understanding of the Virgo cluster. Today the Virgo cluster is used as a laboratory for cluster and galaxy evolution. Since it is the closest dense cluster, it is the best place to study the processes described in the previous section in detail (see Fig. 1.5).

Cluster mass

The total mass of the Virgo cluster is of the order of $10^{14} M_\odot$ solar masses. Fouqué et al. (2001) determined a mass of $1.2 \cdot 10^{15} M_\odot$ out to 8° or 2.2 Mpc (1.7 virial masses), based on measured distances for some galaxies and assuming a Tolman-Bondi model for the cluster (Ekholm et al., 1999). This is largely consistent with estimates based on the hot cluster gas imaged in X-rays. McLaughlin (1999) estimated a virial radius of 1.5 Mpc, which corresponds to a mass of $4.0 \cdot 10^{14} M_\odot$, obtained with the X-ray image of the cluster, and the velocities of early-type galaxies, assuming a Navarro, Frenk, & White (NFW) profile (Navarro et al., 1997). The X-ray method allows also to determine masses for the different clumps in the cluster. Böhringer et al. (1994) found a mass range of $1.2 - 5.0 \cdot 10^{14} M_\odot$ for the M87 subcluster within a radius of 1.5 Mpc. Schindler et al. (1999) estimated the mass of the M87 subcluster to be $1.7 \cdot 10^{14} M_\odot$ within 1.2 Mpc, and Urban et al. (2011) estimated the virial mass of this subcluster to be $1.4 \cdot 10^{14} M_\odot$. Schindler et al. (1999) found the M87 subcluster to be 2.4 times more massive than the M49 subcluster. The M87 subcluster is the dominant part of the cluster, even though M49 is the brightest individual galaxy.

Inventory of the Virgo cluster

The Virgo cluster catalog (VCC; Binggeli et al. 1985) comprises more than 1000 member galaxies above the completeness limit of the catalog. How the different galaxy types contribute at different galaxy brightnesses can be seen in the LFs in Fig. 1.6, taken from Binggeli et al. (1988). There are about twice as many elliptical and lenticular (E and S0) galaxies than spirals, while for early-type dwarfs (dE) and irregular galaxies (Irr) the factor is about 4.

A number of pointed and blind surveys have targeted the Virgo cluster and made data at all wavelengths available: ALFALFA (H I, Giovanelli et al. 2005), HeViCS (far-infrared, Davies et al. 2010), SMAKCED (near-infrared, papers V&VI), SDSS (optical, Stoughton et al. 2002), ACSVCS (high-resolution optical, Côté et al. 2004), GuViCS (UV, Boselli et al. 2011), and the cluster was also imaged in the X-rays (with ROSAT, Böhringer et al. 1994). There will be soon also the NGVS available (deep optical, Ferrarese et al. 2012).

Lieder et al. (2012) studied deep optical images of the core of the Virgo cluster and found several tens of dwarf spheroidal galaxies (dSphs). Durrell et al. (2007) resolved one dSph in the Virgo cluster with HST imaging. Surprisingly, they found no signs of tidal threshing and concluded that this galaxy is pristine, probably just falling into the cluster. Furthermore, a number of UCDs were found in the Virgo cluster by Evstigneeva et al. (2005), Jones et al. (2006), Haşegan et al. (2005), and by Paper IV in this study.

Several studies have revealed a number of objects in the Virgo cluster that are not bound to a galaxy anymore: *(i)* the diffuse intra-cluster light was mapped by Mihos et al. (2005)

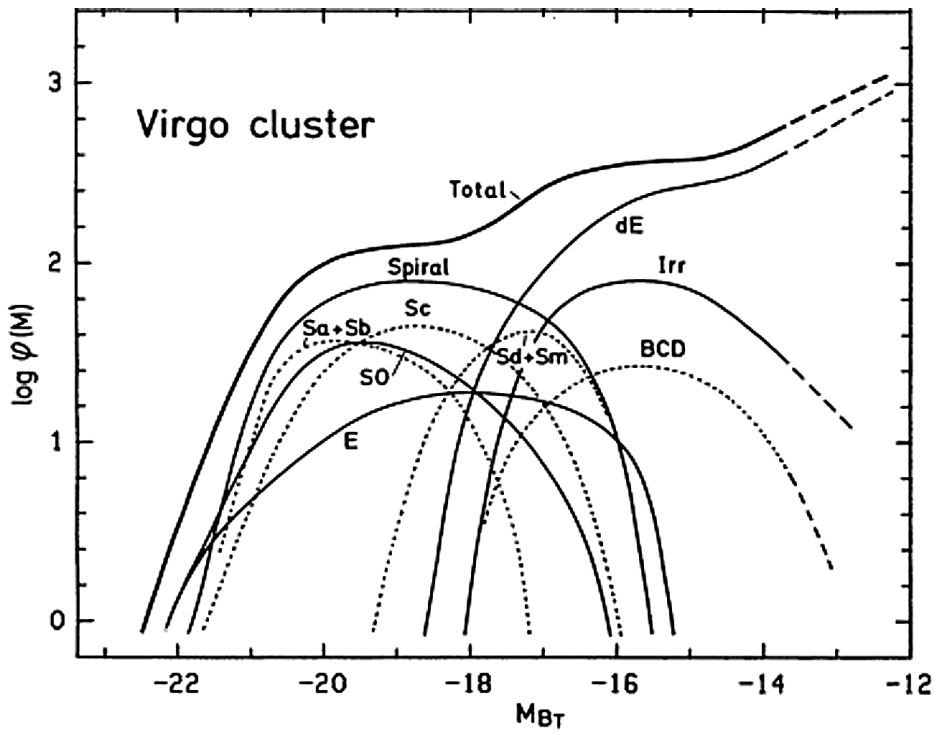

FIGURE 1.6: The galaxy LUMINOSITY FUNCTION (LF) of the galaxies in the Virgo cluster and the contributions from various galaxy types. The Figure is taken from Binggeli et al. (1988).

with impressively deep images, obtained with a small telescope. *(ii)* Intergalactic stars can contribute up to 10% of the stars (Ferguson et al., 1998; Durrell et al., 2002). *(iii)* Intergalactic planetary nebulae (Feldmeier et al., 1998) and intergalactic globular clusters (Lee et al., 2010) have also been found. *(iv)* Even isolated star forming regions (Gerhard et al., 2002), and *(v)* possibly an isolated HI cloud with a substantial amount of DM (Minchin et al., 2005), have been detected. This material and these objects may partly be the remains of the galaxy cluster assembly, and, therefore, offer valuable insights to the processes of galaxy evolution inside this massive galaxy cluster.

The population of early-type dwarf galaxies

The population of early-type dwarf galaxies is quite heterogeneous. They span a mass range of about $10^7 \lesssim M \lesssim 10^{10} M_\odot$ (Grebel, 2001). Already the VCC divided the early-type dwarf galaxies into two distinct classes: dE and dS0, with the latter having revealed direct disk indications or a two-component structure in the surface brightness profile (Sandage & Binggeli, 1984; Binggeli & Cameron, 1991). Lisker et al. (2006b) searched systematically for disk features like bars, spiral arms, and edge-on disks using unsharp masking applied to SDSS images. Indeed, they found a few more examples of early-type dwarf galaxies with spiral arms, continuing the pioneering work of Jerjen et al. (2000) and Barazza et al. (2002). Lisker et al. grouped galaxies with spiral arms or other disk indicators in the subclass of dE(di)s. The fraction of this galaxy type rises as high as 50% at the high-mass end of the early-type dwarfs' LF.

The VCC made a further distinction between nucleated and non-nucleated dwarfs. Lisker et al. (2006a) identified early-type dwarf galaxies with blue cores, dE(bc), hinting at residual star formation in the galaxy centers. In fact, the stellar populations of early-type dwarf galaxies have been found to span a large range of ages (Michielsen et al., 2008; Paudel et al., 2010b).

Furthermore, the amount of rotation in the early-type dwarf galaxies varies. Some of them are rotationally supported, while others do not show any hints of rotation (Simien & Prugniel, 2002; Pedraz et al., 2002; Geha et al., 2003; van Zee et al., 2004; Chilingarian, 2009; Toloba et al., 2009, 2011). The low surface brightness of the dwarf galaxies makes it hard to measure the kinematics to larger radial distances. In fact, such observations are still rather rare. Within the SMAKCED project we obtained spectra for a number of galaxies (Toloba et al., in prep.). Two other approaches to determine the dynamics in early-type dwarfs should be mentioned: Ryś et al. (2012) obtained integral field spectroscopy for a small number of galaxies with the spectrographic Areal Unit for Research on optical Nebulae (SAURON) on the William Herschel Telescope (WHT). The data are of very high quality and their two-dimensional character offers additional information. Beasley et al. (2009) circumvented the problem of the low surface brightness and measured the rotation curves by detecting the velocities of the GCs of the galaxies, instead. The GCs appear as point-sources and are independent of the surface brightness, allowing to trace the rotation out to several half-light radii.

Distribution of galaxies within the cluster

The morphology of galaxies depends in general on the environment. Spiral galaxies are more common in low density environments, while giant ellipticals are preferentially located in high density regions like galaxy clusters. This is the well-known morphology-density relation (Dressler, 1980). Also within the clusters the galaxies have different clustering properties: E galaxies are the most centrally concentrated, whereas S0, dE, dS0, spiral, and irregular galaxies are more and more spread throughout the cluster. For the Virgo cluster Binggeli et al. (1987) studied the clustering properties of various galaxy types. The overall number density of galaxies peaks somewhere between M87 and M86. The subcluster around M87 is called Virgo A and is assumed to be the main subcluster. The different clustering properties of the various galaxy types become even more evident when the cluster is binned over heliocentric velocities (Binggeli & Cameron, 1993): M87 and M86 have different velocities, and the types preferring higher densities clump in velocity space around these galaxies.

The Virgo cluster has another subcluster, Virgo B, around M49, which is actually the brightest galaxy in the cluster. This subcluster is especially rich of spiral and irregular galaxies and is assumed to be currently merging with the Virgo A subcluster. Furthermore, Gavazzi et al. (1999) identified different smaller substructures of the cluster called N, S, and E clouds. They may also be currently merging with the main cluster. The M & W clouds probably consist of background objects, since their galaxies have significantly higher heliocentric velocities. Binggeli et al. pointed out that the outer isophotes of M87 are aligned to the axis M100-M86, while the jet in M87 is aligned to the axis M87-M49. This may or may not be a coincidence.

With the growing number of measured distances to individual galaxies, it has become possible to determine the three-dimensional structure of the cluster. Fukugita et al. (1993) found the spiral galaxies in the Virgo cluster using the Tully-Fisher relation to lay along a prolate filament, which is four times deeper than wide (see also Gavazzi et al., 1999). There was a similar proposition for dEs by Young & Currie (1995), based on their profile shapes. However, the claim was disputed by Binggeli & Jerjen (1998), who concluded that the variations of the profile shapes are intrinsic, instead of being caused by different distances. Jerjen et al. (2004) determined, for the first time, the three-dimensional distribution of the early-type dwarfs by measuring the distances to 16 early-type dwarfs using the surface brightness fluctuation method. Mei et al. (2007) did the same thing for a larger sample using HST. The extent of the cluster determined with these galaxies is qualitatively consistent with the previous finding that the cluster is deeper than wide.

along the line-of-sight is not as extreme, but qualitatively the result that the cluster is deeper than wide remained.

Lisker et al. (2007) showed that also within the early-type dwarf galaxies the various subclasses exhibit different clustering properties: the nucleated early-type dwarfs, dE,N, are most centrally concentrated, while those with blue cores, dE(bc), and galaxies with disk features, dE(di), spread most throughout the cluster. In Paper III we show that the

apparent flattening of the nucleated early-type dwarfs in the (projected) cluster center depends on their orbital characteristics.

In spiral galaxies it was shown that their HI deficiency depends on the cluster distance (e.g. Chamaraux et al., 1980), also indicating the influence of the cluster environment on galaxy parameters. Furthermore, the degree of rotation in early-type galaxies was found to be a function of the clustercentric distance, both in bright (Cappellari et al., 2011) and in dwarf early-type galaxies (Toloba et al., 2011).

Dynamical state of the Virgo cluster

The Virgo cluster is assumed to be a dynamically young, still evolving system, for several reasons:

The shape of the cluster seen in the X-rays has not a simple centrally concentrated spheroidal shape (Schindler et al., 1999). As seen in the previous section, it also has several clumps, which is a clear hint that the cluster is still being assembled. The clump around M86 seems to be merging with the main subcluster around M87 falling in from the far side of the cluster (Binggeli & Cameron, 1993; Jerjen et al., 2004). Some of the low-mass galaxies around M86 are the most blue-shifted galaxies in the Universe. The group around M49 apparently merges with the main subcluster, in a direction perpendicular to the line-of-sight. Furthermore, the Virgo cluster has a higher ratio of late to early-type galaxies than other clusters in the local Universe (e.g. Paper ii, Fig. 6).

The peculiar velocities of the galaxies inside the Virgo cluster (velocity dispersion $\sigma \sim 700$ km/s; Binggeli et al. 1993) are comparable to the heliocentric recession velocity of the cluster itself ($v_h \sim 1100$ km/s; Binggeli et al. 1987). The apparent motions are, therefore, not dominated by the Hubble flow. Conselice et al. (2001) studied the velocity distributions of the different galaxy types in the Virgo cluster. They found that the elliptical galaxies are the only relaxed population with a Gaussian (projected) velocity distribution and a pronounced concentration towards the cluster center. All the other galaxy types have wider, non-Gaussian velocity distributions, and their spatial distributions are more spread. Conselice et al. calculated theoretically that the velocity dispersion is 1.4 times larger for an in-falling than for a virialized population. They also found that the ratios of the velocity dispersions of any other type and the ellipticals is close to that value. This was seen as evidence for an in-fall of those other galaxy populations. The authors argued that from the exact values of these velocity dispersion ratios average in-fall times can be inferred. They concluded that the S0 and early-type dwarf galaxies should have fallen into the cluster earlier than the more recently accreted spiral and irregular galaxies.

With the same argument the nucleated early-type dwarfs, dE,N, should be the oldest early-type dwarf galaxy population in the Virgo cluster. They are more centrally concentrated (Binggeli et al., 1987; Lisker et al., 2007), and their velocity distribution is the most virialized one. The longer time that they spent in the cluster may have allowed for the formation of a nucleus. Secular evolution processes could have driven material to the galaxy core (see also Chapter 9), or the cluster potential may have stabilized the central

part of the galaxy enough to allow GCs to sink into the center and to merge to form the nucleus (Oh & Lin, 2000).

In Paper III we find that the apparent shapes of dE,N in the projected cluster center depend on their orbital characteristics. The flat dE,N move probably on radial orbits, while the orbits of the round dE,N are more circularized. This fits into the picture described above, with the round dE,N having spent more time in the cluster, allowing for a prolonged dynamical heating of the galaxy.

Conselice et al. (2001) calculated the expected number of early-type dwarf galaxies, assuming that they had fallen into the Virgo cluster in galaxy groups. They counted the number of spiral galaxies in the cluster, including potential spirals that underwent a major merger and are now seen as elliptical galaxies. Assuming a number of early-type dwarf galaxies per spiral galaxy in the galaxy group similar to this number in the Local Group, the number of early-type dwarfs was obtained. However, this is too small in comparison with the early-type dwarf population in the Virgo cluster. The discrepancy may be explained by forming the early-type dwarfs from other galaxy types by a transformation processes. However, the number of dwarfs per spiral may also have been different at earlier times.

The Virgo cluster is the closest massive galaxy cluster, but is it a typical cluster? When comparing it to other clusters, an important point is that the other clusters have different masses. For example, the Perseus and Coma clusters are more massive, while the Fornax cluster is less massive (see, e.g., Paper ii and references therein). Furthermore, we have seen that the Virgo cluster shows signs of currently being assembled. Also, we find in Paper ii that the fractions of red galaxies in these other clusters are well reproduced in the SAM of Guo et al. (2011). However, this is not the case for the Virgo cluster. It has a low red fraction compared to model clusters of the same mass, which is consistent with the Virgo cluster being dynamically young. Both the mass and the current evolutionary stage are expected to determine the appearance of a cluster. We may observe the Virgo cluster at a moment, when it is not the most typical cluster. On the other hand, comparisons to model clusters of the same mass (Paper VIII) show that in general the time since the clusters gained half of their present-day mass varies considerably. In that sense, it may even be the rule that the even clusters of the same mass are different.

1.6 THESIS CONTENT

In this thesis the morphologies of the early-type dwarf galaxies are studied with optical and near-infrared data. The photometric scaling relations of early-type dwarfs, and their detailed morphologies are compared to those of bright early-type and spiral galaxies, and of Blue Compact Dwarf galaxies (BCDs). The stellar population characteristics of a subsample of nucleated early-type dwarfs are compared to Ultra-Compact Dwarf galaxies (UCDs). The goal is to look for similarities or differences between these galaxy types, and to lighten possible evolutionary paths between them. It is particularly interesting to

search disk galaxies among the early-type dwarf galaxies, since they are assumed to be evidence for late-type progenitor galaxies. Furthermore, the observations are compared to state-of-the-art SAMs and to N-body simulations. The galaxies' present-day appearance is in that way used to decipher details of their past, with the ultimate goal of determining their origin(s).

The thesis is structured in the following way. The second part introduces the galaxy samples of the different studies and describes the observations. The data reductions are described in the third part, and the different analysis methods in the fourth part. In the fifth part the results are summarized and then conclusions are given.

Part II

SAMPLE AND OBSERVATION

SAMPLES AND OBSERVATIONS

2.1 VARIOUS SAMPLES

We have selected several samples to study the characteristics of the Virgo cluster early-type dwarf galaxies and to compare them to other galaxy types in the cluster. All of these samples are based on the Virgo cluster catalog (VCC, Binggeli et al., 1985). In a few cases the VCC classification was later changed (Barazza et al., 2002, 2003; Geha et al., 2003), when new higher quality data has been obtained. The cluster membership was also updated, when new heliocentric velocities have become available, with the galaxies having $v_{hel} > 3500$ km/s being assigned to the background (Binggeli & Cameron 1993, also see the Appendix of Paper ii, most of the new velocities came from SDSS spectra.). We consider all the galaxies brighter than $m_B \leqslant 18.0$ mag, which is the completeness limit of the VCC (Binggeli et al., 1985). In the r-band as absolute brightness the completeness limit is $M_r \leqslant -15.2$ mag (see Paper ii).

- In Papers I & II we seek to compare the scaling relations of galaxy brightness versus galaxy size for bright early-type galaxies and early-type dwarfs, as well as their color-magnitude relations, with the very homogeneous SDSS images. We select from the VCC all galaxies from Hubble types E to S0/S0a or SB0/SB0a, and all dwarfs with dE, dE:, and dS0 classifications.
- In Paper III the shapes of the early-type dwarfs with nuclei, 'dE,N' (Binggeli et al., 1985), in the cluster-core are studied, and compared to the line-of-sight velocities relative to the cluster. All dE,N galaxies with measured velocities are selected within the central $1.^{\circ}27$, corresponding to about a quarter of the virial radius.
- In Paper IV the stellar population characteristics of nuclei in early-type dwarf galaxies are compared with the stellar populations of UCDs. The nuclei are selected to be brighter than $m_{r,nuc} < 21$ mag, and to be strong, $s_{r,nuc} < -1$. The nuclear strength is here defined as $s_{r,nuc} = m_{r,nuc} - \mu_{r,eff}$, with the brightness of the nucleus, $m_{r,nuc}$, and the mean effective surface brightness of the galaxy, $\mu_{r,eff}$. The comparison sample of UCDs is based on Evstigneeva et al. (2005) and Jones et al. (2006), and includes additionally one newly discovered UCD.
- In the SMAKCED project (Papers V & VI) we aim at obtaining deep near-infrared images for a sample of all early-type galaxies in the Virgo cluster within $-19 \leqslant M_r \leqslant -16$ mag. The number of 174 galaxies in the sample guarantees that binning such parameters as subclass, galaxy brightness, and clustercentric distance is possible with a sufficient number of galaxies in each bin. The brightness range ensures that galaxies of all the subclasses are contained in the sample and spans over a region of particular interest, since galaxies both with dwarf and non-dwarf classification

TABLE 2.1: Samples

Paper	Sample selection	# of galaxies
I	early types	475
II	early types	468
III	dE,N in central region with measured heliocentric velocities	46
IV	dE,N with strong and not too faint nuclei + UCD	34 + 10
V	early types within $-19 \leqslant M_r \leqslant -16$ mag	101
VI	early types within $-19 \leqslant M_r \leqslant -16$ mag	121
VII	BCDs	60
VIII	$M_r \leqslant -15.2$ mag	1013

NOTE. — Summary of the various samples. The last column gives the number of galaxies in the working sample. Early types include E to S0/S0a and SB0/SB0a + dE, dE:, dS0.

overlap. These may or may not be similar (see e.g. Papers I & II). At the time of writing Paper V 101 galaxies were observed. In Paper VI, 20 more galaxies were included The final, observed sample contains 121 galaxies and is complete down to $M_r = -16.73$ mag (Paper VI).

- In Paper VII BCDs are studied. All galaxies with primary, secondary, and tertiary BCD classification in the VCC are selected. Further 3 galaxies are added to the study after inspection of SDSS color images, since they show morphologies and colors similar to the BCDs.
- Finally, in Paper VIII the galaxy population of the Virgo cluster is compared to the SAM of Guo et al. (2011). We select all Virgo galaxies down to $M_r = -15.2$ mag, which we found to be the completeness limit in the r-band in Paper ii. Additionally, we use SDSS based samples for the Coma (down to $M_r = -16.7$ mag) and Perseus clusters (down to $M_r = -16.7$ mag).

We use the AB magnitude system for the optical data and the Vega system for the near-infrared (Oke & Gunn, 1983). The samples are summarized in the Table 2.1.

2.2 OBSERVATIONS

SMAKCED – near-infrared imaging

Near-infrared imaging has been the missing corner stone for a comprehensive spectral coverage of the Virgo cluster (see Part I, 1.5). Moreover, it has two major advantages for

studying galaxy morphology: the observations are almost not affected by dust, which is present even in some early-type dwarf galaxies (de Looze et al., 2010). Also, it provides the most direct tracer of the long-lived low-mass stars that make up the bulk of the galaxy mass (Bell & de Jong, 2001). We choose the H-band, as much towards long wavelengths as possible, to minimize contribution of young stars, but at the same time still having within reasonable exposure times, and also allowing comparisons to the literature (e.g. Boselli et al., 2008).

The observations were carried out at NTT at the European southern observatory (ESO), and at TNG and NOT, both at the Observatorio del Roque de los Muchachos.

The near-infrared sky

Observations in the near-infrared are quite different from the optical, even though the near-infrared is the range in the electromagnetic spectrum that comes right after the optical region towards longer wavelengths. The difference is not only that this light cannot be perceived by the human eye. If one is lucky enough and can look at the night sky far away from any light polluting cities in a moonless night, the sky is dark so that all the stars and the Milky Way show up with a high contrast. This would not be the impression in the near-infrared. First of all, water vapor creates windows of certain wavelength at which the atmosphere is transparent, at others the H_2O molecules absorb the light. Filters with passbands tuned to the atmospheric windows optimize the amount of light from the sources, while blocking the other wavelengths.

However, that is not all of the difference. Vast amounts of transitions between rotational-vibrational energy levels of the molecules in the atmosphere fall into the near-infrared. In the upper atmosphere energy, which was chemically stored, is released via the decays of rotational-vibrational excitations that are produced by chemical reactions. Mostly hydroxyl radicals are responsible for that radiation. These lines are called the Meinel bands (Meinel, 1950). A typical process is that oxygen is dissociated and forms ozone with another oxygen molecule. The ozone reacts with a hydrogen atom to form an excited hydroxyl radical and an oxygen molecule. Relaxation takes place with emission of a near-infrared photon and the hydroxyl reacts further.

$$H + O_3 \rightarrow OH^* + O_2, \qquad \text{Relaxation: } OH^* + O \rightarrow H + O_2 \tag{2.2}$$

At longer wavelengths thermal emission of the atmosphere and of both the telescope and the instrument start to become important. Furthermore, sunlight is scattered by interplanetary dust grains and seen as *zodiacal* light. These processes make the near-infrared sky bright (for the various contributions see Leinert et al. 1998). The sky brightness is typically 10 mag brighter than the low surface brightness galaxies that we want to observe. In other words every 10.000th detected photon will actually come from the source, while all the others are unwanted foreground.

The atmospheric windows, typical broad band filters, and the sources of unwanted light are illustrated in Fig. 2.1. The black line shows a model of the sky emission at Mauna Kea (Lord 1992 and the Gemini Observatory). The model includes the OH^- emission (orange,

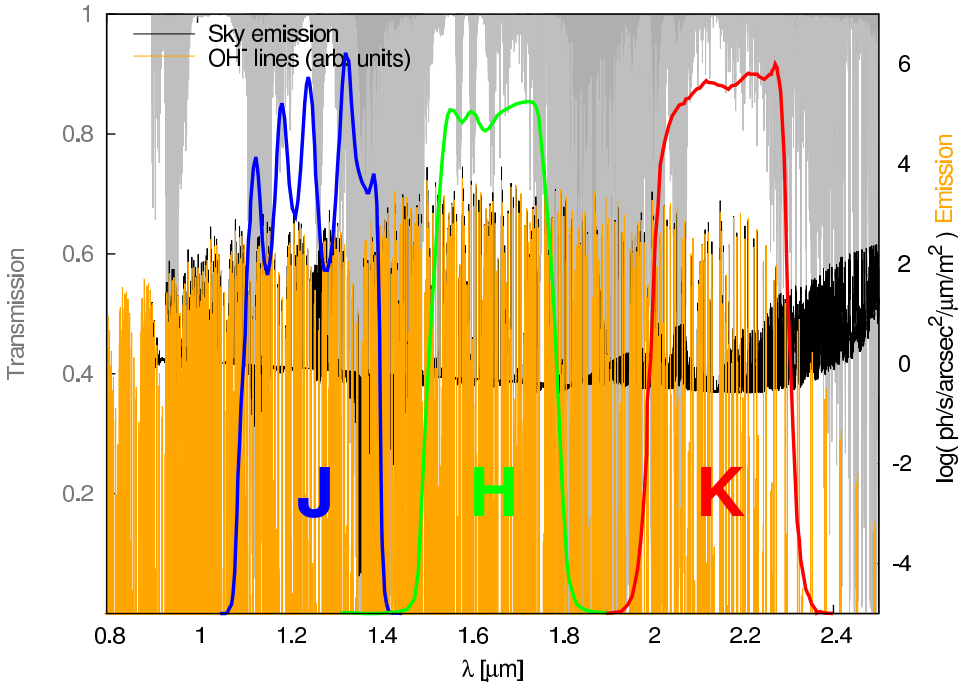

FIGURE 2.1: The blue, green, and red lines display the transmission curves of the J, H, and K (2MASS) filters. The filter bands are designed to fall into the atmospheric windows. The transmission of the atmosphere (white, Lord 1992) is mostly determined by holes in the H_2O bands. The black line shows a model of the sky emission at Mauna Kea (Lord 1992 and the Gemini Observatory). The orange line displays the calculated emission of OH^- (Rousselot et al. 2000, scaled to the observed intensities). While the sky foreground in the H-band is dominated by emission from the hydroxyl radical, thermal emission starts in the K-band to become more important. Not included in the model is thermal emission from telescope and instrument.

Rousselot et al. 2000). Furthermore, it includes emission from other molecules (e.g. O_2, CO_2), zodiacal light (approximated by a grey body of the temperature 5800K, and scaled to the brightness of 18.2 mag/arcsec^2, as observed at Mauna Kea, Maihara et al. 1993), and thermal emission in the atmosphere (here modeled by a black body with a temperature of 273 K; in reality the temperature varies and has different values for different layers in the atmosphere).

Moreover, the sky brightness is variable both in space and time. It depends mostly on the temperature in the atmosphere and the column density of emitting molecules. As a rule of thumb, the sky brightness varies on the order of 10% in 10 minutes. These short period variations can be attributed to gravity waves in the ionosphere, at an altitude of 80-105 km. They modulate the density and temperature, which leads to variations of the reaction rates. The variability of the sky brightness in some of our observations is shown in Fig. 2.2.[11]

Observing strategy in the near-infrared

In order to allow for an adequate subtraction of the variable sky in the near-infrared, it has to be monitored on short time scales. Also, the exposure times for single exposures are limited to ~1 minute. For extended objects usually a sky frame has to be observed in every second exposure. Most of the dwarf galaxies at the distance of the Virgo cluster have angular diameters small enough to allow for more efficient observing strategy: the galaxy can be dithered to the centers of the four quadrants and the empty quadrants can be used for the sky determination. We added small random offsets in order to avoid having bad pixels of the detector always in the same place. We optimize the combinations of single exposure times (DIT) and number of coadds (NDIT), depending on the detector and the sky brightness. The goal is to keep the objects within the linear range of the detector, while minimizing the overheads. The total integration time we calculate for each galaxy individually. The target signal-to-Noise (S/N) is 1 per pixel of $\sim 4' \times 4'$ at two effective radii. The H-band surface brightness is estimated from the optical SDSS images and a conservative color value of $i - H = 1.7$ mag.

Spectroscopy – kinematics and stellar populations

As a follow-up study for Paper III we observed spectra for nucleated dwarfs in the Virgo cluster center, using Focal Reducer and low dispersion Spectrograph (FORS), attached to very Large Telescope (VLT) at ESO. Due to the different resolution and S/N requirements for absorption line index measurements, and for determining the kinematics, it was more

11 Maybe even most impressively the variations of the OH^- airglow are seen in a video of the 2MASS airglow experiment, http://astsun.astro.virginia.edu/?mfs4n/2mass/airglow/airglow.html. They imaged the sky with a large field of view of several degrees. The brightness variations might even mislead to the impression of clouds passing by.

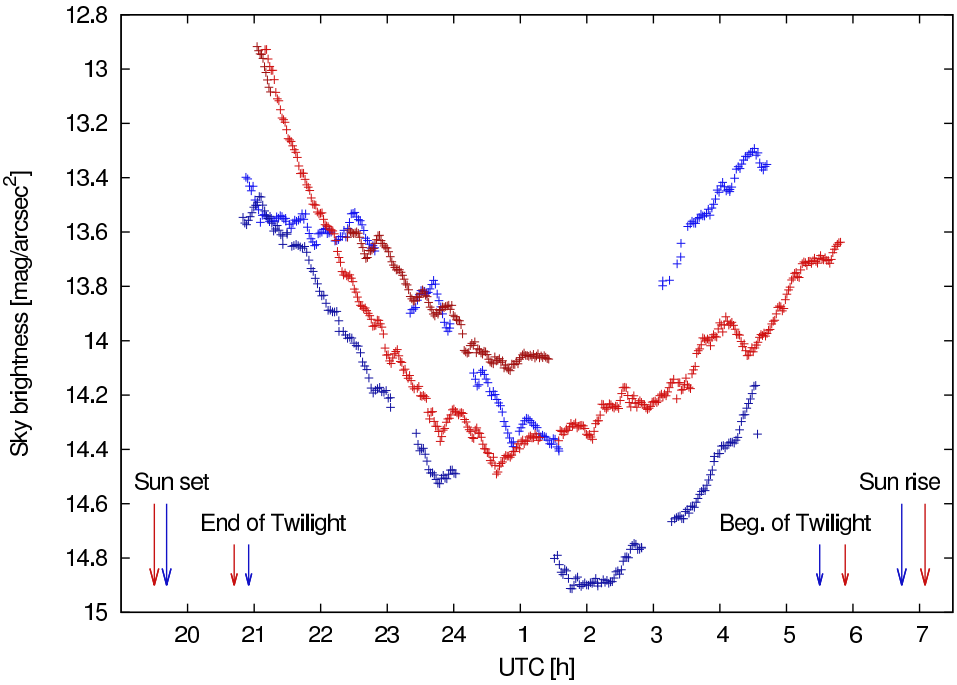

FIGURE 2.2: The curves show the surface brightness of the sky in the images of a few galaxies observed under photometric conditions in two nights in April 2010 at the TNG *(red)*, and in two nights in March 2011 at the NOT *(blue)*. Both telescopes are located at the Observatorio del Roque de los Muchachos in Las Palmas. The times of sun set and rise and the times of the twilight are marked with the arrows. Since all observed galaxies are located in the Virgo cluster, which reached its highest elevation around the middle of the night, the overall trend reflects the change of the sky brightness due to variations of the atmosphere column given by the change of airmass.

efficient to observe spectra for both purposes separately. Long exposure times are needed for the galaxies, which have low surface brightnesses.[12]

For the stellar populations we target the blue part of the spectrum with several metallicity and Balmer line indices. We use grism 300V with a slit width of 1.″0 and the blue-optimized charge-coupled Device (CCD). For the kinematics we target the CaII-triplet at longer wavelengths and use grism 1028z with a slit width of 0.″7 and the red-optimized CCD. The second setup has an instrumental broadening of $\approx$ 35 km/s, allowing for measuring the small expected velocity dispersions and rotation velocities. We measured the surface brightnesses of the galaxies in SDSS images, in order to calculate individually the exposure time needed to reach at least the half-light radius (r_e) with a S/N = 10 per pixel along the dispersion direction. For the calculation a radial bin size of $0.5r_e$ at r_e was used. The exposures are split into chunks of about 10 minutes because of cosmic rays.

For a standard calibration flat fields and arc lamps are needed. Standard stars were observed for the flux-calibration of the stellar population spectra. It is advisable to take exposures with the arc lamps between the single exposures, since the gravity acting on telescope and instrument introduces flexures in the system that lead to varying shifts of the spectra. We decided to do that in a more time-efficient way: in the wavelength range of the CaII-triplet observations there are many bright sky lines of the Meinel bands. We choose to use these lines in the science exposures to determine possible shifts of the spectra during the reduction.

The stellar population data are used in Paper IV.

Sloan Digital Sky Survey

The Sloan Digital sky survey (SDSS) is a large sky survey, which has produced tremendous amounts of scientific results. For the survey a dedicated 2.5m telescope at the Apache Point (New Mexico) is used. SDSS combines a large sky area coverage with reasonable depth, resolution, and multiple filter bands (and additional spectra). The images in the five SDSS filter bands u, g, r, i, and z (Smith et al., 2002) are taken subsequently. This ensures a high relative astrometric accuracy of less than 0.1 pixels (Pier et al., 2003). The absolute astrometric accuracy is better than a Root Mean Sqaure (RMS) $\leqslant$ 0.″1 per coordinate. This precision makes it easy to co-add the images in different filters or to create mosaics for galaxies spanning over more than one survey field.

For the Virgo studies we use the SDSS Data Release Five (DR5) (Adelman-McCarthy et al., 2007). It covers most of the cluster. Six early-type dwarfs in the VCC fall in a region of $2^\circ \times 2.^\circ5$ degree at $\alpha \approx 186.^\circ2$, $\delta \approx +5.^\circ0$ that was not yet observed in SDSS DR 5.

The effective exposure time for each filter band is 54s, with the camera operating in drift-scanning mode (Gunn et al., 1998). The Root Mean sqaure (RMS) of the noise per pixel corresponds to a surface brightness of approximately 24.2 mag/arcsec^2 in the u-band, 24.7 mag/arcsec^2 in the g-band, 24.4 mag/arcsec^2 in the r-band, 23.9 mag/arcsec^2

12 There is a conspiracy between the diameter of a telescope's mirror and the slit width required to achieve the spectral resolution, so that an 8m-class telescope does not perform as much better than a 4m-class telescope, as the difference in light collecting area suggests.

in the i-band, and 22.4 mag/arcsec^2 in the z-band (Lisker et al., 2007). A typical value for the S/N of a bright early-type dwarf image is about 1000 in the r-band within an aperture of two galaxy half-light semi-major axes. For a faint early-type dwarf this value is typically around 50. The pixel scale of the images is $0\farcs396$, which is about a 20th of the typical half-light radius of a small early-type dwarf. The median Full Width at Half Maximum (FWHM) of the Point Spread Function (PSF) in the r band is smaller than $1\farcs4$ or four pixels. The SDSS also provides photometry for the galaxies, but its quality is insufficient due to the treatment of the sky foreground (see Chapter 5).

For the Virgo cluster SDSS provides a very homogenous data set, which is in particular valuable for studies comparing different galaxy types and galaxies of different brightnesses.

Part III

DATA REDUCTION

3

NEAR-INFRARED IMAGING

The various steps in the reduction proceed in the reverse order the effects affect the signal, on the way from the source to the final data product that enters to the scientist's analysis. The first steps are to correct for the instrumental effects. Subsequently, the foreground sky needs to be subtracted, the images to be flux calibrated, and the spectra also to be wavelength calibrated.

3.1 INSTRUMENTAL EFFECTS

Crosstalk

Near-infrared detectors can suffer an effect called *crosstalk*: bright sources cause ghost images on the adjacent quadrant. Moreover, all the pixels in the lines of the bright source and its ghost image will have a slightly enhanced flux. It is not completely understood what the reason for the effect is, but it is well characterized, so that it can be subtracted as long as the bright source is not saturated, or the signal is not too far in the non-linear regime of the detector. Of the three instruments we used two are affected by crosstalk: the Near Infrared Camera spectrometer (NICS) at the Telescopio Nazionale Galileo (TNG), and the son of Isaac (SOFI) at ESO New Technology Telescope (NTT). Both observatories provide scripts to correct for the effect.[1] This step has to be done first, since the amplitude of the crosstalk directly depends on the incident flux on the detector array.

Non-linearity

All array detectors for the near-infrared have ranges of the number of incident photons (or that is electrons), for which the response is close to linear and the output in Analog-to-Digital Units (ADUs) is directly proportional to the number of photons. In the observations we generally stayed within this range of linearity. However, there are reasons why some observations might exceed the upper limit. For example, variations of the sky brightness can make shorter integration times required than those that were chosen at the beginning

1 For SOFI there is an *IRAF*/`crosstalk.cl` script, while for TNG we extracted the FORTRAN script for the crosstalk removal from the SNAP reduction package.

of the observations. Or there can be changes of the seeing, which affect the peak fluxes of point-sources and in the center of the galaxy. In case a brighter source falls into the field of view, one may still decide not to lower the integration times, since the overheads increase with shorter exposure times. If the non-linearities of the detectors' response are well-known, they can be corrected for to some degree. For the NOrdic Optical Telescope near-infrared CAMera and spectrograph (NOTCam) at the NOrdic Optical Telescope (NOT) a pixel-wise correction map was applied to the data of our two last observing runs.

Flat field

The optics of the telescope and the instrument illuminate the detector inhomogeneously. As a result, the system response is not constant, when an image of a surface with constant brightness is taken. In principle, such an image can be normalized and then any science image can be divided by this so-called *flat field*, in order to get a homogeneous response. The surfaces most commonly used are screens in the dome illuminated with a lamp, and the twilight sky. For the ESO/NTT we use 'special' dome flats that combine images of the screen taken with the lamps on and off, and with a partial illumination. The flat field is calculated from these with a script provided by the observatory. For the NOT we take sky flats with high and low counts with the same exposure time, so that thermal effects cancel out when subtracting them from each other. For TNG sky flats are used. Typically, flat fields are stable over weeks. We took flat fields every night when the weather conditions allowed that and calculated one master flat field for each run. This averaging is needed in order not to introduce too much additional noise. The accuracy of the flat fielding is not the most critical, since inaccuracies will largely cancel during the sky subtraction. An example of the raw data, the flat field and the flat-fielded frame is given in the top row of Fig. 3.1.

3.2 SKY SUBTRACTION

This step is the crucial part in the reduction. An accurate sky subtraction is particularly important for our observations, in which faint structures of the early-type dwarfs should be detected. For the brightest sky and the faintest structure this task is comparable to try to observe structures on the moon through a foreground as bright as the sun, concerning the brightness ratio of the foreground and the object. However, on an absolute scale the faint structures are close to the detection limit. This illustrates that a small relative error of 1% in the sky subtraction leads to a huge bias on the science results.

In order to subtract the sky from a certain frame, the observed sky is averaged over those frames observed within a few minutes around the time when that frame was taken. However, in all of the sky frames there are sources. With our dithering strategy the galaxy itself covers a substantial fraction of the detector. The flux of these sources biases the sky values even if a median value is used, so that they need to be carefully masked out. We create the masks using SExtractor on preliminary coadded images (see §3.4) and iterate the sky subtraction with the masks. Only if the masks are obtained that way, the low

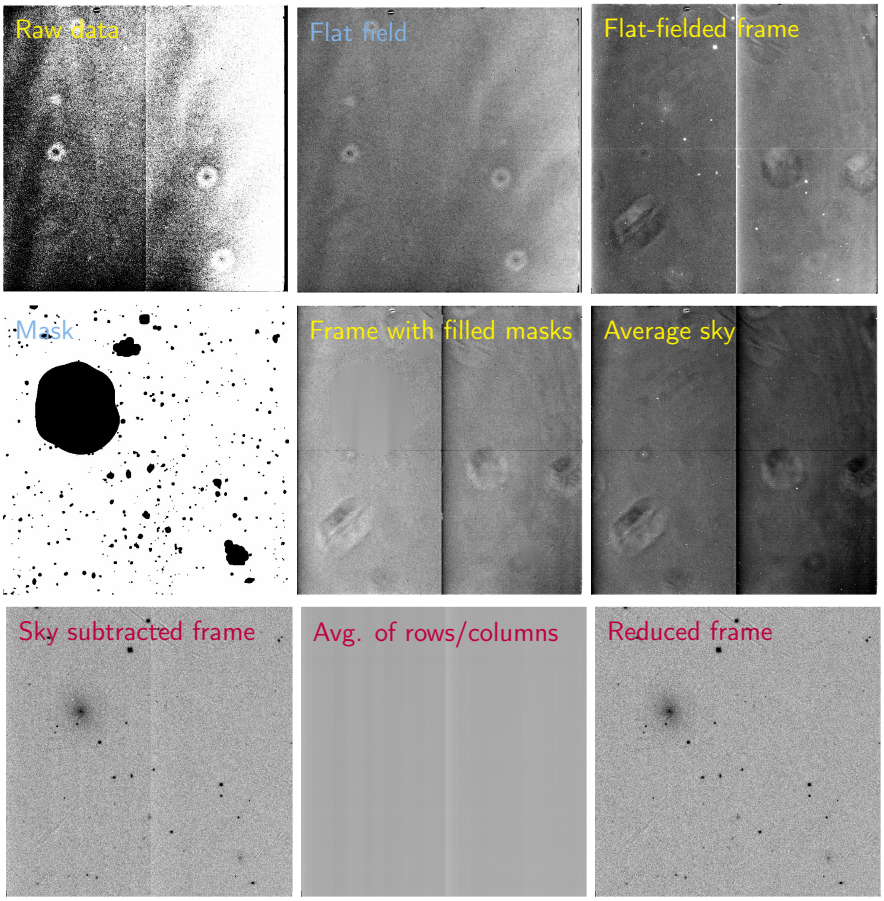

FIGURE 3.1: Illustration of the reduction steps for one single frame of VCC0940. All the images are inverted. In panels with yellow labels the gray scales show the range of 230 to 249 ADU/s. The raw image is divided by the flat field to obtain the flat-fielded image. The mask comes from the previous iteration and was determined on the preliminary coadded image. Note that the masks extend further than the outer isophotes of objects visible on the single frame. In all frames the objects are masked in order to obtain the sky. The masked regions are filled to allow for a proper scaling of the different sky frames. The sky used for the subtraction is obtained by averaging the sky frames within a time window of a few minutes around observation of the frame that is to be sky subtracted. The gray scales in the panels with red labels show −2.5 to 5 ADU/s. Finally, the averages in rows and columns (calculated again taking the masks into account and filling them with appropriate values) are subtracted to reduce artifacts from the detector. North is up and east left. SOFI's x-axis runs from top to bottom.

surface brightness regions can be masked properly, since they have a too low S/N to be detected in a single frame.

Since the sky brightness varies, the different measurements have to be scaled to the same sky level as in the frame, from which the sky will be subtracted. However, the sky can have substantial gradients in the images. The masks can bias the value of the sky brightness determined on the unmasked pixels. If, for example, half of the pixels in one quadrant are masked due to the galaxy, and if there is a gradient so that the sky is brighter in that quadrant, the median value of the remaining pixels will correspond to the score at the 37.5% percentile of the whole frame. Therefore, we fill the masks by averaging and extrapolating the edge pixels around the masks. The scaling factor is then determined taking the recovered pixels into account. For the actual averaging these pixels are discarded. An example of a mask, the sky frame with the reconstructed masked pixels, and the average sky, obtained in a time window of ~10 minutes, are shown in the middle row of Fig. 3.1. If the scaling is done without accounting for the masked pixels ghost images of the masks can appear in the other quadrants.

Finally, the detector can introduce unwanted effects in rows and columns, e.g. due to an reset anomaly. We correct for that by subtracting the average of rows and columns, again masking out any sources and assigning the masked pixels appropriate values. Strictly speaking this is an instrumental effect, but it can only be corrected for after the sky subtraction is done. This step is illustrated in the bottom row of Fig. 3.1.

3.3 ILLUMINATION CORRECTION

During the observing runs in 2012 at NOT and TNG we obtained illumination correction frames. A standard star was shifted to different positions on the detector on a grid of 5×5 positions. The brightness of the star was measured after the images were reduced using the same reduction procedure as for the galaxy images. The variations of the brightness with the position on the detector were then fitted with a second order polynomial using *IRAF*/`surfit` (Fig. 3.2, *upper panels*).[2]

The illumination correction potentially varies with time, although between the observations separated by a few days no changes were found. In order to address a long term evolution we measured the variations of stars in the science frames of two photometric nights in 2010. The stars are much fainter than the standard stars, and the galaxies as extended sources may introduce additional errors in the sky subtraction process. Therefore, the signal is more noisy. However, we conclude that the patterns of the illumination variation are similar to those obtained with the standard stars. Furthermore, the error that might be introduced by using the illumination correction from a different epoch is smaller than not using any correction. We apply the illumination correction by dividing the images by the fitted surface before the final coaddition of the individual frames is done.

2 The same effect can be measured on the raw images. However, the values in the individual positions scatter notably more.

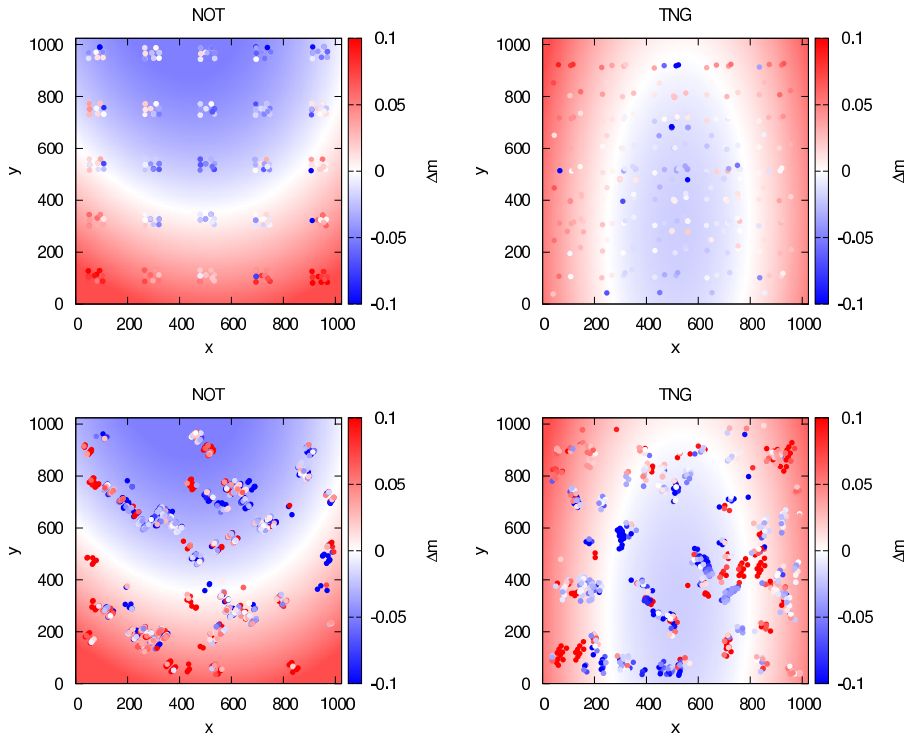

FIGURE 3.2: Variations of the brightness of stars measured across the field of view. The *upper panels* display the dedicated standard star measurements in 2012. The background color shows the fitted surface. The *lower panels* show the same surface and on top the measurements of stars in the science frames of two photometric nights in 2010. The *left* and *right panels* show the data for NOTCam and NICS, respectively.

For the NTT data we do not perform any illumination correction, since the maximum effect is only about 1-3%, as seen on archival illumination correction frames.[3]

3.4 FIELD DISTORTION, ALIGNMENT, AND COADDITION

For low surface brightness objects the exposure time of a single frame is limited by the sky. The sky also dominates the noise in the image. In order to achieve deeper images and to detect faint structures, many short exposures are combined. The averaging enhances the S/N by the square root of the number of exposures, $S/N \sim \sqrt{N}$. Furthermore, imaging the same objects on different parts of the detector allows to remove the bad pixels in an efficient manner.

Before combining them, the single frames need to be aligned. *IRAF*/`xregister` uses a two-dimensional cross-correlation to find the shifts between the images. The initial guesses can be obtained by measuring the coordinates of the same object in the single exposures or by using the coordinates in the header information, if they are accurate and the pointing of the telescope is reliable enough. The images are then shifted with sub-pixel precision using *IRAF*/`iminsert` and *IRAF*/`imshift` and a bicubic spline interpolation between the pixels. The aligned, sky subtracted, single exposures are then combined by coadding them with *IRAF*/`imcombine` taking into account masks for the detector's bad pixels. It is important not to do any clipping in this step, since it will effectively loose some of the stellar fluxes for the following reasons. The seeing conditions change from one image to another, which will modify the stellar images. Furthermore, the alignment of the images is in some cases not perfect over the whole field of view due to field distortions (see below). In both cases a clipping can discard not only outliers, but also meaningful pixel values. This would affect the flux calibration, for which we use the stars in the science frames (see §3.5).

There is an additional effect that complicates the alignment process. The optics can distort the image over the field of view, i.e. two pixels separated by a certain physical distance on the detector can be at different angular distances on the sky, depending on the position of the pixels. For NOTCam and NICS the distortion is substantial, pixels in the corners of the detectors are shifted up to 13 or 10 pixels, respectively, relative to their 'true' position, for which the distance measure would be that of flat euclidean space. As a result the distance between two objects measured close to the center will be different from the distance between the same objects measured close to the edge of the field of view. The image alignment will then find some compromise. In the cross-correlation of the light distributions used by *IRAF*/`ellipse` this will be typically dominated by the best match for the brightest sources. All the other sources are then not necessarily well aligned, which can lead either to complicated widened effective point spread functions, if the images overlap enough, or even to double images.

Since the distortions are not affecting the fluxes but mostly the geometry of the image, we do the correction just before the final alignment and coaddition of the single exposures.

3 The SOFI manual claims that the effect is caused by a different illumination of the flat field screen and the night sky.

Distortion maps can be obtained by measuring the positions of stars in crowded fields and comparing the relative distances as a function of location on the detector. For NICS we extracted such a distortion map from the SNAP reduction pipeline and for NOTCam M. Gålfalk kindly provided us with data to calculate that. The correction maps are applied to the data with *IRAF*/`geotran`. Subsequently, the region to be considered by *IRAF*/`xregister` for the alignment is carefully chosen, in case bright stars bias the cross-correlation.

3.5 FLUX CALIBRATION

Traditionally images are flux calibrated by observing standard stars, for which the brightness is known. The fluxes measured for these standards are compared to their literature brightnesses and the zeropoint of the observing system is found. A problem with this method is that it is restricted to observations made under photometric conditions. Nowadays, extensive catalogs with reliable photometry from large surveys provide data for an alternative approach, which we use: a number of stars in the final coadded images are measured and their brightnesses are compare to the catalog brightnesses in the 2MASS and the UKIDSS. Even faint stars can be used, since they are measured on the coadded images. Some of the stars might be variable stars, though most of them will be low mass main sequence stars. Using several stars avoids that problem and minimizes the uncertainty of the zeropoint determination (see e.g. McDonald et al. 2011).

The UKIDSS and 2MASS filter systems are slightly different. We convert the UKIDSS catalog values to the 2MASS system using the transformations given in Hewett et al. (2006). The photometry of the stars in the 2MASS and UKIDSS then does not show any systematic offsets, with the exception of a very small number of fields. The obtained zeropoints for NOTCam are shown in Fig. 3.3.

Additionally, we compare the galaxy photometry measured in circular apertures of 5″, 7″, 10″, 15″, and 20″. The 2MASS values are taken directly from the extended source catalog. The zeropoints obtained with the galaxy photometry are consistent with the stellar comparisons in spite of the shallow image depth in 2MASS. For fainter galaxies the scatter increases and the 2MASS galaxy apertures loose some of the galaxies' light due to data quality.

The UKIDSS pipeline reductions apparently have a problem with the sky subtraction. There are significant systematic offsets of the zeropoints in comparison to those obtained with the stars, or with the 2MASS galaxy aperture photometry. The offsets become systematically larger from small to large apertures, which hints at a background issue causing the offset. In order to verify that, we downloaded the UKIDSS images and determined the sky values as median values after masking the objects in the images. The offsets of the zeropoints were slightly reduced, but still remained significant.

In the next step, we identify semi-automatically stars listed in the catalogs using SExtractor. Also, the photometry is obtained with SExtractor. Here the best result, with the least scatter, was obtained by assuming that our careful sky subtraction achieves a global background of zero, instead of using local backgrounds determined around the measured star apertures. The aperture sizes are chosen according to the average FWHM of

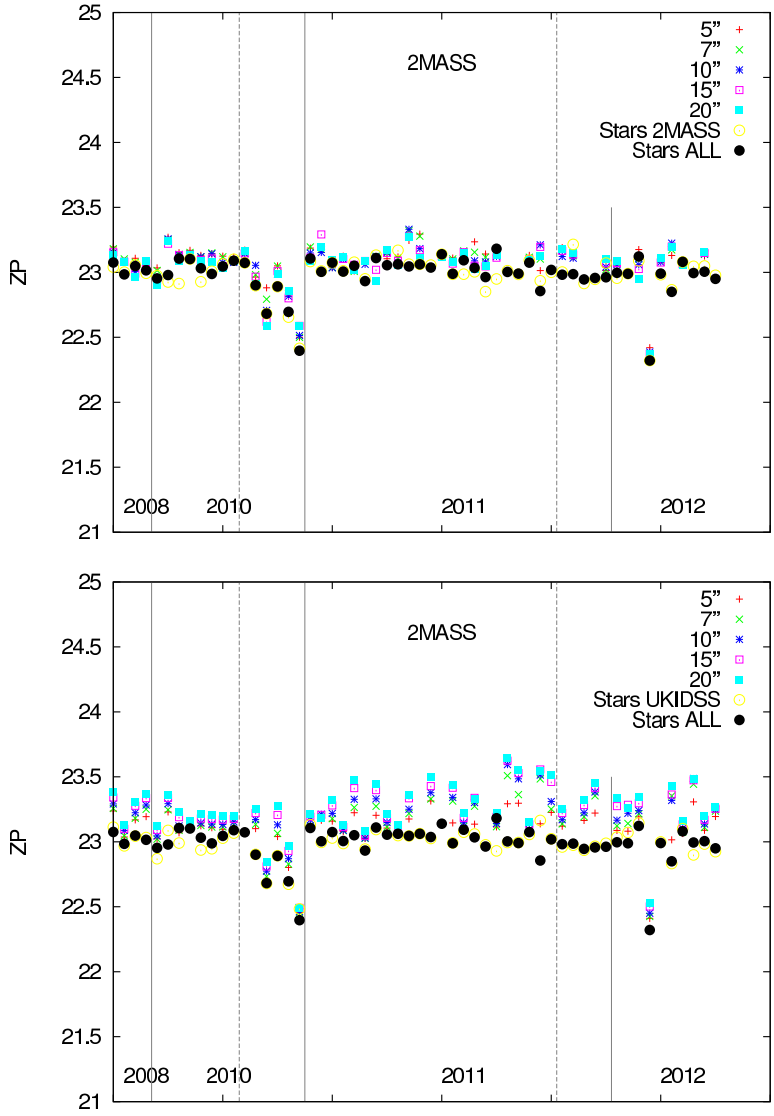

FIGURE 3.3: Zeropoints for the NORDIC OPTICAL TELESCOPE (NOT) obtained by comparison of the star brightnesses in the field of view to the values in the 2MASS *(upper panel)* and UKIDSS *(lower panel)* catalogs. The final zeropoints using stars from both sources are marked with *black symbols*, while those obtained with 2MASS or UKIDSS, respectively, are displayed with *yellow open circles*. The additionally measured zeropoints using various galaxy apertures are shown with the other colored symbols. The gray lines separate the different observing runs (with the years displayed in the bottom).

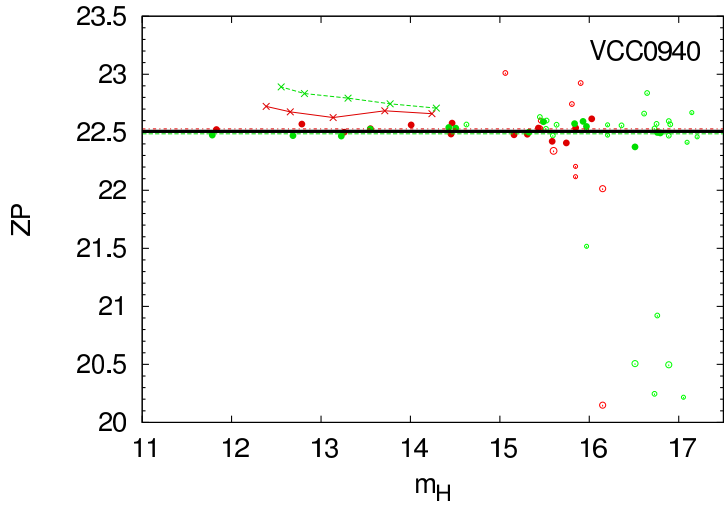

FIGURE 3.4: *Upper panel:* Example for the zeropoint determination of the field with VCC0940. The colors indicate the comparison catalog (*red* – 2MASS, *green* UKIDSS). *Open* symbols indicate sources that were discarded, while *filled* symbols display those measurements used for the zeropoint determination. The zeropoints from galaxy photometry indicated with the colored lines.

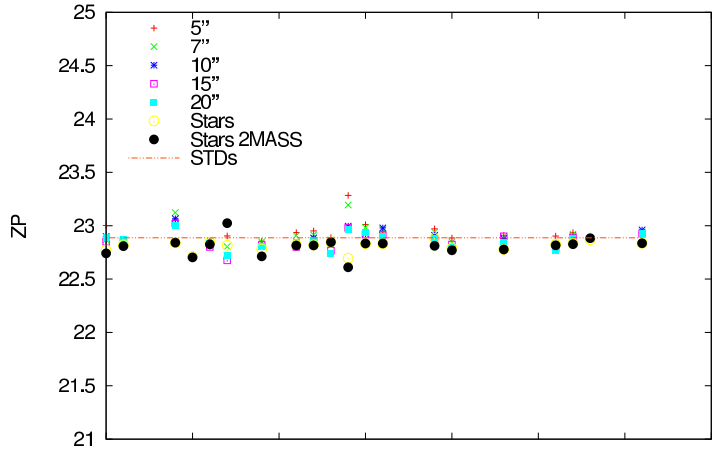

FIGURE 3.5: The obtained zeropoints for the archival NTT data from 2000 (Gavazzi et al., 2001) are displayed as in Fig. 3.3. This run had mostly photometric conditions and a zeropoint (one for the whole run) was determined using observations of standard stars *(red line)*. The results of the catalog comparison method are consistent.

the PSF in the image. For the the zeropoint determination we exclude sources that fulfill one of the following conditions:

(a) sources that are not sufficiently point-like, i.e. for which SExtractor gives a probability of less than 85% of being a point source,

(b) sources that vary too much over the different apertures measured on our images with slightly different sizes,

(c) very bright sources,

(d) faint sources, for which the combined photometric uncertainty of the catalog values and the SExtractor measurement is large,

(e) sources excluded by a clipping of the resulting zeropoints 0.2 below the score at the 75% percentile (in order to eliminate misidentifications and edge detections),

(f) sources excluded by a subsequent 2.33 σ-clipping.

For one field, VCC0940, the comparison of the different zeropoint determinations is shown in Fig. 3.4. Typically, there are 15 stars in the field-of-view of the coadded image, which can be used for the comparison. The final zeropoint is then calculated as a weighted average of the these objects. In order to estimate the precision of the flux calibration, we calculate the scatter of the zeropoints of the individual objects in each field. The median value of this uncertainty is of the order of 2%. This accuracy is only achieved when including the illumination correction. Also, the obtained averaged zeropoints in a given observing run scatter less when the illumination corrections were applied. For the archival data from NTT in 2000 (Gavazzi et al., 2001) a zeropoint for the run was also determined by the observations of standard stars. In Fig. 3.5 we compare our zeropoints for the galaxies observed during this run with the zeropoint determined that way and conclude that they are consistent.

Galactic extinction

Finally, the magnitudes are corrected for Galactic extinction according to Schlegel et al. (1998).[4] Schlegel et al. mapped the galactic dust with Diffuse Infrared Background Experiment (DIRBE) data from the Cosmic Background Explorer (COBE) satellite. Additionally, they used higher resolution infrared data from the Infrared Astronomy satellite (IRAS), and H I data to separate flux contributions from zodiacal light. The dust corrections to our images are small, on the 1% level, since they were observed in the near-infrared, and also due to the high galactic latitude of the Virgo cluster.

4 This is strictly speaking not considered as a part of the data reduction.

4

SPECTROSCOPY

In Paper IV we use long-slit spectra obtained with FORS on the VLT. The first steps of the reduction dealing with the instrumental effects are similar to the reduction of optical or near-infrared images. In the following the reduction of the long-slit data obtained for kinematics, targeting the CaII triplet, is described. The data for stellar population analyses were reduced in a somewhat simpler fashion using the GASGANO pipeline (not described here), since it could also be applied in the same way to previously obtained spectra that were observed using multiple slitlets instead of a long slit. The draw-back of the simpler method is less severe for the blue spectra used in the stellar population analysis, since at the shorter wavelengths the sky lines are weaker and less frequent.

The reduction steps include bias and flat field corrections. Unlike a near-infrared array, a CCD is sensitive to cosmic rays, which have to be identified. The spatial and dispersion directions do not exactly coincide with the axes of the detector and are, in fact, distorted. Therefore, the spectra have not only to be wavelength calibrated, but also rectified. The CaII triplet has a restframe wavelength of $8500 - 8665$Å, which means that the sky is also polluted by atmospheric emission, mainly from the Meinel bands. The subtraction is different than for the images, since the emission is split up into separate spectral lines.

4.1 BIAS SUBTRACTION, FLAT-FIELDING, AND REMOVAL OF COSMIC RAYS

First the bias level has to be subtracted. The bias is a voltage added to the signal before it enters the A/D converter in order to have only positive values.[1] The bias subtraction can be achieved by subtracting a clipped average of bias frames taken with 0s exposure time. However, in our dataset the bias level jumped in one night to a different level, so that not for all frames appropriate bias frames were available. The appropriate alternative is to subtract a low-order polynomial fit to the overscan region in each image, since the FORS bias frame does not have any large spatial variations. After that, the spectra are divided by the flat field, which is obtained by averaging the dome flats taken during the observing run.

1 This bias subtraction is unnecessary in the reduction of near-infrared data, since everything is processed in a differential way.

We identify pixels affected by cosmic rays with a Laplacian edge detection algorithm (van Dokkum 2001, with the python implementation by M. Tewes) and a σ-rejection on the highly sampled data (see below).

4.2 SUBTRACTION OF SKY LINES

The air glow is visible in the spectra as strong emission lines. They are unresolved, since they have FWHMs of less than 1Å (Hanuschik, 2003). These telluric lines are bright and narrow, and thus have sharp edges. The distortions lead to a curvature both in the spatial and dispersion directions. The sharpness and shape of the lines make the subtraction of the sky lines challenging: the pixels sample the lines as they arrive at the detector, always over a wavelength range corresponding to the width of the pixel in wavelength. However, due to the curvature of the spectrum, different pixels do that at different subpixel positions, i.e. the central wavelengths of the pixels vary (Fig. 4.1). The usual procedure is to rectify the spectra and identify the sky lines afterwards, for example, as the median of pixel values over the spatial direction. For the rectification the pixels have to be interpolated. Due to varying sampling of the sky lines the form of the interpolation depends on the spatial coordinate of the row. For most rows the averaged line is not a good representation and the quasi-periodic artifacts in the upper panel of Fig. 4.2 are introduced.

This problem can be solved by using the additional information hidden in the distorted spectrum: the sampling at different subpixel positions allows to construct a super-sampled sky spectrum (Kelson, 2003). The sky spectrum is convolved with the instrumental line broadening and and sampled with a width of 1 pixel, but at many different positions. With this information a spectrum convolved with the instrumental line broadening and with a sampling of 1 pixel, but at any subpixel position can be re-constructed. This re-constructed super-sampled sky spectrum is exactly what is needed for a more sophisticated sky subtraction.

As a first step a rectified coordinate system has to be found. We use *IRAF*`/identify` and *IRAF*`/reidentify` to trace the lines over the rows on each image and to find possible shifts of the spectra between the single exposures. The latter can occur due to different absolute positions of the rotator, and due to flexure caused by gravity acting on the instrument. The line positions are fitted with Chebyshev-polynomials and the solutions determine the position of each pixel on the rectified coordinate system with a subpixel precision. For the high precision required for a good sky subtraction it is important to include many sky lines in the *IRAF*`/identify` and *IRAF*`/reidentify` tasks. There are enough lines to choose from. However, not all of them can be used, since the tasks have problems with lines that have too close neighboring lines. The outer envelope of the used lines will also determine the region where the sky subtraction works in an optimal way. Therefore, it is desirable to include lines both redward and blueward of the CaII triplet.

The super-sampled sky spectrum has another advantage: subsequent pixels in the order of their central wavelength are not anymore necessarily neighboring pixels on the detector. This makes an identification of cosmic rays by a simple σ-clipping possible. We use the remaining sky pixels to fit bi-variate B-splines to the super-sampled sky spectrum (with

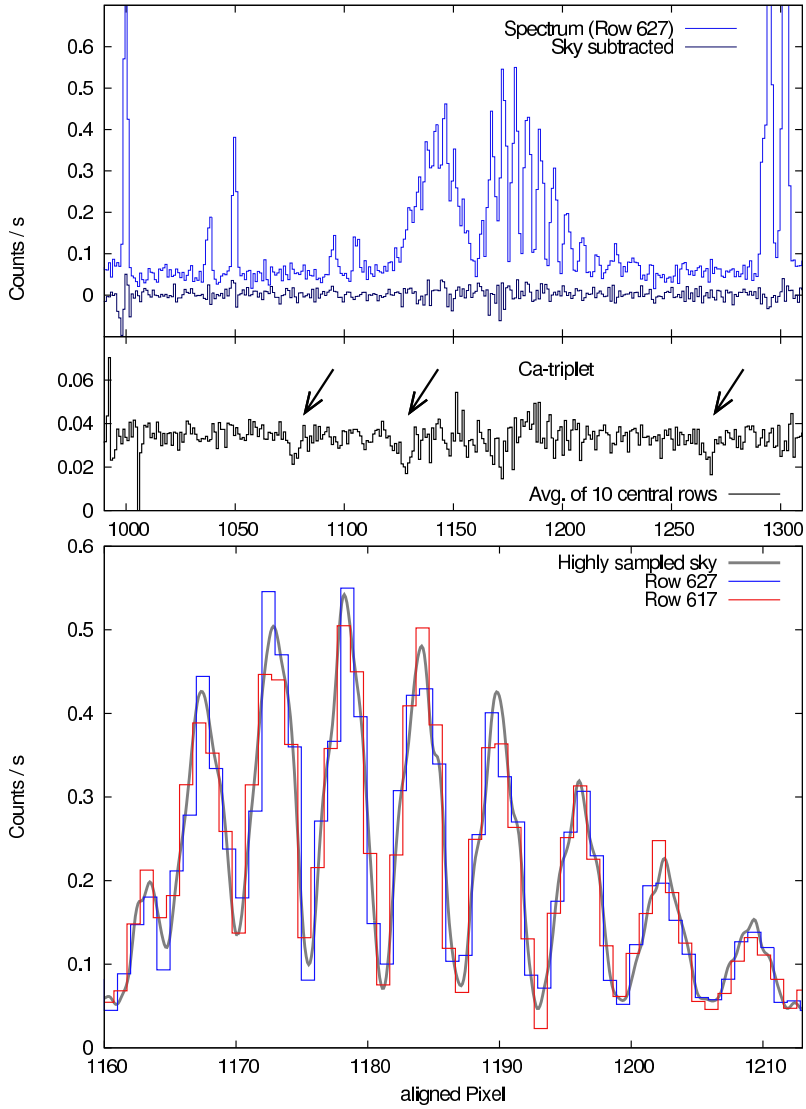

FIGURE 4.1: *Upper panel:* A row without any object in a FORS long-slit spectrum shows the strong sky emission lines (mostly OH^-), which need to be subtracted by the reduction. The *darker* line shows the same row after the sky subtraction, illustrating how well it works. *Middle panel:* After the subtraction the CaII triplet absorption lines at the center of the galaxy become visible (shown here is one single exposure of VCC0786, t_{exp} ~10 min; the rest-frame wavelengths are 8498Å, 8542Å, 8662Å, e.g. Kormendy et al. 2010). *Lower panel:* A zoom of the unsubtracted spectrum of the *upper panel* is compared to the one in the row ten pixels below on the detector. Since spatial and dispersion direction are neither aligned on the CCD rows and columns, nor linear, the pixels in each line sample the sky lines *(gray)* at slightly different wavelengths, with a bin width of one pixel.

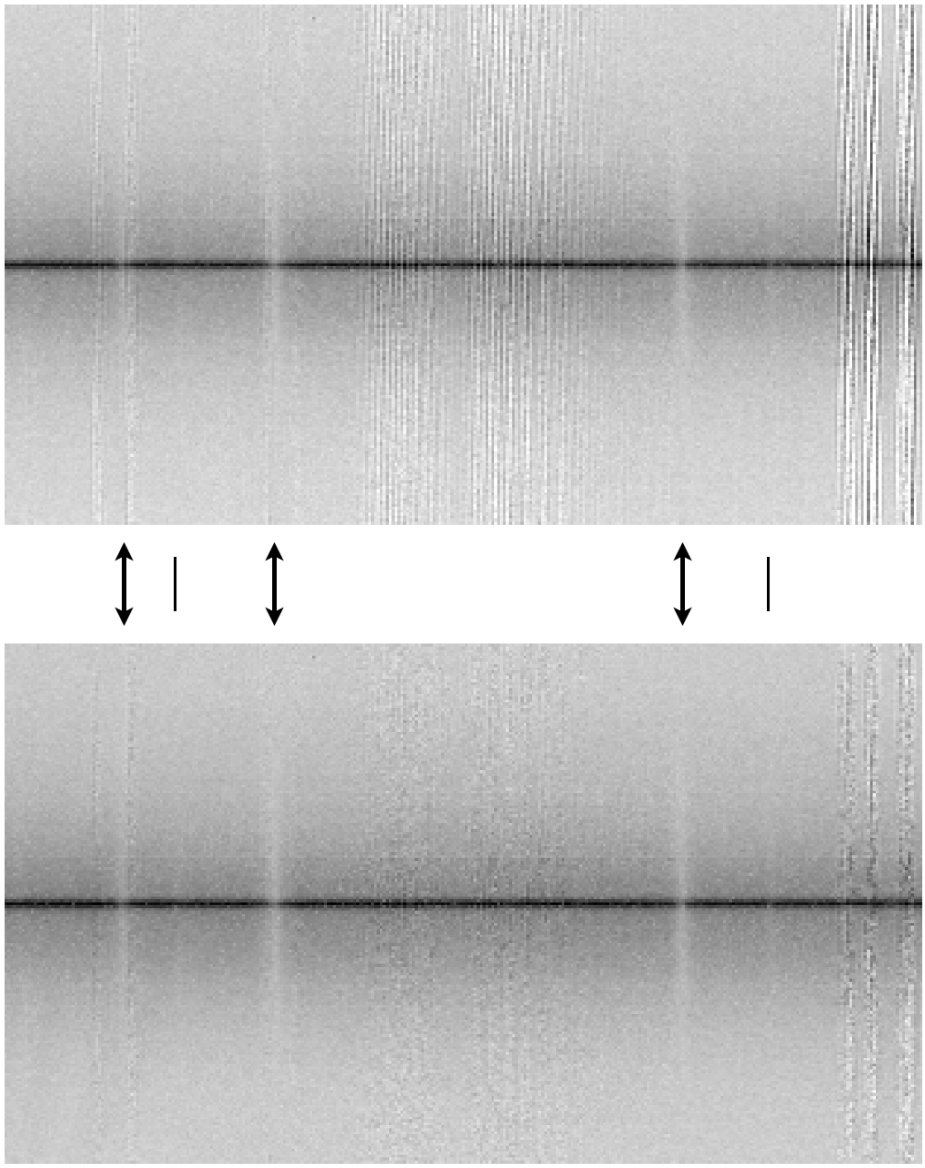

FIGURE 4.2: Comparison of the sky subtraction after rectifying the spectra *(upper panel)* with our method *(lower panel)*. The example shows the spectrum of VCC1104 with inverted gray scales and a wavelength range of 8511.2Å to 8781.6Å. The spatial direction covers 44.″5 or 1.55 half-light radii to each side of the galaxy center. The positions of the CaII triplet lines are marked with the arrows (the lines indicate the positions of two weak iron lines). In this case the two CaII triplet lines at shorter wavelengths (left) are affected by weak sky lines and the need for a high quality sky subtraction is evident. The sky lines remain visible in the *lower panel* as lines of enhanced noise. However, as opposed to the *upper panel* the noise is close to the expected Poisson noise.

the python wrapper of the FITPACK package, P. Dierckx), and subtract obtained model sky spectrum from the science spectra.

4.3 WAVELENGTH CALIBRATION AND LINEARIZATION

After the sky subtraction, the spectra have not anymore the sharp edges of the narrow bright telluric emission lines and can be rectified and wavelength calibrated.

The wavelength solution is found using spectra of arc lamps (He, Ne, Ar). Small shifts between the wavelengths of the pixels in the different exposures, due to flexures in the instrument, are found using the sky lines (see above). As a reference we use the exposure with the smallest airmass. The calibration spectra were obtained in the afternoon with the telescope pointing to zenith. There is a possible small offset between the correct calibration and the one in the reference image. This offset is small (a fraction of a pixel) and can be neglected, if the purpose is not to measure precise heliocentric velocities of the galaxies. However, the shifts between the exposures have to be taken into account properly, since otherwise the absorption lines of interest would be artificially widened.

The position of the galaxy center is traced again with *IRAF*/`identify` and *IRAF*/`reidentify` on preliminarily sky subtracted images. The rectification and wavelength calibration are then finally done with *IRAF*/`transform` in one step, and therefore only one interpolation of the smoothly varying galaxy spectrum is needed.

4.4 COADDITION AND NOISE SPECTRA

The single exposures are then coadded with *IRAF*/`imcombine`. The spectra are scaled to the same flux level, which is measured in the central region of the galaxy. Furthermore, they are weighted with the inverse of the variance of sky pixels in a region without any object, or strong sky lines, in order to optimize the S/N of the final spectrum. We calculate the error spectra from the flux in the single image after bias subtraction and rectification without subtracting the sky, using the gain of the detector, assuming Poisson statistics for the signal and taking into account the readout noise. These single variance spectra are combined using the scales and weights of the coaddition of the spectra squared, divided by the square of the summed weights. The square root of this variance spectrum gives the noise spectrum of the coadded spectrum.

Alternatively, we calculated the pixel-wise noise by determining the RMS scatter of each pixel through the individual reduced spectra. Both methods give consistent results.

5

NOTES ON SLOAN DIGITAL SKY SURVEY IMAGES

In this thesis we use extensively the optical SDSS images. The galaxies in the Virgo cluster have quite large angular sizes (typical half-light radius $\sim 12\farcs5$). The photometry provided by the SDSS pipeline has two problems with such extended objects and cannot be used in a simple manner. In some cases the galaxies are split into more than one *photoObj* catalog entry and several separate measurements exist for different parts of one galaxy.

The other problem has been pointed out by several authors (e.g. Lauer et al., 2007; Bernardi, 2007; Lisker et al., 2007; Chen et al., 2010): the SDSS pipeline overestimates the sky foreground around bright extended sources. In order to remove scattered light (Stoughton et al., 2002) the pipeline measures the median sky value in a box of $100'' \times 100''$ shifted in steps of $50''$ across the image, and then subtracts the bi-linear interpolation of that sky. Extended objects bias these medians towards too large values. As a result of the overestimated sky, the measured radii and brightnesses are too small (Fig. 5.1). For galaxies with a large angular size this can be quite severe: a half-light radius of about $30''$ is on average underestimated by a factor of 2.5, and the total brightness of the same galaxy is underestimated by 0.75 mag. The effect is less strong for the typical angular sizes of dwarf galaxies at a distance of the Virgo cluster. However, it is not negligible and it is essential to be considered for comparing galaxies of different sizes and brightnesses in a consistent way.

Therefore, we performed the photometry on the images only after a proper sky subtraction was made (Lisker et al., 2007). The sky subtraction and removal of scattered light were done in a similar manner as in the SDSS pipeline. However, all sources were masked before calculating the medians. The masks were created after coadding the images in the g, r, and i-bands, in order to improve the S/N, and to mask also areas with low surface brightnesses. Furthermore, a smaller box and smaller offsets, as compared to the SDSS pipeline, were used for the interpolation of the scattered light.

The SDSS collaboration acknowledged the problem and estimated it quantitatively. They added 1300 artificial galaxies at random positions to SDSS images. The galaxy brightnesses and radii were motivated by observed galaxies. The pipeline measurements of the artificial galaxy brightnesses were compared to the true values. In Fig. 5.1 their findings are compared to the differences between the SDSS pipeline and our measurements. Here we consider only galaxies that appear as one single *photoObj* in the catalog. The trends are consistent with our photometry recovering the galaxies' true brightnesses and radii.

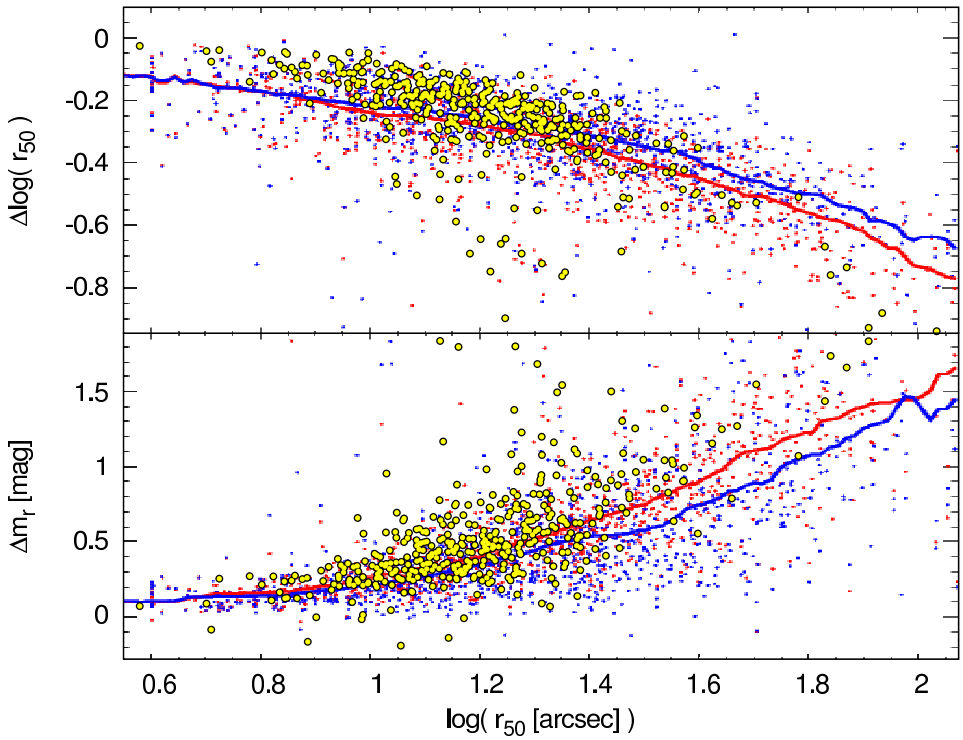

FIGURE 5.1: The *yellow points* show a comparison of the photometry of Virgo cluster early types (Janz & Lisker, 2008) with the SDSS DR5 pipeline values, for the half-light radii *(upper panel)* and the total magnitudes *(lower panel)*. *Red* and *blue points* show comparisons of the true and SDSS pipeline values for artificial galaxies added to SDSS images, for the old pipeline used in DR5 and after the pipeline update in DR8 (SDSS collaboration). The lines indicate the mean relations. The graph of the SDSS collaboration is taken from `http://www.sdss3.org/dr9/imaging/caveats.php`.

Second order deviations are caused by the different methods of the photometric measurements (profile fitting in the SDSS pipeline; our method see next chapter) and possibly also a different sampling of profile shapes of the artificial galaxies and the observed galaxies in the Virgo cluster. Furthermore, our photometry is consistent with the photometry of Chen et al. (2010). Their study used also SDSS data with their own independent sky foreground subtraction and photometry.

The SDSS zeropoints in the u and z band are slightly shifted in comparison to the AB system (Oke & Gunn 1983, see http://www.sdss.org/dr5/algorithms/fluxcal.html). Our SDSS magnitudes take this offset into account. Finally, they are corrected for Galactic extinction according to Schlegel et al. (1998).

Part IV

METHODS

6

PHOTOMETRY AND RADIAL PROFILES

In all the following we describe how the photometric and other characteristic parameters of the galaxies such as the boxiness are determined. In all these analyses fore- and background sources are masked. The masks are mostly created with the help of SExtractor, commonly after subtraction of a galaxy model in order to reliably identify also sources that are blended with the galaxy of interest. The masks are all checked visually and modified if needed. The galaxy centers are determined mostly in two ways: with *IRAF*/`imcntr` and using an iterative approach with asymmetry centering (e.g. Papers I, II): the point of the highest symmetry in the image is found by minimizing the asymmetry, which is calculated as (Conselice et al., 2000)

$$A = \frac{\sum_i |f_i - f_{i,180}|}{\sum_i |f_i|},$$

where f_i is the flux of the ith pixel, and $f_{i,180}$ is the flux of the pixel in the image rotated by 180°. The asymmetry is calculated for the initial guess for the galaxy center, and then for the center shifted by one step-size to each of the eight directions that are parallel or diagonal to the axes. The point with the lowest asymmetry is then taken as the starting point for the next iteration. This process is repeated until a minimum is found. To avoid local minima we apply this algorithm twice with different step-sizes of 1 pixel and 0.3 pixels. The point of highest symmetry is then considered to be the center of the galaxy. The centers determined by either of the two methods are typically closer than 1 pixel to a visual estimate.

6.1 NON-PARAMETRIC PHOTOMETRY

Galaxy brightness and size

In order to characterize a galaxy we measure such parameters as its brightness and size. We want to determine the values in a model-independent way. Furthermore, the method should be consistent for galaxies spanning many magnitudes in brightness, from the brightest elliptical to the faintest early-type dwarf galaxy in the Virgo cluster catalog. Due to the galaxies smoothly fading into the background, even the simple question of "how

bright is a galaxy" is non-trivial. A popular way of measuring galaxy brightnesses is to use the Petrosian radius (Petrosian, 1976). At the Petrosian radius the intensity reaches a level of a fifth of the mean intensity inside that radius,

$$\frac{I(r_P)}{< I >_{r_P}} = 0.2\,. \tag{6.1}$$

The Petrosian magnitude is then given by the flux contained within two Petrosian radii, $2r_P$. This definition is at least to first order independent of the brightness and contains the bulk of light also for faint galaxies, unlike for example magnitude in apertures at a specific surface brightness.

Instead of circular apertures we use elliptical apertures (see, e.g. Lotz et al. 2004). The masked pixels are replaced with the median value inside an elliptical annulus. The axis ratio and the position angle are initially determined by the image moments (Abraham et al., 1994) in a circular aperture, and using *IRAF*/`ellipse` at $2r_e$ in the subsequent iterations. Once the aperture for the brightness measurement and the contained flux is determined, the half-light radius (or semi-major axis, SMA) is given as the radius that contains half of the light of the galaxy. Likewise, radii containing a different fraction of the light can be obtained, i.e. the radii containing 20%, 80%, 90% of the light, denoted by r_{20}, r_{80}, r_{90}, respectively.

However, some of the galaxy's light falls outside the $2r_P$ aperture used for the brightness measurement. The amount of the missed flux depends on the profile shape of the galaxy (Strauss et al., 2002, §3.2). For a galaxy with a de Vaucouleurs profile the difference between the Petrosian and total magnitude is larger than for a galaxy with an exponential profile. Since bright early-type galaxies have steeper profiles than faint ones, this difference makes the measurement inconsistent. Graham et al. (2005) quantified the missed flux under the assumption of a Sérsic profile and provided a formula to recover both the size and brightness of a galaxy using r_{50} and r_{90}:

$$\Delta m \approx P_1 \exp\left[(r_{90}/r_{50})^{P_2}\right], \tag{6.2}$$

where $P_1 = 5.1^{-4}$ and $P_2 = 1.451$. For the radius the correction is given by

$$r_e \approx \frac{r_{50}}{1 - P_3 (r_{50}/r_{90})^{P_4}}, \tag{6.3}$$

with $P_3 = 8.0^{-6}$ and $P_4 = 8.47$. Typical values for the correction are $\Delta m = 0.01$ and $\Delta m = 0.20$, and $r_{50}/r_e = 0.99$ and $r_{50}/r_e = 0.73$, for an exponential or a de Vaucouleurs profiles, respectively.

The corrections according to Graham et al. (2005) implicitly assume a Sérsic profile, although for their calculation only the radii containing 50% and 90% of the light are needed. In Papers V & VI we find that many galaxies are better represented by more complex profiles, e.g. a superposition of two exponentials, instead of a single Sérsic func-

tion. We numerically calculate the error introduced if the concentration and the specific combination of r_{50} and r_{90} is not caused by the assumed Sérsic profile, but rather by a superposition of two exponential profiles (Fig. 6.1).

Another popular method for estimating galaxy brightnesses is the so-called *curve of growth*. It is also non-parametric and achieves to measure a galaxy's total magnitude. Our method was shown to be consistent with that method (see Chen et al. 2010 for early types in Virgo using SDSS data).

Galaxy concentration

Furthermore, we want to quantify the galaxies' light concentrations in a model-independent way. We follow Conselice (2003) and measure the concentration within 1.5 Petrosian SMA as $C = 5 \log r_{80}/r_{20}$ (Bershady et al., 2000), with the radii containing 20% and 80% of the light of a galaxy.

6.2 ELLIPSE FITTING

So far, we have considered only single values characterizing the galaxies. In many cases it is insightful to study also the radial profiles of different parameters. We run *IRAF*/`ellipse` (Jedrzejewski, 1987) to measure light profiles, profiles of ellipticity and position angle, as well as profiles of the parameters for non-elliptical isophotal shape (see below). Depending on the purpose, we choose the step size and whether or not to fix the center of the galaxy, the position angle, or the ellipticity.

For obtaining colors

Colors are defined as the difference of brightness in magnitudes in two different filter bands, i.e. they are related to the relative fluxes in those bands. We use fixed apertures to determine colors. In that way problems with determining total magnitudes in different filter bands with varying image qualities can be avoided. Furthermore, the masks can be used without special corrections as long as the same masks are used for the different wavelengths. *IRAF*/`ellipse` calculates the flux contained within an isophote, which we use to measure colors. This is in particular convenient for SDSS data: since the observations in the different filter bands are taken nearly at the same time, the FWHM of the PSF is nearly the same. Moreover, the images in the different bands are readily aligned. Also, profiles of the color can be obtained with *IRAF*/`ellipse`.

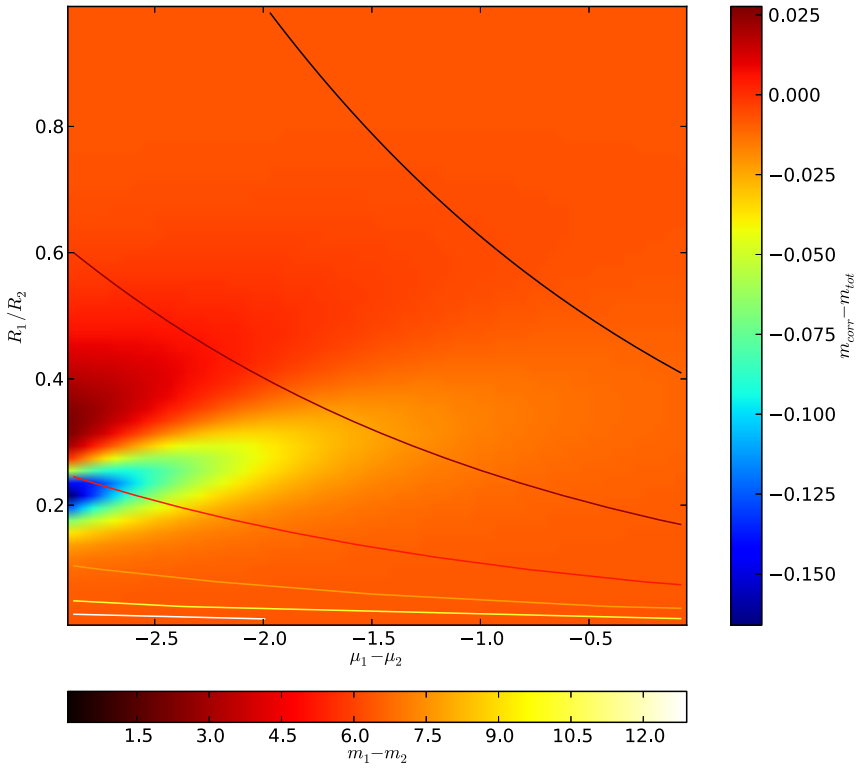

FIGURE 6.1: The colors display the error introduced by the corrections for the missed flux outside the Petrosian aperture if the galaxy's light profile does not follow a Sérsic function, but a superposition of two exponentials *(right color bar)*. The offset is calculated as a function of the ratio of sizes and the flux ratio at r_e of the two exponential profiles. The lines indicate constant ratios of the two components' brightness *(bottom color bar)*.

For obtaining isophotal shapes

The galaxy isophotes are not necessarily elliptical. Deviations from an elliptical shape can be parametrized by a Fourier series. An ellipse, generalized this way, can be described in a parametric form as:

$$\begin{aligned} f_x(\phi) &= a\cos\phi + b\sin\phi + \cos\phi \sum_n c_n \cos n\phi + s_n \sin n\phi \\ f_y(\phi) &= -a\cos\phi + b\sin\phi + \sin\phi \sum_n c_n \cos n\phi + s_n \sin n\phi\,, \end{aligned} \tag{6.4}$$

where a and b are the semi-major and minor axis lengths (here for simplicity aligned with the axes), the angle ϕ is the position angle with respect to the x-axis, and c_n and s_n are the coefficients of the Fourier series. *IRAF*/`ellipse` rather fits an ellipse to the isophote and determines then the intensity variations along the ellipse:[1]

$$I(\theta) = I_0 + \sum_{n=1}^{\infty} (C_n \cos n\theta + S_n \sin n\theta)\,. \tag{6.5}$$

The first parametrization (eq. 6.4) quantifies the distance of the isophote to the ellipse and the second one (eq. 6.5) measures the variations in the flux along an ellipse. The coefficients can be converted by division with the gradient dI/dr of the light profile (Fig. 6.2):

$$c_n = C_n/(dI/dr)\,, \qquad s_n = S_n/(dI/dr)\,. \tag{6.6}$$

IRAF/`ellipse` actually uses these transformations. The coefficients are then normalized with the length of the SMA, in order to quantify the distance of the isophote to the ellipse, relative to its size. The first terms of the Fourier series represent egg-shaped distortions. The terms with $n = 2$ are a different way of describing the flattening of an ellipse. The terms with $n = 3$ are variations with a period of 120°. Such distortions are usually not observed in galaxies. The interesting terms are those having $n = 4$, illustrated in Fig. 6.2: the coefficient c_4 is known as the boxiness, i.e. the parameter describing how boxy ($c_4 < 0$) or disky ($c_4 > 0$) an isophote is. The sine coefficient of the same order describes deviations that correspond to warped distortions. For pure boxy or disky shapes the sine coefficient is irrelevant and should remain close to $s_4 \approx 0$. Otherwise the isophote has a more complex deviation from an elliptical shape, in which case the reason for the non-ellipticity is less clear.

In studies of the boxiness, typically one single value of c_4 is assigned to a galaxy. Traditionally an average or maximum value is used. This is not necessarily the optimal way for the early-type dwarf galaxies. The profiles of the c_4 and s_4 can be noisy, and

1 *IRAF*/`ellipse` uses a notation with A_n and B_n for the coefficients of the sine and cosine terms, respectively, while in the literature A_4 (or a_4 in eq. 6.6) is often used for the coefficient of the fourth order cosine term.

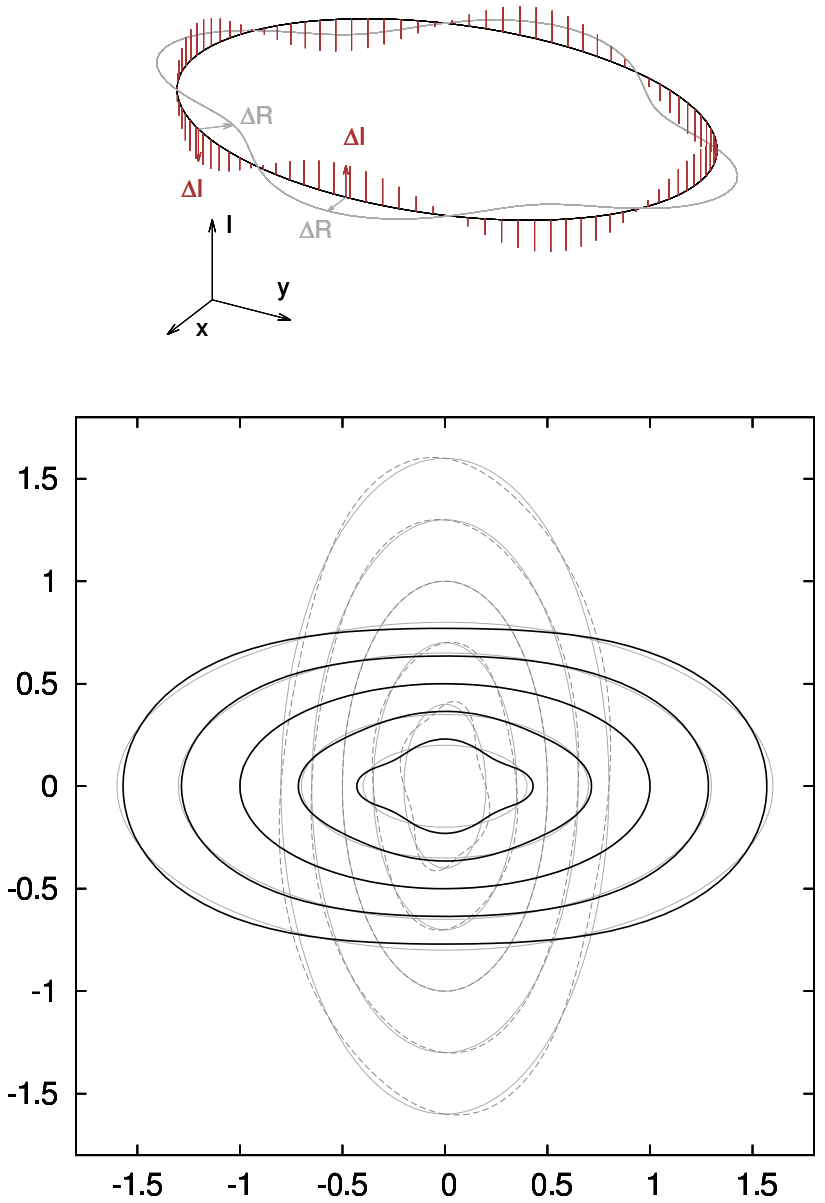

FIGURE 6.2: Illustration of boxi- and diskiness. The *top panel* shows an ellipse *(black)* in the xy-plane, the corresponding disky isophote *(gray)*, and the brightness variations along the ellipse perpendicular to the plane of the ellipse *(red)*. The *bottom panel* illustrates isophotes with different c_4, from inside out $0.2, 0.1, 0, -0.1, -0.2$ *(black lines)*. The gray solid lines show the corresponding ellipses for comparison. The ellipses rotated by 90° and the dashed gray lines display the deviations with the same values for s_4 instead of c_4.

there can be subsections with a positive and negative c_4 values, i.e. disky and boxy parts, in the same galaxy. Therefore, we adopt an additional measure: we search in the profiles for regions with significant deviations and assign all of these subsections in the profiles of each galaxy values. This way each galaxy can also have multiple or not any values at all. The features in the profiles are quantified by numerical integration of the boxiness over the region with the same sign.

6.3 THE SPECIAL CASE OF BLUE COMPACT DWARFS

Blue Compact Dwarf galaxies (BCDs) are characterized by their blue color and compactness. They host possibly several star forming regions that make their appearances patchy, much less regular than the other galaxies studied in this thesis. The lack of a well-defined center and axial symmetry makes it difficult to measure a meaningful profile. We use the procedure described by Papaderos et al. (2002) and calculate the photometric radius corresponding to an intensity as

$$R^* = \left(\frac{A_I + A_{I-\Delta I}}{2\pi}\right)^{1/2}, \tag{6.7}$$

with the areas A_I and $A_{I-\Delta I}$ where the intensity is higher than I and $I - \Delta I$, respectively.

While most of the light in BCDs is emitted by massive stars in the star forming regions, most of the mass is located in the underlying Low surface Brightness (LSB) component with old stars. In order to measure the contribution of the LSB component, we fit an exponential function to the outer part of the light profile, where the LSB component is dominant. The transition radius between the regions dominated by the old and young stellar populations is inferred from a break in the color profile.

7

MULTICOMPONENT DECOMPOSITIONS

7.1 TWO-DIMENSIONAL LIGHT DISTRIBUTIONS VERSUS LIGHT PROFILES

Studies of the morphology of bright galaxies often fit model functions to the light distributions of the different structure components such as bulges and disks. Several authors have shown that this is best done two-dimensionally (Byun & Freeman, 1995; de Jong et al., 2004; Laurikainen et al., 2005; Noordermeer & van der Hulst, 2007). Non-axisymmetric components like bars can be hidden in azimuthally averaged profiles, while they are clearly detectable using the full information of the two-dimensional light distributions. Even axisymmetric structures are easier to separate that way, since in addition to the light profiles also the position angles and flattenings are considered. The two-dimensional fitting technique has not been widely used for dwarfs, so far.

However, the light profiles have been used to search for characteristic profile types and multiple components. For example, Binggeli & Cameron (1991) grouped the profiles of the early-type dwarf galaxies in the Virgo cluster to five different types. The types were defined by the existence of a nucleus, whether or not the profiles show breaks, and whether or not the sections of the profiles are exponential. Binggeli & Cameron found that also many dwarfs without previous indications of being disk galaxies (dEs as opposed to dS0s) can have complex profiles. This result was largely forgotten, when the Sérsic function started to be routinely fitted to the surface brightness profiles of the early-type galaxies.

Aguerri et al. (2005) classified dwarf galaxies in the Coma cluster as dEs, if the light profiles follow a Sérsic function, and dS0s, if the largest deviation from the best-fitting Sérsic function at any radius is larger than 0.15 mag/arcsec^2. Fig. 7.1 illustrates the problem of decompositions using the azimuthally-averaged profiles. The residual profile after subtraction of a Sérsic model shows limited structure and stays at all radii within Aguerri et al.'s goodness limit. The bar is revealed, when the residual profiles are calculated in sectors at different position angles separately. Along the bar there is an excess of light, while perpendicular to it the observation is fainter than the model.

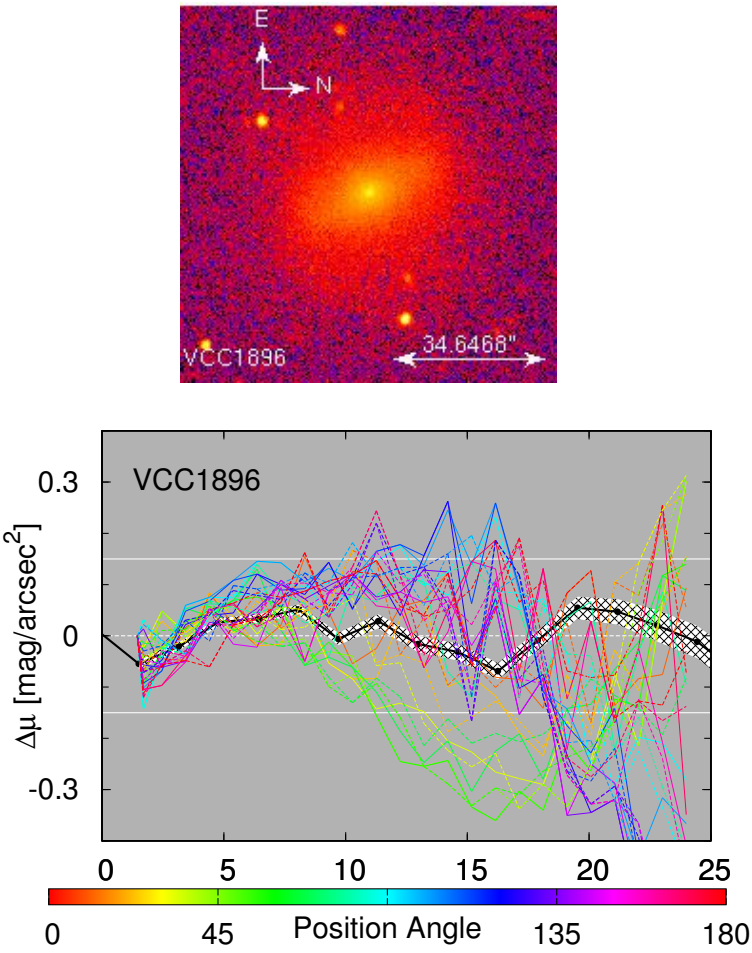

FIGURE 7.1: *Upper panel:* Image of VCC1896 in the H-band (VCC classification: dSB012;N; dE(di) in Lisker et al. 2006b). *Lower panel:* residual profile after subtraction of a Sérsic + nucleus model, the corresponding SMAs on the x-axis are given in arcseconds. The azimuthally averaged profile is shown with the black line together with the surface brightness uncertainties given by *IRAF*/`ellipse`. The colored lines display the residual profiles in sectors at different angles to the semi-major axis. The angle can be read from the color bar, for the solid and dashed lines the angle differs by 180°. When the bar is fitted, the residual profiles in the different sectors flatten.

7.2 MODEL FITTING

We use GALFIT 3.0 (Peng et al., 2010) to decompose the early-type dwarf galaxies into multiple components taking advantage of the full two-dimensional information of the image. GALFIT fits the two-dimensional models by minimizing the $\chi^2 = \sum_i (O_i - M_i)/\sigma_i^2$, where the sum runs over all (unmasked) pixels, O and M are the observed and model fluxes, respectively, and σ_i^2 is the pixel-wise variance. The latter is determined as the variances of each pixel in the many individual exposures that were taken for each galaxy.

The decompositions should answer the following question: does the galaxy have several structural components or can the surface brightness distribution be fitted by a single Sérsic function with a constant position angle and ellipticity of the isophotes. Here, we consider the presence of a nucleus as a separate question. We add a central point source for all galaxies that show an unresolved excess of light in the center, but do not consider it as additional complexity of the profile.[1] We fit two kind of models to the galaxies: a simple model with one component, and a complex model with an inner and outer component. The functions used for these components are summarized in Table 7.1, together with the functions of components that were added later (see below). The simple and two-component models are then visually[2] compared with each other using GALFIDL[3], a set of IDL procedures to illustrate the fitting results.

In Figs. 7.2 and 7.3 two example galaxies are shown, VCC2019 and VCC0490. The Figures show the galaxy image, the residuals after subtracting a simple and the final model (which is the same in the first case), and the profiles of the two-dimensional light distributions for the images and models. By two-dimensional we mean that the surface brightnesses of all pixels are shown as a function of their angular distance to the galaxy center. These representations contain the information of the two-dimensional light distribution, but they display a profile instead of an image: the spread of pixel values for a given radius corresponds to the apparent flattening of the observed galaxy, the model, or a component. The first example also illustrates that a galaxy with a nucleus can still be considered to be a one-component galaxy. Furthermore, both galaxies have spiral arms.[4] The examples illustrate that it is possible to find both simple and complex structures apart of the spiral arms, with the profile shape determining which model is better. VCC2019 has an exponential profile and including further components will not fit the spiral arms any better. In the profile of VCC0490 two distinct extended components are visible.

1 The nucleus needs to be added, if present, in order to obtain good fits of the inner component in particular.

2 In Paper VI we demonstrate that with numerical quantifications of the model quality similar conclusions can be reached.

3 H. Salo, http://cc.oulu.fi/~hsalo/galfidl.html.

4 While GALFIT in principle provides a possibility to fit spiral arms with coordinate rotations, this option was not used.

TABLE 7.1: Functions and components

Sérsic function	$I(r) = I_0 \exp\left[-\left(\frac{r}{h}\right)^{1/n}\right]$	One-component, inner component, 'truncated' outer component
Exponential function	$I(r) = I_0 \exp\left(-\frac{r}{h}\right)$	Outer component
Delta function	$I(r) = I_0\, \delta(r)$	Central point source
Ferrers function	$I(r) = I_0 \left(1 - (r/r_{out})^{2-\beta}\right)^{\alpha}$	Lens, bar

NOTE. — The parameters are: the central intensity I_0; the scale length h, which is related to the half-light radius via $r_e = b^n h$ with $b = 1.9992n - 0.3271$ (Capaccioli, 1989); the Sérsic index n, which corresponds to the profile shape; and the truncation radius r_{out}, the central slope β, and the sharpness of the truncation α. All components except the point sources have two additional parameters: the position angle and axis ratio. For the outer components these are fixed to the values of the outer isophotes. The model is convolved with the seeing during the fitting.

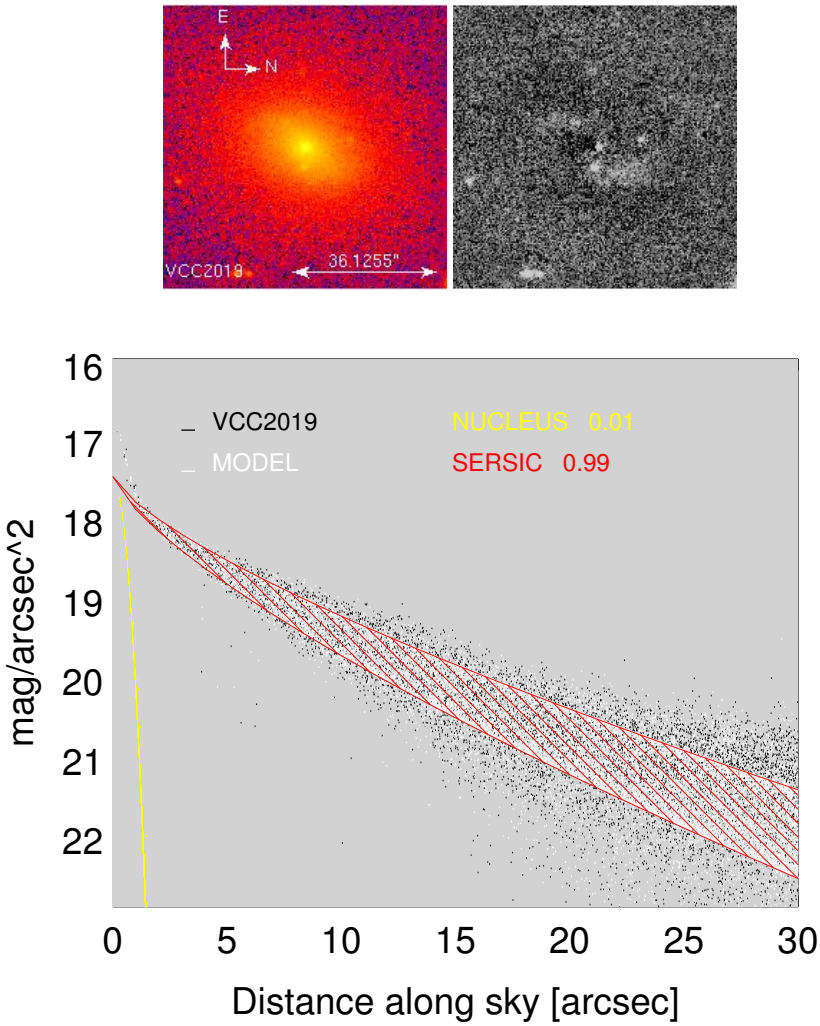

FIGURE 7.2: *Upper panel:* Image of VCC2019 and the residual after subtraction of the model. In the VCC the galaxy is classified as dE4;N; Lisker et al. (2006b) find possible disk features. *Lower panel:* Two-dimensional profile displaying all pixels. The colors indicate different components. The fraction of the light in each component is given after the label. The total model *(white)* is plotted twice: without noise and including the noise of the observed image *(black)*. The noiseless model shows a spread due to the apparent flattening of the light distribution. It is visible as an area filled with white points. Since this galaxy has a nucleus and one component, which dominates the model for all larger radii, the model is overlaid by the display of the extended component *(red)*. Only at the pixels in the inner $2''$ the model departs from the extended component. The model including the noise has a broader distribution at larger radii, due to an approximately constant noise, displayed on the logarithmic magnitude scale. These white points of the model including the noise spread around the black points of the observed pixels.

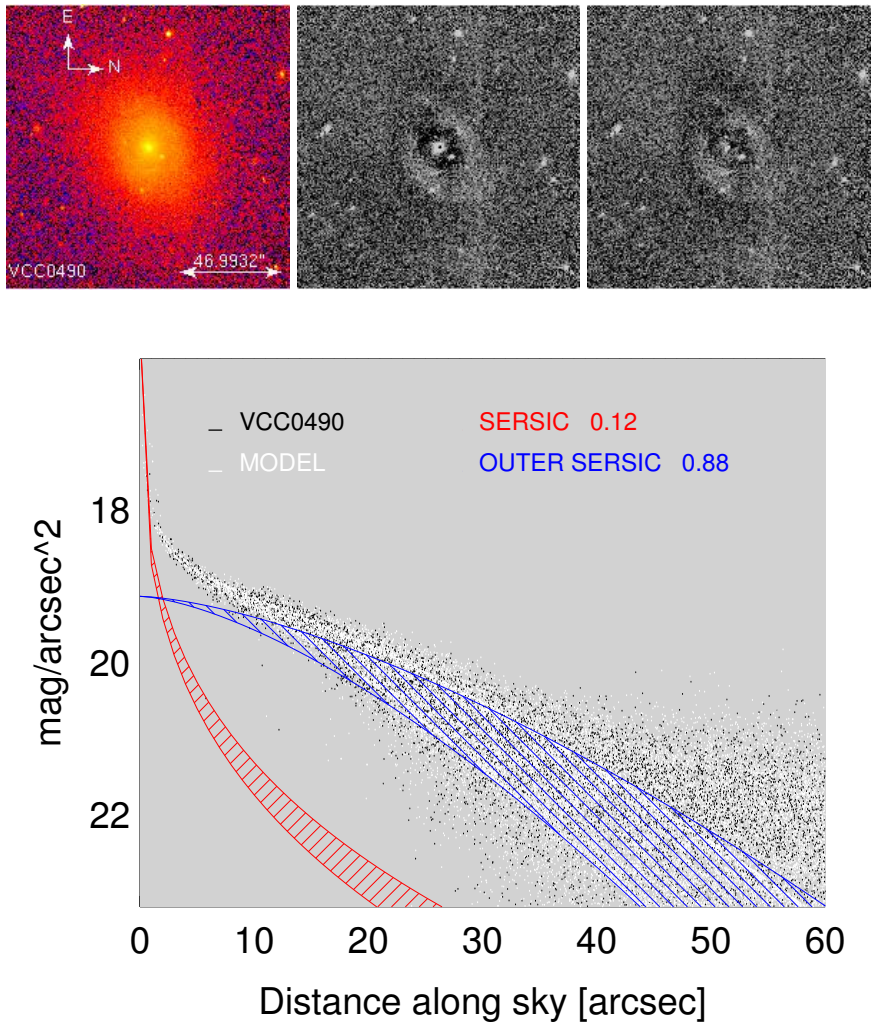

FIGURE 7.3: *Upper panel:* Image of VCC0490 and the residuals after subtraction of a simple and the final model. In the VCC the galaxy is classified as dS03;N; dE(di) in Lisker et al. (2006b). *Lower panel:* Two-dimensional profile displaying all pixels. The colors indicate different components. The fraction of the light in each component is given after the label. The total model *(white)* is plotted twice: without noise and including the noise of the observed image *(black)*. The noiseless model shows a spread due to the apparent flattening of the light distribution. It is visible as an area filled with white points. At radii larger than $\sim$ 15″ it is overlaid by the display of the outer component *(blue)*. The model including the noise has a broader distribution at larger radii, due to an approximately constant noise, displayed on the logarithmic magnitude scale. These white points of the model including the noise spread around the black points of the observed pixels.

7.3 BARS AND LENSES

In the evaluation we take into account possible large scale variations of the background, which are determined by the scatter of the median sky values in small boxes distributed over the image. In some cases both of the aforementioned models still significantly deviate from the observation. In those cases we try first the following changes to the models: we vary the starting values; in a few cases, we allow for the outer component to have Sérsic index $n < 1$ (instead of an exponential); or we use different centers for the different structure components. However, about 30% of the galaxies are really more complex. For example, in some galaxies bars are identified. Bars have a characteristic profile shape with a rather flat central part and a steep truncation beyond an outer radius (Fig. 7.4). In about as many galaxies we find components that have similar profiles, but which are fairly round (*lenses*, Fig. 7.5).

One complete set of models is shown in Fig. 7.6 for VCC0940. Again, the information contained in the two-dimensional profile should be emphasized: the excess of light in the profile due to the bar is not very prominent, since the bar is faint. In the azimuthally averaged profiles it is almost invisible. However, in the two-dimensional profile at about 10-20″, the bar clearly thickens the pixel distribution.

5 VCC1614 is one example for the E and S0 galaxies at the same brightness, which were included in the sample

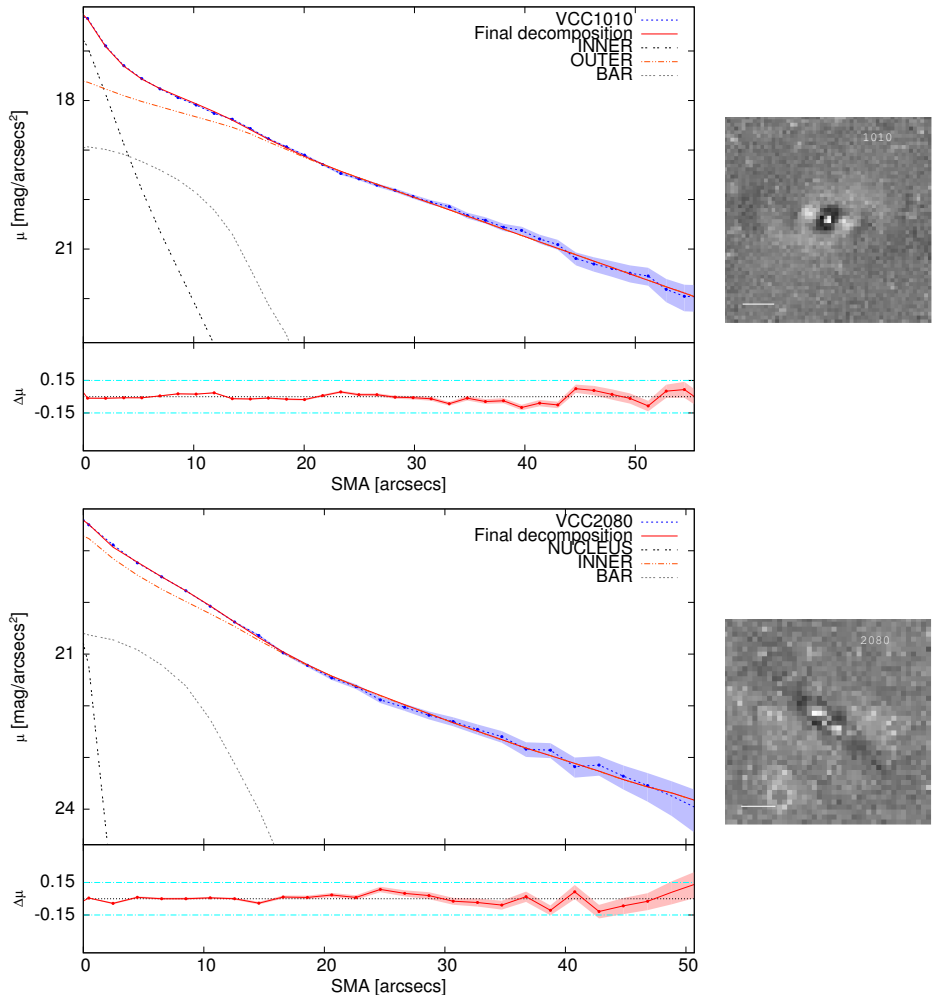

FIGURE 7.4: Profiles of barred galaxies. The *upper panels* show a clear example, VCC1010 – classified as dS0$_{5}$;N in the VCC; dE(di) in Lisker et al. (2006b) –, and the *lower panels* a weaker bar in VCC2080, classified as dE6pec: in the VCC; Lisker et al. (2006b) find possible disk features. The shaded areas correspond to the photometric uncertainty in the residual profiles and the possible influence of large scale background variations in the profiles. The white bars in the residual images correspond to 20″.

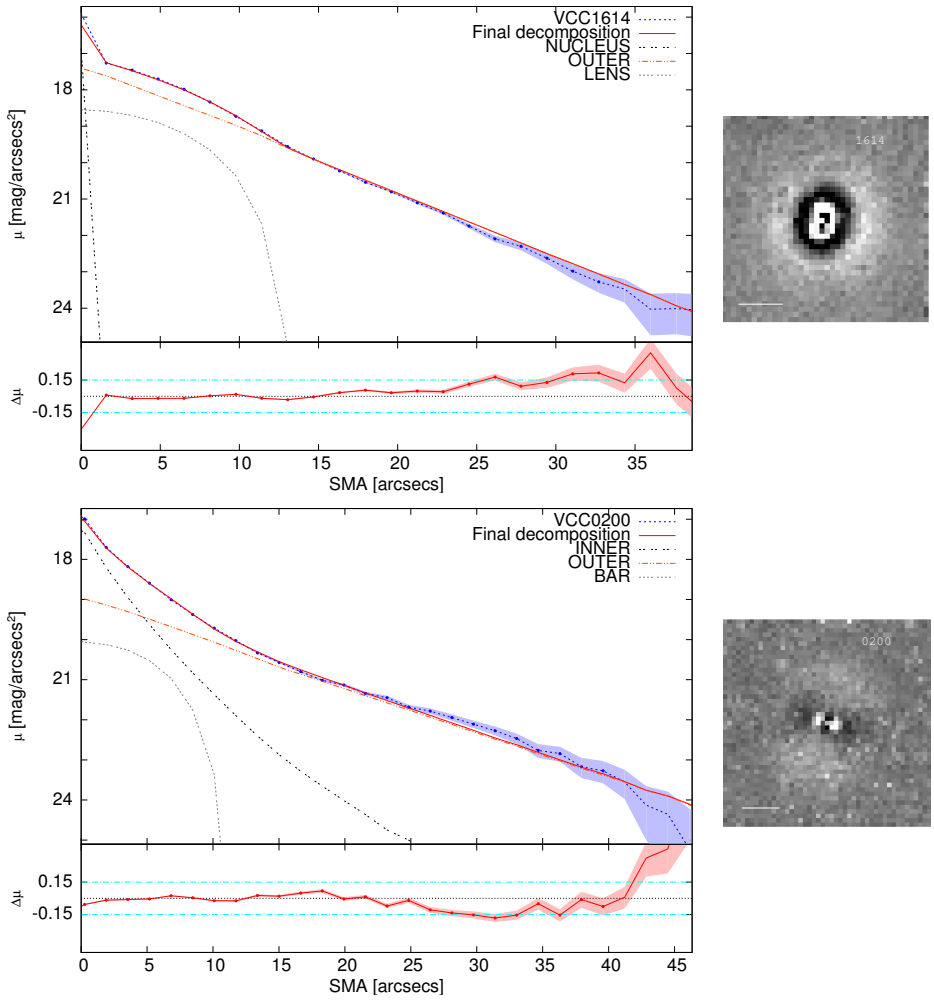

FIGURE 7.5: Profiles of galaxies with lenses. The *upper panels* show a clear example, VCC1614 (classified as $S0_3(2)$ in the VCC[5]), and the *lower panels* a weaker lens in VCC0200, classified as dE2;N in the VCC. The shaded areas correspond to the photometric uncertainty in the residual profiles and the possible influence of large scale background variations in the profiles. The white bars in the residual images correspond to 20″.

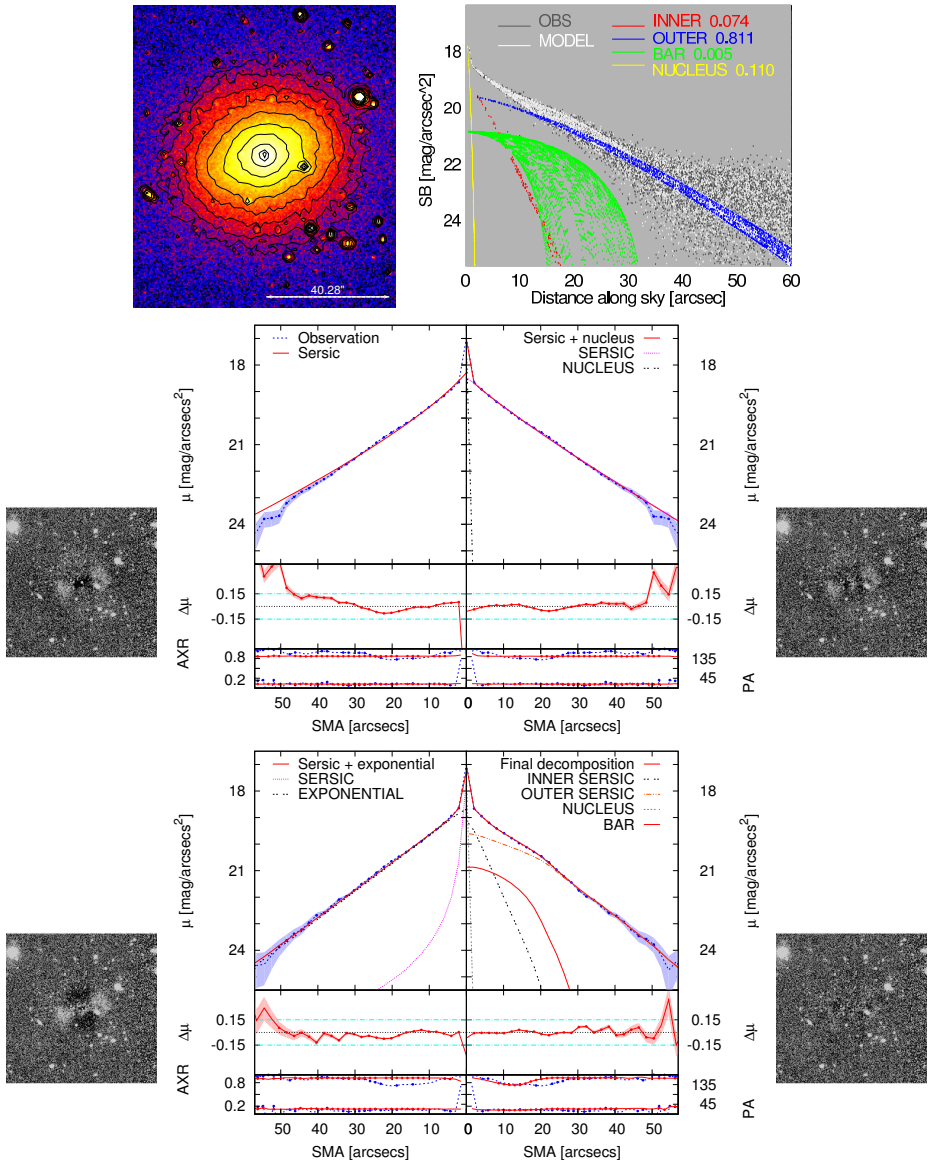

FIGURE 7.6: Illustration of the information used in the fitting procedure. The *top panels* show the image of the galaxy, VCC0940 (classified as dE1,N in the VCC), and the two-dimensional profile of the final model. The simple models (without and with nucleus) are shown in the *middle*. The *bottom row* displays the two-component model and the final model with a bar. The profiles in each panel from top to bottom show the profile, the residual profile, and the profiles of axis ratio (AXR) and position angle (PA). The residual images display $\pm 3\sigma$. The width and height of the residual images are $\sim 30''$. The error regions in the profiles and residual profiles illustrate the estimate of large scale variations and the surface brightness uncertainties given by *IRAF*/`ellipse`, respectively.

8

INFORMATION FROM SPECTROSCOPY

Absorption lines in the spectra of galaxies are used to infer ages, metallicities, and stellar kinematics. The used lines are caused by various elements in the stellar atmospheres. The spectrum of a galaxy is composed of the spectra of millions of individual stars. It can be used to determine characteristics of the stellar population as a whole. Some of the absorption lines trace the heavy elements and provide information about the stellar metallicity, while others trace the age of the stellar population. Furthermore, the position of the lines and partly their widths are determined by the Doppler shifts due to movements of the stars and the galaxy relative to us. This information can be used to measure the velocity of the galaxy relative to us, galaxy rotation, as well as random motions of the stars inside the galaxy.

8.1 CaII TRIPLET – KINEMATICS

For the kinematics the Mgb and CaII triplets are often used, since they occur only in absorption. In a follow-up study of Paper III we target the CaII triplet for a small sample of early-type dwarf galaxies. The rotation velocity and random motions are extracted from the reduced spectra using the penalized pixel-fitting code pPXF (Cappellari & Emsellem, 2004). *Penalized* means that the line of sight velocity distribution is fitted with a Gauss-Hermite series. However, the more complicated the fitting function becomes, the higher penalty is added to the χ^2, so that a simple Gaussian is preferred in case there are no significant deviations. Simultaneously, the template for the spectrum is fitted using a library of stellar spectra. This minimizes errors introduced by a possible template mismatch. We use the stellar library for the CaII triplet region by Cenarro et al. (2001). Furthermore, the code applies an adaptive radial binning in order to achieve a target S/N. One example of the extracted data is shown for the rotating galaxy VCC1491 in Fig. 8.1.

8.2 LICK INDICES – STELLAR POPULATION CHARACTERISTICS

The strengths of many absorption lines are often quantified using the system of Lick indices (Worthey et al., 1994). This system defines, for each line, a passband for the feature and two passbands on either side of the feature, in order to define a pseudo-continuum.

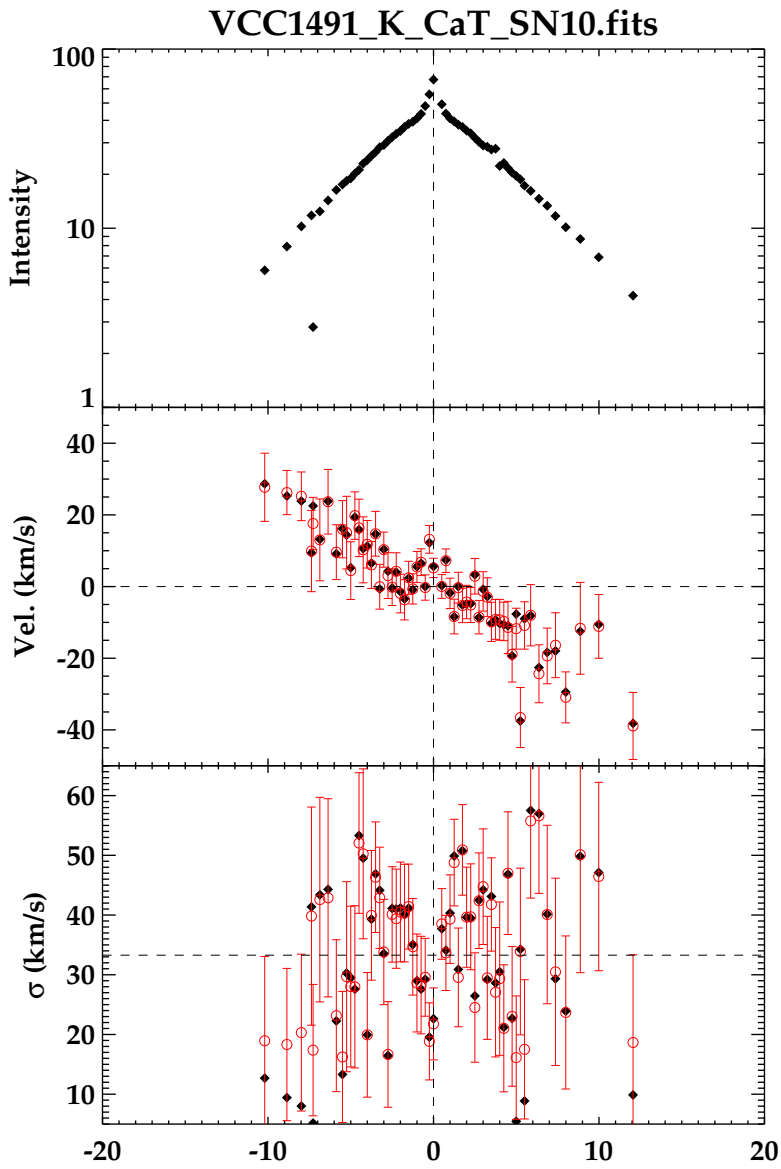

FIGURE 8.1: Kinematics from long-slit spectroscopy using pPXF (Cappellari & Emsellem, 2004). The panels show from top to bottom the intensity profile (in arbitrary units), the rotation velocity, and the velocity dispersion (measured by J. Falcón-Barroso). The radius is given in arcseconds. The black points show the direct measurements with pPXF, while the red points and error bars are obtained by running a Monte-Carlo simulation of the measurements using the error spectra. VCC1491 clearly rotates.

The average intensities and wavelengths of the spectrum in the pseudo-continuum passbands define a beginning and end of the baseline for the integration over the spectral line. The strength of the line is then quantified with the equivalent width of the feature. We use nine indices, three from the age-sensitive Balmer series ($H\delta_F$, $H\gamma_F$, $H\beta$; the Hydrogen lines only occur in hot massive stars that are short lived), the magnesium Mgb line index, and several iron line indices (Fe4383, Fe5015, Fe5270, Fe5335, Fe5406) in the same wavelength regime. The indices are measured with INDEXF (Cardiel, 2007). The program also estimates their uncertainties by running a Monte-Carlo simulation of the measurements using the error spectra and the uncertainties of the radial velocities.[1]

We are interested in the parameters of the nuclei, which are the dominant light sources in the centers of the galaxies. However, the galaxies contribute also to the light. This contribution we try to subtract in order to obtain a pure measurement of the nucleus. The galaxy spectrum is extracted on both sides of the galaxy in the interval from 3″ to 8″. The intensity is scaled with a factor obtained by a exponential fit to the light profile, in order to approximate the contribution of the galaxy light in the galaxy center (Paudel et al., 2011, Appendix A1). The obtained galaxy spectrum is then subtracted from the spectrum of the nucleus.

The index strengths are then compared to the single stellar population (SSP)-models of Thomas et al. (2003). These have the advantage that they consider the α-abundance as a parameter. We interpolate their model grid and perform a χ^2-minimization for the nine indices with ages, metallicities and α abundances as parameters (Proctor & Sansom, 2002). For illustration Fig. 8.2 shows a model grid and measured galaxies with metallicity and age-sensitive indices on the x and y-axes, respectively.

1 We do not correct for the velocity dispersions, since they are expected to be small ($\sigma_{gal} \leqslant 50$ km/s) compared to the spectral resolution ($\sigma_{instr} \sim 280$ km/s).

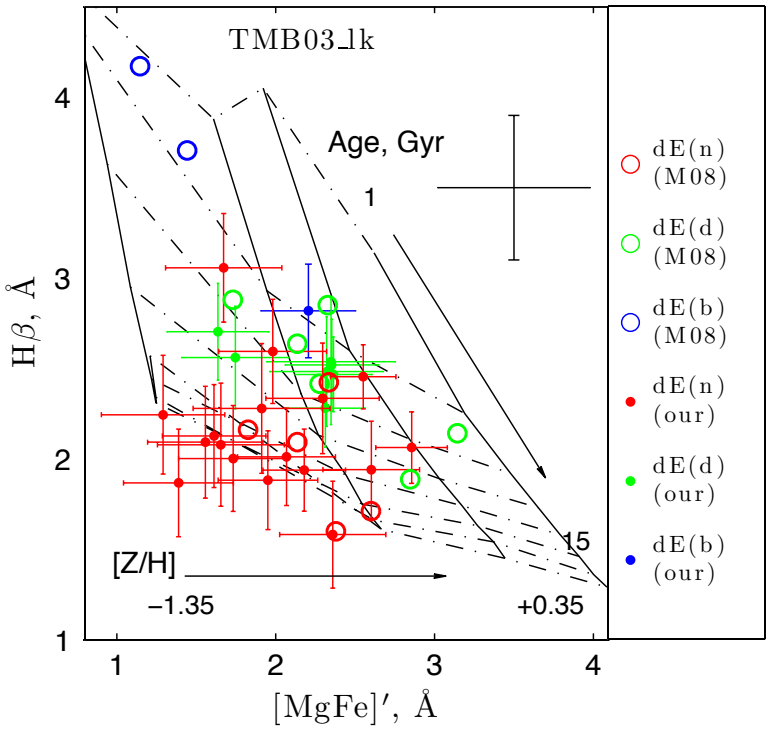

FIGURE 8.2: This figure illustrates, how SSP-equivalent ages and metallicities are related to absorption line indices. On the axes are the age and metallicity sensitive indices [MgFe]′ and Hβ, respectively. The [MgFe]′ index is defined as $[\mathrm{MgFe}]' = \sqrt{\mathrm{Mgb} \times (0.72 \times \mathrm{Fe5270} + 0.28 \times \mathrm{Fe5335})}$ and traces total metallicity unaffected of [α/Fe] (Thomas et al., 2003). The model grid shows different SSP models (with [α/Fe] = 0.0, Thomas et al. 2003), the *dashed* lines indicate constant ages (from 1 to 15 Gyrs in steps of 2 Gyrs), and the *solid* lines show the metallicities of the models ([Z/H] = −1.35, −0.33, 0, +0.35). The data points are early-type dwarf galaxies (*red* – nucleated dEs, *green* – dEs with disk signatures, and *blue* – dEs with blue cores, according to Lisker et al. 2006b,a, 2007). Figure taken from Paudel et al. (2010b). The *filled* points are measurements by Paudel et al., while the *open symbols* show values from Michielsen et al. (2008). For the latter the mean error is given by the black cross.

9

SIMULATIONS

It has been suggested that early-type dwarfs are former late-type galaxies that have been transformed by harassment (Moore et al., 1998; Mastropietro et al., 2005; Smith et al., 2010). In Papers V and VI we find that many early-type dwarfs have more than one structural component. Some of the parameters of the structural components are clearly offset from the extrapolated scaling relations of the bulges and disks in bright galaxies. We wanted to investigate how the components may be altered in fast galaxy encounters as in the harassment scenario. Our toy model consists of the initial model galaxy, the perturber, and their relative orbit, and the simulation is run with GADGET2 (Springel, 2005). It does not incorporate any gas or stellar physics. Also, the cluster potential was considered only in some final simulations.

9.1 INITIAL MODEL

The initial model (Fig. 9.1) is constructed to resemble a late-type galaxy using the self-consistent model of Kuijken & Dubinski (1995). The parameters of the bulge and disk components are motivated by the decompositions of this galaxy type in the literature (Laurikainen et al., 2011; Graham & Worley, 2008). Our model has a bulge-to-total mass ratio of $B/T = 0.01$ (here total means bulge plus disk: $T = B + D$) and halo to bulge and disk ratio of $H/(B + D) \approx 10$. The circular rotation curve is dominated by the disk up to one effective radius of the disk. The disk has an exponential profile with the scale length h, it is truncated at $5h$, and it has a scale height of $h_z = 0.1h$. The initial disk is rather cool, with a minimum Toomre parameter (Toomre, 1964) of $Q_{min} = 1.35$, and the Toomre parameter at two scale lengths of $Q_{2h} = 1.6$. The initial model has a ratio of the velocity dispersions perpendicular to the disk and in the radial direction of $\sigma_z/\sigma_r = 0.6$, close to value observed in the Milky Way and for other galaxies (Dehnen & Binney, 1998; Shapiro et al., 2003). The ratio of the velocity dispersions is assumed to be nearly constant with radius. The ratio of the scale height to the scale lengths, h_z/h, is rather small (de Grijs, 1998), but on the other hand Gerssen & Shapiro Griffin (2012) find σ_z/σ_r to be decreasing towards later Hubble types. The bulge effective radius is $0.17h$. We choose units such that $h = 1$ kpc and the maximum circular rotation velocity is $v_c = 100$ km/s (Fig. 9.1).

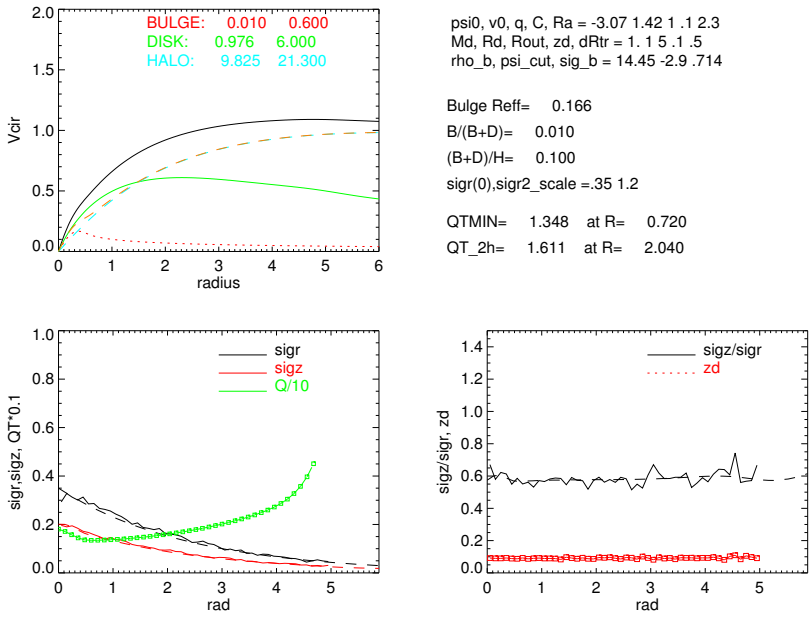

FIGURE 9.1: Model of initial late-type galaxy. The *upper left* panel displays the circular rotation curves of the model galaxy and the different components. The *lower left* panel shows the profiles of the Toomre parameter Q, and the radial and vertical velocity dispersions. The ratio of the latter two and the scale height are shown in the *right* panel. The numbers in the upper right give the parameters for the Kuijken & Dubinski model for reference. For the halo: psi0 – central potential; v0 – given by $v0 = \sqrt{2}\sigma_0$, with the central velocity dispersion σ_0, it corresponds roughly to the maximum circular velocity of the halo; q – flattening parameter; C – core smoothing parameter; Ra – scaling radius. For the disk: Md – mass of disk ignoring the cutoff; Rd – scale length; Rout – truncation radius; zd – scale height; dRtr – truncation width. For the bulge: rho_b – bulge central density; psi_cut – bulge cut-off potential; sig_b – bulge central potential.

TABLE 9.1: Simulation parameters

Component	Particle number	Mass	Softening
Bulge	5000	$2.3 \times 10^7 M_\odot$	0.05 kpc
Disk	100000	$2.3 \times 10^9 M_\odot$	0.05 kpc
Halo	145000	$2.3 \times 10^{10} M_\odot$	0.05 kpc
Perturber	100000	$4.7 \times 10^{11} M_\odot$	0.25 kpc

NOTE. — Basic parameters of the simulations.

9.2 ENCOUNTERS

The perturber is modeled with a King sphere (King, 1966), with a scale radius of 5h. The perturbation strength depends on the perturber's mass and even more on the encounter distance (Smith et al., 2010). We aim to model a case of substantial harassment. Therefore, we select encounter parameters with a large impact from the Smith et al. (2010). The perturber is chosen to be massive, which allows the encounter to be not very close. The perturber is 20 times more massive than the galaxy to be perturbed. The smallest distance between the two galaxies is ten exponential scale lengths of the disk, and the relative velocity is 1000 km/s, 10 times faster than the maximum circular rotation velocity. We model the encounter 12 times with different geometries of the orbit relative to the disk plane, evenly distributed over the relative alignments of the inclination and line of nodes. Although the encounters proceed at high relative velocities, the effect depends also on the orbital geometry, with the direct planar encounter being most efficient, while the retrograde planar encounter has the smallest effect.

The N-body simulations are carried out with GADGET2. First we run the model of the initial late-type galaxy for ~1 Gyr in isolation to allow for relaxation and to see that the model is stable. Subsequently, we place the model on an appropriate orbit relative to the perturber galaxy. We start the simulations about 300 Myrs before the closest approach and let it evolve after that for 1.2 Gyrs. The number of particles in each component of the initial model and the perturber, the masses and the used softening lengths are summarized in Table 9.1. In order not to introduce unphysical effects by simulation parameters as well as the resolution and softening, we re-ran selected simulations with higher particle numbers and different softenings. Furthermore, we did a check with a larger extent for the halo, as that is not well constrained by observations. All these changes did not lead to qualitatively different results.

9.3 EFFECT OF THE ENCOUNTERS ON THE PROFILES

During the encounter a bar forms (see also Mastropietro et al. 2005). The bar transfers angular momentum and moves stars inwards. The profile of the disk component steepens and the galaxy develops a higher concentration. Qualitatively this occurs in all geometries of the orbit, only the strength of the effect is modified. When the simulated galaxy is decomposed into photometric components, it would in many cases be modeled with two distinct components, and in some cases also with an additional bar. However, the two components, illustrated in the lower right panel of Fig. 9.2, form different parts of the disk. The bulge component is much less prominent than the disk and largely unchanged during the encounter. It would not be fitted as a separate component at all. The photometric decomposition does not coincide with the dynamical decomposition, since the transfer of stars from the disk to the dynamically hot bulge component is unlikely (see also Laurikainen & Salo 2001; Scannapieco et al. 2011). The bar formation is inhibited, if the disk is too hot. After the first encounter the galaxies are heated, which prevents a further steepening of the profile in subsequent encounters. Likewise, the effect almost completely disappears, if a hotter initial model is assumed, as seen in test with a disk scale height of $h_z = 0.2h$, instead of $h_z = 0.1h$, and a minimum stability parameter $Q = 2.5$.

9.4 SHORTCOMINGS OF THE MODELS

These simulations should be considered as a test case to study the evolution of the light profile of a late-type progenitor that is transformed into an early-type dwarf galaxy. They do neither include the cluster tidal field, nor do they contain any gas. If there is gas in the galaxy, the bar can efficiently transfer it to the galaxy center (Shlosman et al., 1989, 1990), so that the existence of gas is expected to enhance the effect of increasing the galaxy concentration. Also, ram pressure stripping of the gas by the hot intra-cluster gas could lead to a profile steepening: the gas in the center is retained longer and the star formation may be enhanced (e.g. Vollmer et al. 2001; Bekki & Couch 2003). The effect of the cluster tidal field was tested with modifications to GADGET2, so that it included an analytical cluster potential. Depending on the geometry of the encounter orbit within the cluster the cluster potential can help or hinder the mass loss of the halo. Therefore, a much more thorough study is needed to obtain statistics of a realistic distribution of encounters. However, the result that the inner parts of the profiles become steeper is qualitatively consistent with Mastropietro et al. (2005). Also, the parameter space of the initial model needs to be explored. Our chosen model becomes eventually bar unstable also in isolation, which subsequently leads to a small steepening of the profile. Furthermore, Smith et al. (2010) assume a K-band mass-to-light ratio of $M/L_K = 20$, constant for all galaxies throughout the cluster. In comparison to the SAM of Guo et al. (2011) the value is too high, especially in the cluster center. This makes the probability of encounters with this mass ratio small. They become more probable if larger encounter distances are used, or the mass of the galaxy to be perturbed is smaller. A perturbation with a smaller perturber mass or larger distance has less effect on the profile. It becomes larger for smaller relative velocities, i.e.

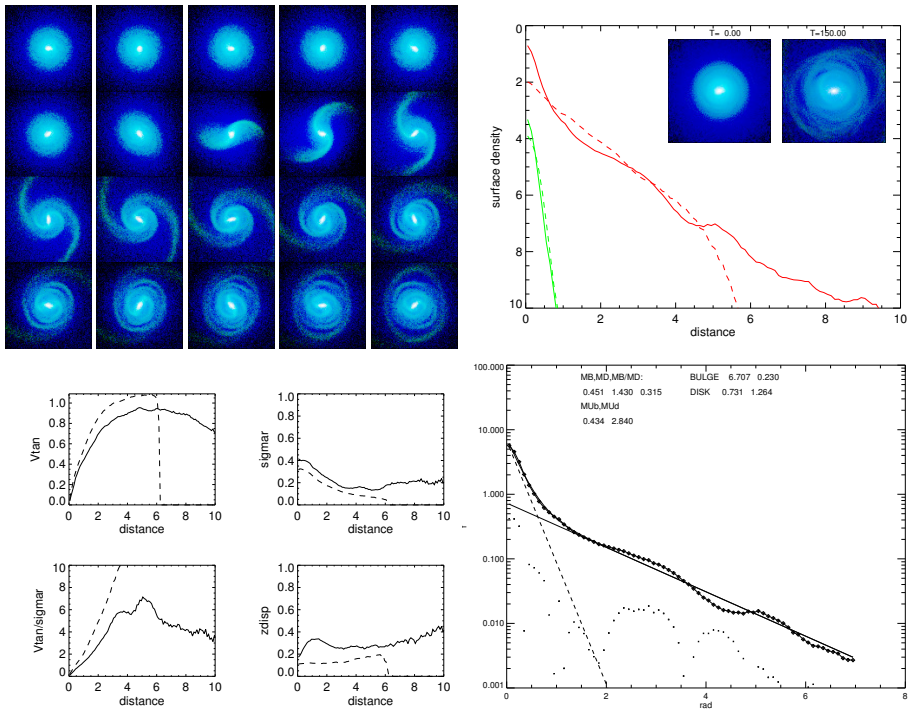

FIGURE 9.2: Illustrated is the direct planar encounter as an example. The *upper left* panel displays snapshots centered on the perturbed galaxies. The contributions of the bulge, disk, and halo are color-coded in *red, green, blue*. The *upper right and lower left* panels show profiles of different parameters for the initial *(dashed)* and final *solid* models. The *lower right* panel illustrates profile fits to the final model, illustrating that a two-component fit is found basically for the modified disk profile.

if the two galaxies fall together into the cluster. Again, a more thorough study would be needed to address all these effects. In spite of those shortcomings, our simulations demonstrate that the transformation process might indeed cause the distribution of stars inside the galaxy disk to be modified in such a manner that the light distributions could be fitted with multiple components.

Part V

RESULTS

RESULTS

In the following our main results are summarized and discussed in their historical context.

10.1 EARLY-TYPES VS. BRIGHT ELLIPTICAL GALAXIES

It is still a matter of debate whether the bright elliptical and early-type dwarf galaxies follow the same scaling relations, and whether these scaling relations can be interpreted as manifestations of different formative processes of the two galaxy types. In the past, early-type dwarfs and giant ellipticals were seen as different species based on their effective surface brightnesses (see classification scheme of Sandage & Binggeli 1984) and especially based on their surface brightness profiles. The dwarfs were believed to have exponential profiles, while the giant ellipticals were fitted with steeper de Vaucouleurs profiles (e.g. Wirth & Gallagher, 1984).

The conclusion of the different origins of dwarfs and giants was further supported by the photometric scaling relations. The mean effective surface brightness was found to increase from faint towards bright dwarfs, and to show the opposite behavior for giant elliptical galaxies (e.g. Binggeli & Cameron, 1991). Likewise, in scaling relations of any other combination of the parameters brightness, mean effective surface brightness, and effective radius, the two types were found to follow their own linear relations, which cross at some angle (Kormendy relation, Kormendy 1985; effective radius versus brightness, e.g. Binggeli & Cameron 1991). These findings have been interpreted as manifestations of different formative processes of the two galaxy types. However, the issue is still under debate (e.g. Kormendy et al., 2009; Kormendy & Bender, 2012).

Later, it was realized that neither all ellipticals have de Vaucouleurs profiles, nor do all early-type dwarfs follow exponential profiles. Instead, there is a smooth variation of the profile shapes (Caon et al., 1993; Jerjen & Binggeli, 1997; Binggeli & Jerjen, 1998). The Sérsic function is a generalization, which reproduces both the exponential and de Vaucouleurs profiles as special cases. When this function was used to fit the profiles, a linear relation between the logarithm of the profile shape parameter n and galaxy brightness was found. Also, a linear relation with brightness was found for the second fit parameter of the Sérsic profile, the central surface brightness (μ_0). In this sense the dwarfs and giants were unified. Moreover, Graham & Guzmán (2003) demonstrated that, as a consequence of the Sérsic profiles and the linear relations of the fit parameters, scaling relations including the effective radius or the mean effective surface brightness have to be curved (their Fig. 12; also see Graham & Worley 2008, Fig. 11; and Paper I, Fig. 1). Both views, that dwarfs and giants follow distinct scaling relations, and that they follow the same curved scaling relations, are extensively described by Kormendy & Bender (2012) and Graham (2011), respectively.

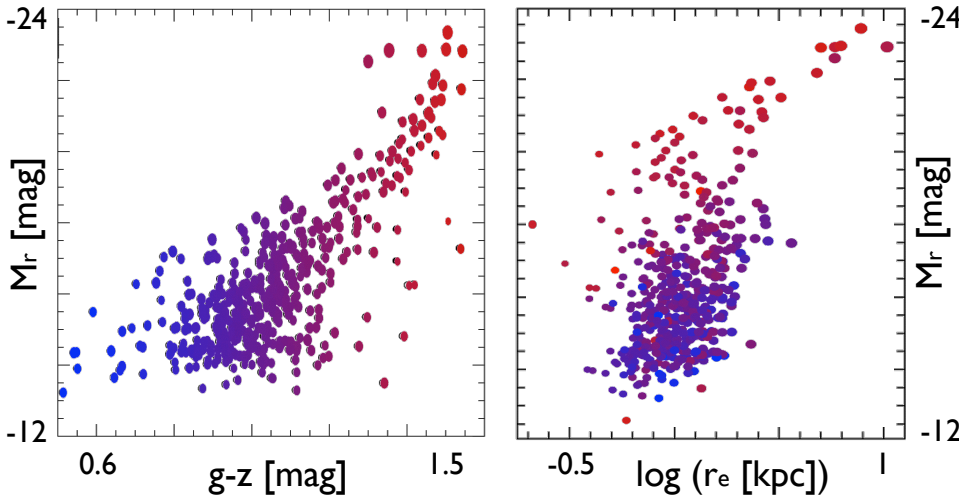

FIGURE 10.1: The color-magnitude relation and the relation of size versus brightness for the early-type galaxies in the Virgo cluster (data from Papers II and I). The colors of the symbols indicates the g-z colors of the galaxies.

In Paper I we revisit the scaling relation of effective radius and galaxy brightness using a homogenous data set of Virgo cluster early-type galaxies, based on SDSS images. We fit Sérsic functions to the light profiles, and fit linear relations to the μ_0 and n vs. brightness diagrams. From these relations we calculate the corresponding size-brightness relation. At intermediate brightnesses dwarfs and non-dwarf galaxies overlap in galaxy brightness. Both show subtle deviations from the expected curved behavior: the brightest dwarf galaxies are too large, while the faintest non-dwarf galaxies are too small. In Paper VI we find a possible explanation for this: namely, the assumption that all the early-type galaxies follow Sérsic profiles is not valid. Instead, many two-component galaxies are found with the multicomponent decompositions. When these multicomponent galaxies are fitted with single Sérsic functions, the dependency of the presence of the multiple components, and of their parameters, on galaxy brightness causes the Sérsic parameter n of the single component profile fits to depend also on galaxy brightness.

Early-type galaxies are known to follow a tight color-magnitude relation (Baum, 1959; de Vaucouleurs, 1960). Comparisons of the color-magnitude relations in different clusters (Visvanathan & Sandage, 1977; Sandage & Visvanathan, 1978a,b), and in less dense environments (Faber, 1973; Bower et al., 1992), have shown a high degree of universality of the color-magnitude relation. Generally, this relation is interpreted as a result of a more efficient chemical enrichment in more massive galaxies (Kodama & Arimoto, 1997; Ferreras et al., 1999; Gallazzi et al., 2006; Chang et al., 2006).

Many studies found the color-magnitude relation from early-type dwarfs to giants to be linear, possibly with an increased scatter for the dwarf galaxies (e.g. Secker et al. 1997 for the Coma cluster; Conselice et al. 2002 for Perseus; Karick et al. 2003 and Mieske et al. 2007 for Fornax; Smith Castelli et al. 2008 for Antlia; Misgeld et al. 2008 for Hyrda I). However, the color-magnitude relation in the Virgo cluster has been found to be curved with high quality HST data (Ferrarese et al., 2006).

In Paper II we find, using a larger sample of SDSS images, that the color-magnitude relation changes the slope twice and has an *S*-shaped structure. It is continuous over many magnitudes, but not linear. This result has been confirmed by Chen et al. (2010).

Interestingly the two findings, the shape of the size vs. galaxy brightness relation, and the non-linearity in the color-magnitude relation, are not independent from each other. In Fig. 10.1 the colors and sizes are shown side by side: the galaxies that are more compact at a given magnitude are systematically redder.

Furthermore, we discuss in Paper VI the deviations of the galaxies' isophotes from an elliptical shape. The giant elliptical galaxies are boxy if they are bright and disky if they are faint (Pasquali et al., 2007). The dwarf galaxies do not follow this trend. They have both boxy and disky shapes and are on average elliptical. Also, the data of the globular cluster systems (Peng et al., 2006) hint at a different behavior of dwarf and bright early-type galaxies. From bright to faint non-dwarf early types the galaxies host less globular clusters normalized to the galaxy brightness. However, the globular clusters systems around the dwarfs do not follow this trend and are richer and also bluer than those around the non-dwarf galaxies at the same galaxy brightness.

10.2 A DETAILED VIEW OF THE EARLY-TYPE DWARF MORPHOLOGY

The search for structures in early-type dwarf galaxies has a long history. Already the classification scheme for the VCC (Sandage & Binggeli, 1984) provided two distinct classes, dE and dS0, the latter showing hints of disk structures, such as bars, high flattening, and multicomponent light profiles. Jerjen et al. (2000) and Barazza et al. (2002) applied unsharp masking to images of early-type dwarfs to reveal low amplitude spiral arms in some of them. Lisker et al. (2006b) applied the unsharp masking technique to SDSS images and made a systematic search for disk features in the early-type dwarfs in the Virgo cluster. They found such disk features in a substantial fraction of the brighter early-type dwarfs. Ferrarese et al. (2006) reported stellar disks on nuclear and kiloparsec scales and found many bars in "intermediate luminosity" early types, making use of the high quality of the HST images.

Several studies looked for departures of the galaxy light profiles from a simple functional form. Binggeli & Cameron (1991) introduced five different profile types to classify the exponential or non-exponential shapes of the profiles or their inner and outer sections. This characterization was largely forgotten when Sérsic profiles started to be routinely fitted to the light profiles. However, it was noticed that the Sérsic profile does not provide satisfactory fits for the light profiles of all early-type dwarfs. For example, Barazza et al. (2003) pointed out in their abstract that "the observed profiles of the brightest cluster

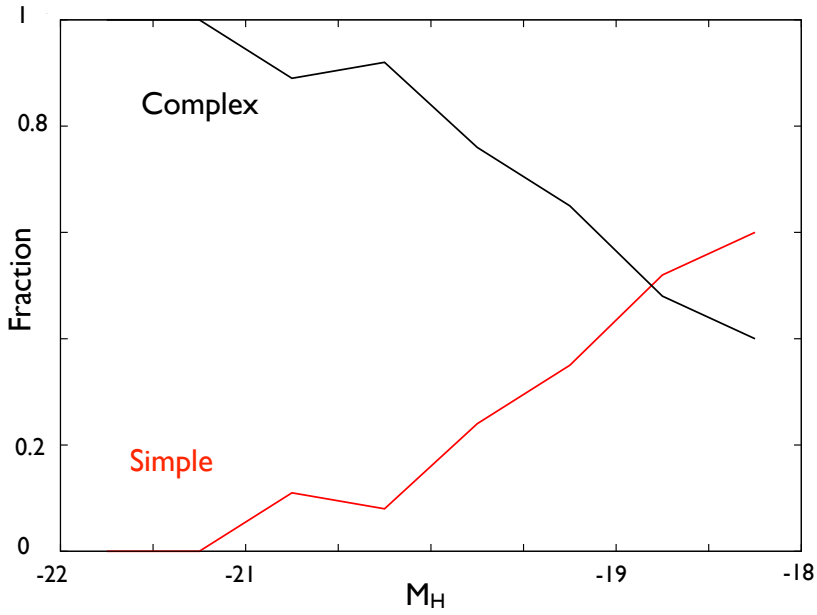

FIGURE 10.2: The fractions of one-component and complex galaxies as a function of galaxy brightness (data from Paper VI).

dwarfs [in the Virgo cluster] show significant deviations from a simple Sérsic model, indicating that there is more inner structure than just a nucleus." They emphasized that this is not restricted to those early-type dwarfs with spiral arms or disk signatures, but is true also in 'normal' early-type dwarfs. Further support for the complexity they found in the profiles of the position angles and ellipticities of these galaxies. Graham & Guzmán (2003) fitted multicomponent models to the light profiles of early-type dwarfs in the Coma cluster, and Aguerri et al. (2005) used the deviations from Sérsic profiles to classify early-type dwarfs as multiple component systems, which they assumed to be disk galaxies.

In Papers V and VI we apply the two-dimensional decomposition technique to an almost magnitude limited ($-19 < M_T < -16$ mag) sample of 121 galaxies. This method is a powerful tool in revealing the complexity of the structures, and is the better choice as compared to profile decompositions (see §7.1). Only for a relatively small fraction of the galaxies the light distributions are well represented by simple Sérsic models, with about two thirds of the galaxies being more complex. Bars are found in about 15%, and lenses are also found in about 15% of the galaxies.

The level of complexity of the galaxies is a strong function of galaxy brightness: at the bright end all of the galaxies have multiple components, while the fraction of complex galaxies drops towards fainter galaxies (Fig. 10.2). This is not a selection effect, since the integration times were chosen in such a manner that the same signal-to-noise is reached at two half-light radii of each galaxy. Moreover, the trend seems plausible, since the high mass galaxies are expected to shield their stars better against dynamical heating, which can wash out structures or prevent their formation.

The fraction of galaxies with simple morphology is highest among those early-type dwarfs, where no disk features or central star formation was detected (Lisker et al., 2006b,a). This may be expected, since they found disk features by applying unsharp masks to the images. This reveals spiral arms, bars, and possibly edge-on disk components. Most of the features are likely to be related to multicomponent structures. However, some of the galaxies with spiral arms we find to be one-component galaxies.

Qualitatively, the frequencies of complex structures we find is consistent with some previous studies (Binggeli & Cameron, 1991; McDonald et al., 2011) that used the light profiles. Also, the bar fraction and its decrease to fainter galaxy brightnesses are similar to the findings for the Coma cluster (Méndez-Abreu et al., 2010).

10.3 EARLY-TYPE DWARFS VS. LATE-TYPE DISK GALAXIES

In order to understand the inner and outer components in the early-type dwarfs, we consider several of their properties. The flattening distributions for the inner and outer components are very similar, so that they should have similar intrinsic shapes. We find that the profiles of the inner components are close to exponentials, i.e. the Sérsic indices are close to unity, the median value being $n = 1.15$.

Furthermore, we compare the parameters of the inner and outer components in the dwarf galaxies to those of the bulges and disks in bright galaxies (NIRS0S for S0, Laurikainen et al. 2011; OSUBSGS for late-type galaxies, Laurikainen et al. 2004). For all these galaxies a similar decomposition method was used. The comparisons are shown in Fig. 10.3. The bulges and disks in the bright galaxies follow more or less tight scaling relations, from which the inner and outer components in the dwarfs are clearly offset. We conclude that the inner and outer components in early-type dwarf galaxies are not of the same nature as the bulges and disks in bright galaxies. However, a comparison sample with similar decompositions for the latest low luminosity spirals would be desirable, in order to confirm or exclude possible similarities. If the whole dwarf galaxies are compared to the bulge and disk components in bright disk galaxies, they rather fall on the extrapolation of the disks' scaling relation than on the extrapolation of the scaling relation of the bulges.

The flattening distributions of the inner and outer components we find to resemble that of the disk galaxies (see also Ferguson & Sandage, 1989; Binggeli & Popescu, 1995). It is also worth noticing that the decreasing fraction of one-component galaxies towards fainter galaxy brightnesses resembles the decreasing complexity in the late-type galaxy mixture. Furthermore, Gavazzi et al. (2000) used profile decompositions for late-type galaxies and

discussed a similar trend from simple exponential to two-component galaxies towards higher brightnesses. The fraction of one-component galaxies they found is similar to what we obtain for the early-type dwarfs: for Sd/m galaxies it is slightly smaller, while it is larger for Sc galaxies.

Our analysis of the properties of the inner and outer components, and the complementary N-body simulations suggest that the inner and outer components of dwarf galaxies are not normal bulge and disk components, but rather phenomena inherent to a disk. The simulations also illustrate that the profile of the disk can be altered during the transformation process of a late-type galaxy to an early-type dwarf by harassment, and resembles afterwards the observed multicomponent structures. This is consistent with the simulations of Mastropietro et al. (2005). We discuss that also ram pressure stripping may increase the concentration and lead to a steepening of the profile in the center: according to the ram pressure stripping criterion of Gunn & Gott (1972), galaxies like the more massive early-type dwarf galaxies could retain some of their gas in the galaxy center for typical orbits within the Virgo cluster. The pressure on the (not yet) stripped gas may even enhance the star formation (see discussion in Roediger 2009). Also, the spiral structures and disk signatures that are found in some of the early-type dwarf galaxies (Jerjen et al., 2000; Barazza et al., 2002; Lisker et al., 2006b) fit into this picture of an evolutionary link. This all is consistent with the parallel sequence classification (Laurikainen et al. 2011; Cappellari et al. 2011; Kormendy & Bender 2012, originally suggested by van den Bergh 1976). These studies suggest that disk galaxies fade into lenticular galaxies after the star formation is stopped. Kormendy & Bender further extrapolate that to low masses and suggest that late-type disk galaxies turn into early-type dwarf galaxies in a similar manner.

One variety of star-forming low-mass galaxies is the class of Blue Compact Dwarf galaxies (BCDs). They are compact star-forming low-mass galaxies. Also for these galaxies an evolutionary connection to early-type dwarfs was envisioned. Davies & Phillipps (1988) suggested that BCDs may turn into early-type dwarfs after several alternating starburst and quiescent phases. However, Drinkwater & Hardy (1991) and Papaderos et al. (1996) concluded that BCDs are so compact that they could only evolve into the most compact early-type dwarfs. Drinkwater et al. (1996) made an even stronger conclusions: there are "no blue star-forming progenitors of dE galaxies". In Paper VII we look for their descendants. If the starburst phase of BCDs is short (Thuan et al., 1991; Thornley et al., 2000), their non-starforming counterparts should be found in a similar spatial region. Possible candidates are the early-type dwarfs and the dIrrs. We extract the photometric parameters of the BCDs' underlying non-starforming component of old stars by fitting exponential profiles to these low-surface brightness components. We find that their radii are compatible with those of the more compact half of early-type dwarfs. While BCDs and early-type dwarfs are in this sense similar, the dIrrs have significantly lower surface brightnesses and are thus unlikely to be related to the BCDs.

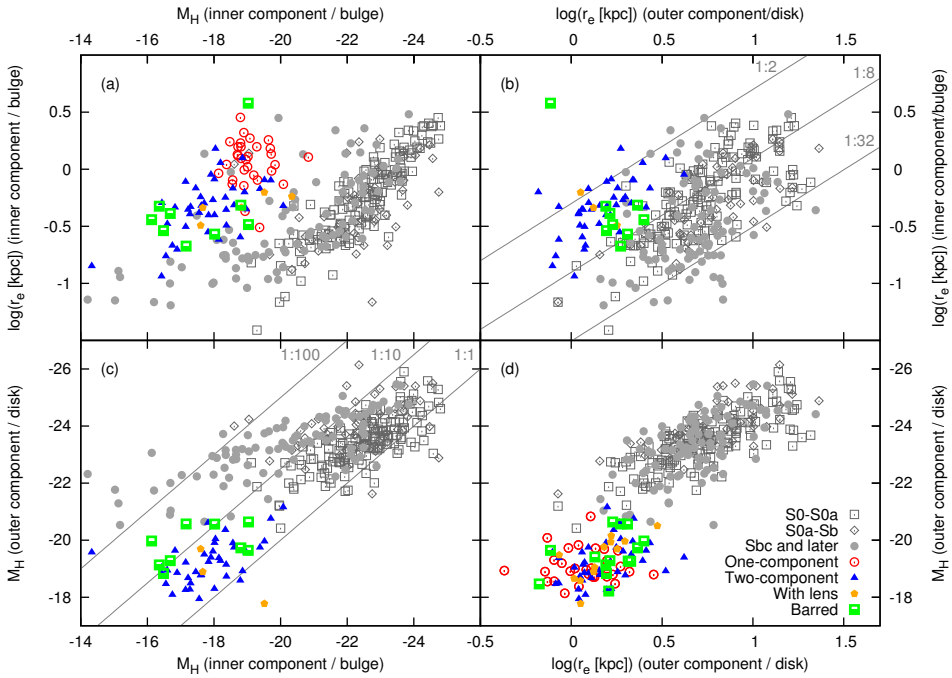

FIGURE 10.3: The inner and outer components of the galaxies in our sample are shown in the scaling relations of the bulge and disk components of the bright galaxies. The earliest bin of Hubble types is taken from NIRS0S (Laurikainen et al., 2011) and the two other from OSUBSGS (Laurikainen et al., 2004). Panels *(a)* and *(d)* display the relations of brightness and radius of the inner/bulge and outer/disk components, respectively. Panels *(b)* and *(d)* show the scalings for radius and brightness, respectively, versus the corresponding parameter of the other component. In panel *(b)* the gray lines show a ratio of the effective radii of bulge and disk (or of the inner and outer component) of 1:2, 1:8 and 1:32, while in panel *(c)* they show a bulge to disk (or inner to outer component) ratio of 1:1, 1:10 and 1:100. The one-component galaxies of our sample are plotted in both the bulge and disk panels. Galaxies with lens or bar are plotted in the respective panels, if there was an inner Sérsic or outer component fitted in the decomposition (Figure from Paper VI).

10.4 GALAXY FLATTENINGS AND ORBITS WITHIN THE CLUSTER

In Paper III we analyze the nucleated early-type dwarf galaxies without disk signatures or residual star formation in the projected center of the Virgo cluster. The nucleated early-type dwarfs are the most centrally concentrated dwarf subclass within the cluster and have the oldest stellar populations (Lisker et al., 2007, 2008). We divide them into slow and fast ones, based on their line-of-sight velocity relative to the cluster. The surprising result is that the galaxies in the two samples have significantly different shapes: the majority of fast moving dwarfs have high ellipticities, while the slow ones are nearly round (Fig. 10.4). It works also the other way round: when dividing the galaxies into flat and round ones, their line-of-sight velocity distributions differ significantly. The round dwarfs' distribution is clearly peaked and rather narrow, whereas the distribution of the flat ones is broader, possibly double-peaked.

The different distributions suggest that the two populations spent different amounts of time in the cluster. The double-peaked distribution is more typical for a population that fell in (Conselice et al., 2001): the galaxies are expected to move on radial, highly eccentric orbits. The round dwarfs probably move on more circular orbits, characteristic for a cluster-born galaxies. Alternatively, these galaxies might have fallen-in early on. In both cases they have experienced a prolonged period of dynamically heating by the cluster environment. We conclude that they might be the first generation of Virgo cluster early-type dwarf galaxies.

The assumed different ages of the two populations are reflected in the color-magnitude relations: the round galaxies are redder in $g-i$ and the difference becomes even more evident in the age-sensitive NUV $-$ r relation. In the FUV $-$ r color the two samples have similar colors. Altogether, the obtained color differences are consistent with a small age difference between the two samples of already relatively old galaxies (Lisker & Han, 2008). However, the tentative results from the kinematics that we obtained for a subsample of fast-moving dwarfs pose further questions: two of the galaxies show no significant rotation out to the half-light radius. One of them looks like being disrupted, based on a deep optical image (Lieder et al., 2012). Literature values for the round galaxies, on the other hand, show rotation for several of them. Therefore, the kinematics fit not readily to the above scenario.

10.5 ISOPHOTAL SHAPE AND KINEMATICS

In Paper VI we study the non-elliptical shapes of the isophotes. Larger deviations are preferentially found in galaxies with higher apparent ellipticities. Especially, most of the large boxy values occur in the outer parts of galaxies with a presumably higher inclination. Furthermore, we find that disky isophotes are not a good proxy for the degree of rotation in a galaxy, contrary to what was claimed previously (Toloba et al., 2011). Unlike for the bright galaxies, the median boxiness values for these lower mass galaxies scatter around the elliptical shape, in a similar manner to disky and boxy shapes. With the boxy sections

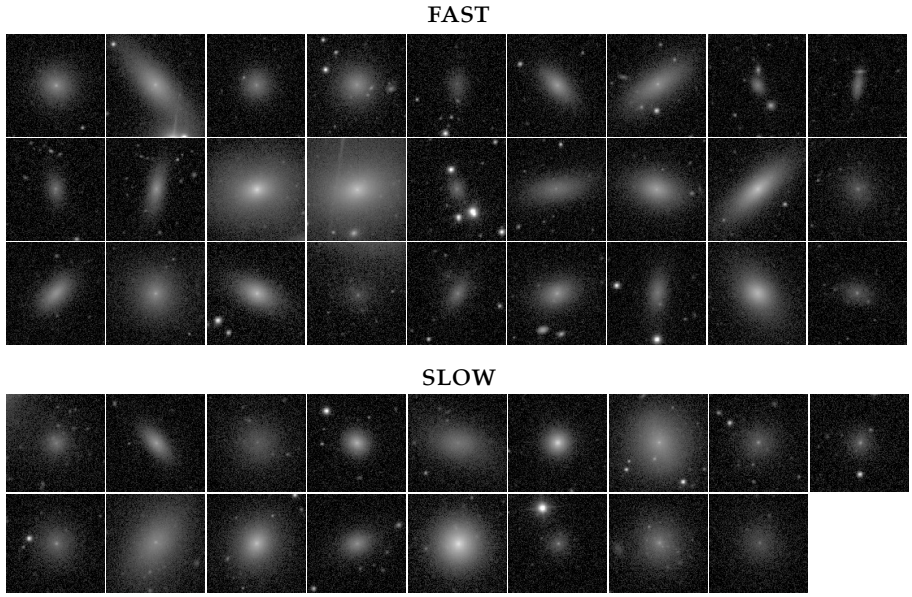

FIGURE 10.4: The stamps show SDSS r-band images of the nucleated early-type dwarfs in the center of the Virgo cluster grouped by their heliocentric velocities relative to the cluster. The boxes are $1'.36 \times 1'.36$.

occurring especially in the outer parts of inclined galaxies, we conclude that also the boxy shapes are related to disk phenomena (see also Paper iii).

10.6 ULTRA-COMPACT DWARFS AND NUCLEI OF EARLY-TYPES DWARFS

Ultra-compact dwarf galaxies (UCDs) are extremely compact, small galaxies, which were first discovered in the Fornax cluster (Hilker et al., 1999; Drinkwater et al., 2000; Phillipps et al., 2001). Their appearance is not much different from globular clusters (GCs), they are just $1-2$ mag brighter, and also have old stellar populations. UCDs are generally assumed to be either the brightest versions of GCs (e.g. Mieske et al., 2002) or, alternatively, to be the remaining nuclei of nucleated early-type dwarf galaxies that have been tidally disrupted (Bekki et al. 2003; also see discussion in Mieske et al. 2004).

In Paper IV we analyze the stellar population characteristics of 10 UCDs and of 34 nuclei in early-type dwarf galaxies. For the nuclei the spectra are taken from the galaxy centers and the light contribution of the galaxy is subtracted. We fit simple stellar population models to the observed absorption line indices to derive stellar ages and metallicities. We find that the nuclei are on average younger and more metal rich than the UCDs. However, the UCDs are present only in regions with high local galaxy density. If they are compared to the nuclei of dwarfs in the same high density environment no significant differences of the stellar population parameters are found. This is consistent with the UCDs being the remaining nuclei of tidally disrupted nucleated early-type dwarfs.

10.7 COMPARISON TO SEMI-ANALYTIC MODELS

In Papers I and II the relation of size versus galaxy brightness, and the color-magnitude relation are studied. There are subtle deviations from a simple joint behavior of bright and dwarf early-type galaxies (see above). However, a comparison to the SAM of Nagashima et al. (2005) shows that in principle the relation can be reproduced in the framework of the SAM.

In Papers VIII and ii the observations in the Virgo cluster and other clusters are compared to the SAM of Guo et al. (2011), which is based on the Millennium-II simulation (Boylan-Kolchin et al., 2009). In Paper ii we have found that the number density profiles of the clusters are reasonably well reproduced. However, the fraction of red galaxies at low galaxy masses is lower in the Virgo cluster than the corresponding fraction in the simulated clusters. The match is better for the Perseus and Coma clusters. The dwarf-to-giant number ratio is generally over-predicted in the simulations. We conclude that this may be related to an insufficient implementation of tidal disruption of faint galaxies.

In Paper VIII we find a remarkable resemblance of the projected clustercentric distance distributions of elliptical, intermediate, and late-type dwarfs, with the distributions of model galaxies whose subhaloes experienced strong, intermediate, or weak mass loss since their infall into a massive halo. Assuming that subhalo mass loss serves as a proxy for the environmental influence on the baryonic configuration of galaxies thus reproduces

the well-known morphology-density relation. At the same time, this is closely correlated with the epoch when the galaxies fell into a massive halo for the first time: this happened at early epochs for today's ellipticals, but much more recently for the present-day late-type galaxies.

Part VI

CONCLUSIONS

In this thesis various aspects of the early-type dwarf galaxies were studied. We collected near-infrared images for a substantial, almost luminosity limited sample of early-type dwarf galaxies. The near-infrared data are the missing cornerstone in the comprehensive photometric analysis of the electromagnetic spectrum of the Virgo cluster, which is the nearest rich galaxy cluster. The obtained data quality is high, some of the images possibly being as deep as achievable for a large sample with current instrumentation from the ground. The deep images together with a two-dimensional multicomponent decompositions allowed for a detailed view on the morphologies of early-type dwarfs. Using the SDSS, we obtained a homogenous data set of galaxy photometry in the optical filter bands, which was well-suited to compare galaxies of different morphological types and over a large range of galaxy brightnesses. Furthermore, it provided the basis for detailed comparisons to state-of-the-art semi-analytic models (SAMs) of galaxy formation and evolution. Finally, spectra were obtained with FORS at VLT in order to study the stellar populations and kinematics of dE,Ns. Both the two-dimensional multicomponent decomposition approach and Kelson (2003)'s *Background Subtraction for the 21st Century* method for the reduction of the kinematics spectra were probably applied for the first time for studying early-type dwarf galaxies in the Virgo cluster.[1]

We found that the early-type dwarfs follow roughly scaling relations as they may be expected from those of bright early-type galaxies. The sizes as a function of brightness follow a curved relation with the bright early-type galaxies, which is expected from the observed continuous variation of the profile shapes, if they follow Sérsic functions. Furthermore, the color-magnitude relation was found to be continuous. However, subtle deviations from this simple joint behavior of dwarf and giant early-type galaxies were found: their sizes depart from the expected relation to opposite directions towards intermediate brightnesses. Also, the color-magnitude relation is not linear but changes the slope twice and has an *S*-shape structure. Nevertheless, comparisons to the SAM of Nagashima et al. (2005) showed that these findings may still be explained within a common framework for the high and low-mass early-type galaxies, with their present day appearance mostly being shaped by internal feedback processes and mergers.

The two-dimensional multicomponent decompositions opened a new viewing angle on the early-type dwarfs. They revealed a surprising complexity in their structure. The comparisons of the scaling relations of dwarf galaxies and their individual components to the scalings of the bright galaxies and their components suggested that the majority of the early-type dwarfs is rather related to disks of late-type galaxies than to the bulges or bright elliptical galaxies. This view is also supported by the flattening distributions of the early-type dwarfs, which we found to be similar to that of late-type galaxies. Complementary N-body simulations illustrated that the observed multicomponent structures can be inherent to a disk, instead of being the result of a combination of a bulge and disk components. As such, the multicomponent structures in the early-type dwarfs may be formed during the transformations from late-type galaxies.

1 Francis et al. (2012) applied the reduction prescriptions of Kelson (2003) to spectra of UCDs.

The flattenings of the nucleated early-type dwarfs (dE,Ns) in the cluster center were found to depend strongly on the line-of-sight velocity relative to the cluster. The fast moving galaxies are flatter than the slowly moving ones. A possible interpretation was found by comparisons to the subhalo dynamics in the Millennium-II simulation (Boylan-Kolchin et al., 2009): the flat fast moving dE,Ns move along radial orbits, while the rounder more slowly moving galaxies are on circularized orbits. The latter galaxies spent a longer time in the cluster as the flat fast moving ones, allowing for the circularization of the orbits and prolonged dynamical heating of the galaxies, which gave them their rounder shape. The difference of time spent in the cluster was found to be consistent with difference in stellar population age.

Furthermore, we found that the stellar population characteristics of the nuclei of dE,Ns are compatible with those of the UCDs. This is evidence for the scenario of UCDs forming by tidal disruption of dE,Ns. Also, the BCDs were found to be possibly linked to early-type dwarfs by transformations through the cluster environment. The low surface brightness components of old stars in the BCDs were shown to have similar sizes as the more compact half of the early-type dwarfs of the same brightness.

In future, the obtained near-infrared data will be further exploited. In combination with optical data the age-metallicity degeneracy can be overcome, and the broad band colors can be used to estimate stellar population characteristics. The ages and metallicities of the different identified structural types can be compared, as well as the stellar population characteristics of the different components. Trends with the position inside the cluster and gradients in the individual galaxies can be studied. Decompositions similar to those in this study need to be carried out also for the possible early-type dwarf progenitors, the late-type galaxies. Further possibilities will be offered by comparisons to two-dimensional kinematics that will become available soon (Ryś et al., 2012). The decompositions of the early-type dwarfs are a benchmark study of the largest galaxy population in the nearest cluster. It will be exciting to compare them to similar studies in different clusters and environments.

Part VII

APPENDIX

A.1 REDUCTION OF NEAR-INFRARED IMAGES – A SCHEMATIC OVERVIEW

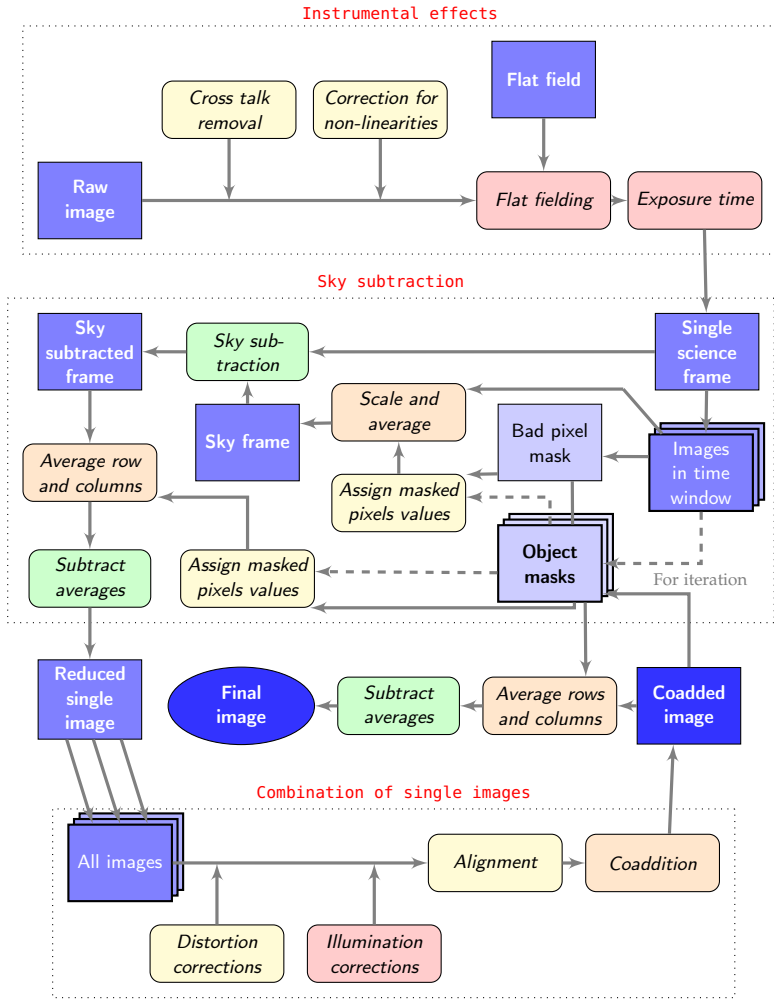

Blue boxes mark images and masks. Steps with divisions, subtractions, and scaling and averaging are displayed with red, green, and orange backgrounds, respectively. Yellow backgrounds indicate other steps. The reduction is done with one iteration to obtain the object masks on the preliminary coadded image, which are then used in the sky subtraction of the final iteration.

A.2 REDUCTION OF NEAR-INFRARED LONG-SLIT SPECTRA – A SCHEMATIC OVERVIEW

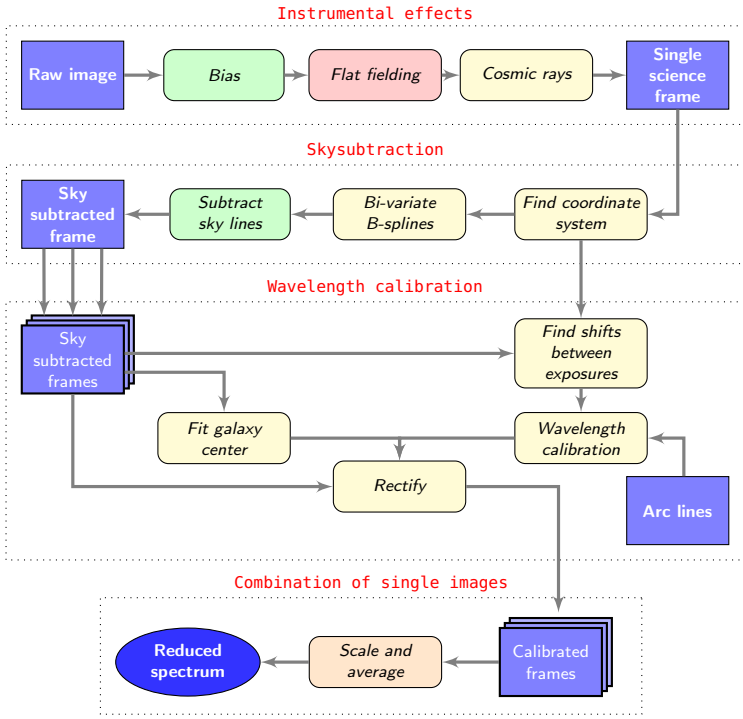

Blue boxes mark images and masks. Steps with divisions, subtractions, and scaling and averaging are displayed with red, green, and orange backgrounds, respectively. Yellow backgrounds indicate other steps. The reduction is done with one iteration to obtain the object masks on the preliminary coadded image, which are then used in the sky subtraction of the final iteration.

LIST OF FIGURES

LIST OF TABLES

ACRONYMS

2MASS	Two Micron All sky survey
ADU	Analog-to-Digital Unit
BCD	Blue Compact Dwarf galaxy
CCD	charge-coupled Device
CMBR	Cosmic Microwave Background Radiation
DM	Dark Matter
DR	Data Release
ESO	European southern Observatory
FORS	FOcal Reducer and low dispersion Spectrograph – imager/speectrograph at ESO/VLT
FWHM	Full Width at Half Maximum
GC	globular Cluster
HST	Hubble space Telescope
IRAF	Image Reduction and Analysis Facility
ΛCDM	Cosmological constant Cold Dark Matter – concordance cosmology
LF	Luminosity Function
LSB	Low Surface Brightness

NASA	National Aeronautics and Space Administration
NED	NASA/IPAC Extragalactic Database
NFW	Navarro, Frenk, & White profile (Navarro et al., 1997)
NICS	Near Infrared Camera Spectrometer – near-infrared instrument at TNG
NOT	Nordic Optical Telescope
NOTCam	Nordic Optical Telescope near-infrared CAMera and spectrograph – near-infrared instrument at NOT
NTT	New Technology Telescope
PSF	Point Spread Function
RMS	Root Mean Sqaure
SAM	semi-Analytic Model
SAURON	Spectrographic Areal Unit for Research on Optical Nebulae – integral field spectroscopy unit at WHT
SDSS	Sloan Digital Sky Survey
SMA	semi-Major Axis
SMAKCED	Stellar content, Masses And Kinematics of Cluster Early-type Dwarfs
S/N	Signal-to-Noise
SN	SuperNova
SOFI	Son OF Isaac – near-infrared instrument at ESO/NTT
SSP	Single Stellar Population
TNG	Telescopio Nazionale Galileo
UCD	Ultra-Compact Dwarf galaxy
UKIDSS	UKIRT Infrared Deep Sky Survey
UKIRT	United Kingdom InfraRed Telescope
VCC	Virgo Cluster Catalog (Binggeli et al., 1985)
VLT	Very Large Telescope
WFI	Wide-Field Imager – optical instrument at ESO/2.2m
WHT	William Herschel Telescope

BIBLIOGRAPHY

Abel, T., Bryan, G. L., & Norman, M. L., 2002. *The Formation of the First Star in the Universe*. Science, 295, 93.

Abraham, R. G., Valdes, F., Yee, H. K. C., & van den Bergh, S., 1994. *The morphologies of distant galaxies. 1: an automated classification system*. The Astrophysical Journal, 432, 75.

Adelman-McCarthy, J. K., Agüeros, M. A., Allam, S. S., Anderson, K. S. J., Anderson, S. F., Annis, J., Bahcall, N. A., et al., 2007. *The Fifth Data Release of the Sloan Digital Sky Survey*. The Astrophysical Journal Supplement Series, 172, 634.

Aguerri, J. A. L. & González-García, A. C., 2009. *On the origin of dwarf elliptical galaxies: the fundamental plane*. Astronomy & Astrophysics, 494, 891.

Aguerri, J. A. L., Iglesias-Páramo, J., Vílchez, J. M., Muñoz-Tuñón, C., & Sánchez-Janssen, R., 2005. *Structural Parameters of Dwarf Galaxies in the Coma Cluster: On the Origin of dSo Galaxies*. The Astronomical Journal, 130, 475.

Allen, S. W., Evrard, A. E., & Mantz, A. B., 2011. *Cosmological Parameters from Observations of Galaxy Clusters*. Annual Review of Astronomy & Astrophysics, 49, 409.

Alpher, R. A., Bethe, H., & Gamow, G., 1948. *The Origin of Chemical Elements*. Physical Review, 73, 803.

Amanullah, R., Lidman, C., Rubin, D., Aldering, G., Astier, P., Barbary, K., Burns, M. S., et al., 2010. *Spectra and Hubble Space Telescope Light Curves of Six Type Ia Supernovae at 0.511 < z < 1.12 and the Union2 Compilation*. The Astrophysical Journal, 716, 712.

Bacon, D. J., Refregier, A. R., & Ellis, R. S., 2000. *Detection of weak gravitational lensing by large-scale structure*. Monthly Notices of the Royal Astronomical Society, 318, 625.

Baldry, I. K., Driver, S. P., Loveday, J., Taylor, E. N., Kelvin, L. S., Liske, J., Norberg, P., et al., 2012. *Galaxy And Mass Assembly (GAMA): the galaxy stellar mass function at z < 0.06*. Monthly Notices of the Royal Astronomical Society, 421, 621.

Balogh, M. L., Navarro, J. F., & Morris, S. L., 2000. *The Origin of Star Formation Gradients in Rich Galaxy Clusters*. The Astrophysical Journal, 540, 113.

Barazza, F. D., Binggeli, B., & Jerjen, H., 2002. *More evidence for hidden spiral and bar features in bright early-type dwarf galaxies*. Astronomy & Astrophysics, 391, 823.

Barazza, F. D., Binggeli, B., & Jerjen, H., 2003. *VLT surface photometry and isophotal analysis of early-type dwarf galaxies in the Virgo cluster*. Astronomy & Astrophysics, 407, 121.

Barnes, J. E., 1988. *Encounters of disk/halo galaxies*. The Astrophysical Journal, 331, 699.

Barnes, J. E. & Hernquist, L., 1992. *Formation of dwarf galaxies in tidal tails*. Nature, 360, 715.

Baum, W. A., 1959. *Population Inferences from Star Counts, Surface Brightness and Colors*. Publications of the Astronomical Society of the Pacific, 71, 106.

Beasley, M. A., Cenarro, A. J., Strader, J., & Brodie, J. P., 2009. *Evidence for the Disky Origin of Luminous Virgo Dwarf Ellipticals from the Kinematics of Their Globular Cluster Systems*. The Astronomical Journal, 137, 5146.

Bekki, K. & Couch, W. J., 2003. *Starbursts from the Strong Compression of Galactic Molecular Clouds due to the High Pressure of the Intracluster Medium*. The Astrophysical Journal Letters, 596, L13.

Bekki, K., Couch, W. J., Drinkwater, M. J., & Shioya, Y., 2003. *Galaxy threshing and the origin of ultra-compact dwarf galaxies in the Fornax cluster*. Monthly Notices of the Royal Astronomical Society, 344, 399.

Bell, E. F. & de Jong, R. S., 2001. *Stellar Mass-to-Light Ratios and the Tully-Fisher Relation*. The Astrophysical Journal, 550, 212.

Bennett, C. L., Halpern, M., Hinshaw, G., Jarosik, N., Kogut, A., Limon, M., Meyer, S. S., et al., 2003. *First-Year Wilkinson Microwave Anisotropy Probe (WMAP) Observations: Preliminary Maps and Basic Results*. The Astrophysical Journal Supplement Series, 148, 1.

Benson, A. J., Lacey, C. G., Frenk, C. S., Baugh, C. M., & Cole, S., 2004. *Heating of galactic discs by infalling satellites*. Monthly Notices of the Royal Astronomical Society, 351, 1215.

Bernardi, M., 2007. *The σ-L Correlation in Nearby Early-Type Galaxies*. The Astronomical Journal, 133, 1954.

Bershady, M. A., Jangren, A., & Conselice, C. J., 2000. *Structural and Photometric Classification of Galaxies. I. Calibration Based on a Nearby Galaxy Sample*. The Astronomical Journal, 119, 2645.

Bertin, E. & Arnouts, S., 1996. *SExtractor: Software for source extraction*. Astronomy & Astrophysics Supplement Series, 117, 393.

Binggeli, B., 1994. *A Note on the Definition and Nomenclature of Dwarf Galaxies*. Dwarf Galaxies, 49, 13.

Binggeli, B. & Cameron, L. M., 1991. *Dwarf galaxies in the Virgo cluster. I - The systematic photometric properties of early-type dwarfs*. Astronomy & Astrophysics, 252, 27.

Binggeli, B. & Cameron, L. M., 1993. *Dwarf galaxies in the Virgo cluster. II - Photometric techniques and basic data*. Astronomy & Astrophysics Supplement Series, 98, 297.

Binggeli, B. & Jerjen, H., 1998. *Is the shape of the luminosity profile of dwarf elliptical galaxies an useful distance indicator?* Astronomy & Astrophysics, 333, 17.

Binggeli, B. & Popescu, C. C., 1995. *Dwarf galaxies in the Virgo cluster. III. Flattening distributions*. Astronomy & Astrophysics, 298, 63.

Binggeli, B., Popescu, C. C., & Tammann, G. A., 1993. *The kinematics of the Virgo cluster revisited*. Astronomy & Astrophysics Supplement Series, 98, 275.

Binggeli, B., Sandage, A., & Tammann, G. A., 1985. *Studies of the Virgo Cluster. II - A catalog of 2096 galaxies in the Virgo Cluster area*. The Astronomical Journal, 90, 1681.

Binggeli, B., Sandage, A., & Tammann, G. A., 1988. *The luminosity function of galaxies*. Annual Review of Astronomy & Astrophysics, 26, 509.

Binggeli, B., Tammann, G. A., & Sandage, A., 1987. *Studies of the Virgo cluster. VI - Morphological and kinematical structure of the Virgo cluster*. The Astronomical Journal, 94, 251.

Binney, J. & Tremaine, S., 2011. *Galactic Dynamics*. (Second Edition). Princeton University Press.

Böhringer, H., Briel, U. G., Schwarz, R. A., Voges, W., Hartner, G., & Trumper, J., 1994. *The Structure of the Virgo Cluster of Galaxies from ROSAT X-Ray Images*. Nature, 368, 828.

Bond, J. R., Kofman, L., & Pogosyan, D., 1996. *How filaments of galaxies are woven into the cosmic web*. Nature, 380, 603.

Boselli, A., Boissier, S., Cortese, L., & Gavazzi, G., 2008. *The Origin of Dwarf Ellipticals in the Virgo Cluster*. The Astrophysical Journal, 674, 742.

Boselli, A., Boissier, S., Heinis, S., Cortese, L., Ilbert, O., Hughes, T., Cucciati, O., et al., 2011. *The GALEX Ultraviolet Virgo Cluster Survey (GUViCS)*. Astronomy & Astrophysics, 528, A107.

Boselli, A. & Gavazzi, G., 2006. *Environmental Effects on Late-Type Galaxies in Nearby Clusters*. The Publications of the Astronomical Society of the Pacific, 118, 517.

Bosma, A., 1978. *The distribution and kinematics of neutral hydrogen in spiral galaxies of various morphological types*. PhD Thesis, Rijksuniversiteit Groningen.

Bournaud, F. & Duc, P.-A., 2006. *From tidal dwarf galaxies to satellite galaxies*. Astronomy & Astrophysics, 456, 481.

Bournaud, F., Duc, P.-A., Brinks, E., Boquien, M., Amram, P., Lisenfeld, U., Koribalski, B. S., et al., 2007a. *Missing Mass in Collisional Debris from Galaxies*. Science, 316, 1166.

Bournaud, F., Jog, C. J., & Combes, F., 2007b. *Multiple minor mergers: formation of elliptical galaxies and constraints for the growth of spiral disks*. Astronomy & Astrophysics, 476, 1179.

Bouwens, R. J., Illingworth, G. D., Labbe, I., Oesch, P. A., Trenti, M., Carollo, C. M., van Dokkum, P. G., et al., 2011. *A candidate redshift z~10 galaxy and rapid changes in that population at an age of 500Myr*. Nature, 469, 504.

Bower, R. G., Lucey, J. R., & Ellis, R. S., 1992. *Precision Photometry of Early Type Galaxies in the Coma and Virgo Clusters - a Test of the Universality of the Colour / Magnitude Relation - Part Two - Analysis*. Monthly Notices of the Royal Astronomical Society, 254, 601.

Boylan-Kolchin, M., Springel, V., White, S. D. M., Jenkins, A., & Lemson, G., 2009. *Resolving cosmic structure formation with the Millennium-II Simulation*. Monthly Notices of the Royal Astronomical Society, 398, 1150.

Bromm, V. & Yoshida, N., 2011. *The First Galaxies*. Annual Review of Astronomy & Astrophysics, 49, 373.

Butcher, H. & Oemler, A. J., 1978. *The evolution of galaxies in clusters. I - ISIT photometry of C1 0024+1654 and 3C 295*. The Astrophysical Journal, 219, 18.

Byun, Y. I. & Freeman, K. C., 1995. *Two-dimensional Decomposition of Bulge and Disk*. The Astrophysical Journal, 448, 563.

Caffau, E., Bonifacio, P., François, P., Sbordone, L., Monaco, L., Spite, M., Spite, F., et al., 2011. *An extremely primitive star in the Galactic halo*. The Astrophysical Journal Supplement Series, 477, 67.

Caon, N., Capaccioli, M., & D'Onofrio, M., 1993. *On the Shape of the Light Profiles of Early Type Galaxies*. Monthly Notices of the Royal Astronomical Society, 265, 1013.

Capaccioli, M., 1989. *Photometry of early-type galaxies and the R exp 1/4 law*. World of Galaxies (Le Monde des Galaxies). Springer-Verlag, New-York.

Cappellari, M. & Emsellem, E., 2004. *Parametric Recovery of Line-of-Sight Velocity Distributions from Absorption-Line Spectra of Galaxies via Penalized Likelihood*. The Publications of the Astronomical Society of the Pacific, 116, 138.

Cappellari, M., Emsellem, E., Krajnović, D., McDermid, R. M., Serra, P., Alatalo, K., Blitz, L., et al., 2011. *The ATLAS3D project - VII. A new look at the morphology of nearby galaxies: the kinematic morphology-density relation*. Monthly Notices of the Royal Astronomical Society, 416, 1680.

Cardiel, N., 2007. *Measuring line-strength indices in a systematic way*. In F. Figueras, J. M. Girart, M. Heranz, & C. Jordi, eds., *Highlights of Spanish Astrophysics IV, Proceedings of the 7th Scientific Meeting of the Spanish Astronomical Society*. CD–ROM.

Cenarro, A. J., Cardiel, N., Gorgas, J., Peletier, R. F., Vazdekis, A., & Prada, F., 2001. *Empirical calibration of the near-infrared CaII triplet - I. The stellar library and index definition*. Monthly Notices of the Royal Astronomical Society, 326, 959.

Chaboyer, B., Demarque, P., Kernan, P. J., & Krauss, L. M., 1996. *A Lower Limit on the Age of the Universe*. Science, 271, 957.

Chamaraux, P., Balkowski, C., & Gerard, E., 1980. *The H I deficiency of the Virgo cluster spirals*. Astronomy & Astrophysics, 83, 38.

Chang, R., Gallazzi, A., Kauffmann, G., Charlot, S., Ivezić, Ž., Brinchmann, J., & Heckman, T. M., 2006. *The colours of elliptical galaxies*. Monthly Notices of the Royal Astronomical Society, 366, 717.

Chen, C.-W., Côté, P., West, A. A., Peng, E. W., & Ferrarese, L., 2010. *Homogeneous UGRIZ Photometry for ACS Virgo Cluster Survey Galaxies: A Non-parametric Analysis from SDSS Imaging*. The Astrophysical Journal Supplement Series, 191, 1.

Chilingarian, I. V., 2009. *Evolution of dwarf early-type galaxies - I. Spatially resolved stellar populations and internal kinematics of Virgo cluster dE/dSo galaxies*. Monthly Notices of the Royal Astronomical Society, 394, 1229.

Chwolson, O., 1924. *Über eine mögliche Form fiktiver Doppelsterne*. Astronomische Nachrichten, 221, 329.

Clowe, D., Gonzalez, A., & Markevitch, M., 2004. *Weak-Lensing Mass Reconstruction of the Interacting Cluster 1E 0657-558: Direct Evidence for the Existence of Dark Matter*. The Astrophysical Journal, 604, 596.

Conselice, C. J., 2003. *The Relationship between Stellar Light Distributions of Galaxies and Their Formation Histories*. The Astrophysical Journal Supplement Series, 147, 1.

Conselice, C. J., Bershady, M. A., & Jangren, A., 2000. *The Asymmetry of Galaxies: Physical Morphology for Nearby and High-Redshift Galaxies*. The Astrophysical Journal, 529, 886.

Conselice, C. J., Gallagher, J. S., & Wyse, R. F. G., 2002. *Galaxy Populations and Evolution in Clusters. II. Defining Cluster Populations*. The Astronomical Journal, 123, 2246.

Conselice, C. J., Gallagher, J. S. I., & Wyse, R. F. G., 2001. *Galaxy Populations and Evolution in Clusters. I. Dynamics and the Origin of Low-Mass Galaxies in the Virgo Cluster*. The Astrophysical Journal, 559, 791.

Côté, P., Blakeslee, J. P., Ferrarese, L., Jordán, A., Mei, S., Merritt, D., Milosavljević, M., et al., 2004. *The ACS Virgo Cluster Survey. I. Introduction to the Survey*. The Astrophysical Journal Supplement Series, 153, 223.

Côté, P., Piatek, S., Ferrarese, L., Jordán, A., Merritt, D., Peng, E. W., Haşegan, M., et al., 2006. *The ACS Virgo Cluster Survey. VIII. The Nuclei of Early-Type Galaxies*. The Astrophysical Journal Supplement Series, 165, 57.

Cowan, J. J., McWilliam, A., Sneden, C., & Burris, D. L., 1997. *The Thorium Chronometer in CS 22892-052: Estimates of the Age of the Galaxy*. The Astrophysical Journal, 480, 246.

Cowan, J. J., Pfeiffer, B., Kratz, K. L., Thielemann, F. K., Sneden, C., Burles, S., Tytler, D., et al., 1999. *r-Process Abundances and Chronometers in Metal-poor Stars*. The Astrophysical Journal, 521, 194.

Croton, D. J., Springel, V., White, S. D. M., de Lucia, G., Frenk, C. S., Gao, L., Jenkins, A., et al., 2006. *The many lives of active galactic nuclei: cooling flows, black holes and the luminosities and colours of galaxies*. Monthly Notices of the Royal Astronomical Society, 365, 11.

Dabringhausen, J. & Kroupa, P., 2012. *Dwarf elliptical galaxies as ancient tidal dwarf galaxies*. arXiv:1211.1382.

Davies, J. I., Baes, M., Bendo, G. J., Bianchi, S., Bomans, D. J., Boselli, A., Clemens, M., et al., 2010. *The Herschel Virgo Cluster Survey*. Astronomy & Astrophysics, 518, L48.

Davies, J. I. & Phillipps, S., 1988. *The evolution of dwarf galaxies*. Monthly Notices of the Royal Astronomical Society, 233, 553.

de Blok, W. J. G., 2010. *The Core-Cusp Problem*. Advances in Astronomy, 2010, 5.

de Grijs, R., 1998. *The global structure of galactic discs*. Monthly Notices of the Royal Astronomical Society, 299, 595.

de Jong, R. S., Simard, L., Davies, R. L., Saglia, R. P., Burstein, D., Colless, M., McMahan, R., et al., 2004. *Structural properties of discs and bulges of early-type galaxies*. Monthly Notices of the Royal Astronomical Society, 355, 1155.

de Looze, I., Baes, M., Zibetti, S., Fritz, J., Cortese, L., Davies, J. I., Verstappen, J., et al., 2010. *The Herschel Virgo Cluster Survey . VII. Dust in cluster dwarf elliptical galaxies*. Astronomy & Astrophysics, 518, L54.

de Rijcke, S., Van Hese, E., & Buyle, P., 2010. *The Conversion of Late-type Into Early-type Dwarf Galaxies by Ram-pressure Stripping in the Fornax Cluster*. The Astrophysical Journal Letters, 724, L171.

de Vaucouleurs, G., 1960. *Integrated Colors of Bright Galaxies in the u, b, V System.* The Astrophysical Journal Supplement Series, 5, 233.

de Vega, H. J. & Sanchez, N. G., 2011. *Warm dark matter in the galaxies:theoretical and observational progresses. Highlights and conclusions of the chalonge meudon workshop 2011*. arXiv:1109.3187.

Dehnen, W. & Binney, J. J., 1998. *Local stellar kinematics from HIPPARCOS data*. Monthly Notices of the Royal Astronomical Society, 298, 387.

Dekel, A. & Silk, J., 1986. *The origin of dwarf galaxies, cold dark matter, and biased galaxy formation*. The Astrophysical Journal, 303, 39.

Dekel, A. & Woo, J., 2003. *Feedback and the fundamental line of low-luminosity low-surface-brightness/dwarf galaxies*. Monthly Notices of the Royal Astronomical Society, 344, 1131.

Dicke, R. H. & Peebles, P. J. E., 1979. *The Big Bang Cosmology: Enigmas and Nostrums*. General Relativity: An Einstein Centenary Survey.

Dietrich, J. P., Werner, N., Clowe, D., Finoguenov, A., Kitching, T., Miller, L., & Simionescu, A., 2012. *A filament of dark matter between two clusters of galaxies*. The Astrophysical Journal Supplement Series, 487, 202.

Dine, M. & Kusenko, A., 2003. *Origin of the matter-antimatter asymmetry*. Reviews of Modern Physics, 76, 1.

Djorgovski, S. & Davis, M., 1987. *Fundamental properties of elliptical galaxies*. The Astrophysical Journal, 313, 59.

Doroshkevich, A. G., Zel'dovich, Y. B., & Novikov, I. D., 1967. *The Origin of Galaxies in an Expanding Universe.* Astronomicheskii Zhurnal, 44, 295.

Dotter, A., Sarajedini, A., Anderson, J., Aparicio, A., Bedin, L. R., Chaboyer, B., Majewski, S., et al., 2010. *The ACS Survey of Galactic Globular Clusters. IX. Horizontal Branch Morphology and the Second Parameter Phenomenon*. The Astrophysical Journal, 708, 698.

Dressler, A., 1980. *Galaxy morphology in rich clusters - Implications for the formation and evolution of galaxies*. The Astrophysical Journal, 236, 351.

Dressler, A. & Gunn, J. E., 1983. *Spectroscopy of galaxies in distant clusters. II - The population of the 3C 295 cluster*. The Astrophysical Journal, 270, 7.

Dressler, A., Lynden-Bell, D., Burstein, D., Davies, R. L., Faber, S. M., Terlevich, R., & Wegner, G., 1987. *Spectroscopy and photometry of elliptical galaxies. I - A new distance estimator*. The Astrophysical Journal, 313, 42.

Drinkwater, M. & Hardy, E., 1991. *Extreme blue compact dwarf galaxies in the Virgo Cluster*. The Astronomical Journal, 101, 94.

Drinkwater, M. J., Currie, M. J., Young, C. K., Hardy, E., & Yearsley, J. M., 1996. *Blue compact dwarf galaxies and new velocities in Virgo*. Monthly Notices of the Royal Astronomical Society, 279, 595.

Drinkwater, M. J., Jones, J. B., Gregg, M. D., & Phillipps, S., 2000. *Compact stellar systems in the Fornax Cluster: Super-massive star clusters or extremely compact dwarf galaxies?* Publications of the Astronomical Society of Australia, 17, 227.

Duc, P.-A., Braine, J., Lisenfeld, U., Brinks, E., & Boquien, M., 2007. *VCC 2062: an old tidal dwarf galaxy in the Virgo cluster?* Astronomy & Astrophysics, 475, 187.

Durrell, P. R., Ciardullo, R., Feldmeier, J. J., Jacoby, G. H., & Sigurdsson, S., 2002. *Intracluster Red Giant Stars in the Virgo Cluster*. The Astrophysical Journal, 570, 119.

Durrell, P. R., Harris, W. E., Geisler, D., & Pudritz, R. E., 1996. *Globular Cluster Systems in Dwarf Elliptical Galaxies. II. The Virgo Cluster*. The Astronomical Journal, 112, 972.

Durrell, P. R., Williams, B. F., Ciardullo, R., Feldmeier, J. J., von Hippel, T., Sigurdsson, S., Jacoby, G. H., et al., 2007. *The Resolved Stellar Populations of a Dwarf Spheroidal Galaxy in the Virgo Cluster*. The Astrophysical Journal, 656, 746.

Eggen, O. J., Lynden-Bell, D., & Sandage, A. R., 1962. *Evidence from the motions of old stars that the Galaxy collapsed.* The Astrophysical Journal, 136, 748.

Einasto, J., Kaasik, A., & Saar, E., 1974a. *Dynamic evidence on massive coronas of galaxies*. Nature, 250, 309.

Einasto, J., Saar, E., Kaasik, A., & Chernin, A. D., 1974b. *Missing mass around galaxies: morphological evidence*. Nature, 252, 111.

Einstein, A., 1916. *Die Grundlage der allgemeinen Relativitätstheorie*. Annalen der Physik, 354, 769.

Einstein, A., 1936. *Lens-Like Action of a Star by the Deviation of Light in the Gravitational Field*. Science, 84, 506.

Eisenstein, D. J., Zehavi, I., Hogg, D. W., Scoccimarro, R., Blanton, M. R., Nichol, R. C., Scranton, R., et al., 2005. *Detection of the Baryon Acoustic Peak in the Large-Scale Correlation Function of SDSS Luminous Red Galaxies*. The Astrophysical Journal, 633, 560.

Ekholm, T., Lanoix, P., Teerikorpi, P., Paturel, G., & Fouqué, P., 1999. *Investigations of the Local supercluster velocity field. II. A study using Tolman-Bondi solution and galaxies with accurate distances from the Cepheid PL-relation*. Astronomy & Astrophysics, 351, 827.

Evstigneeva, E. A., Gregg, M. D., & Drinkwater, M. J., 2005. *The Origin of UCDs in the Virgo Cluster*. arXiv:astro-ph/0504289, 4289.

Faber, S. M., 1973. *Variations in Spectral-Energy Distributions and Absorption-Line Strengths among Elliptical Galaxies*. The Astrophysical Journal, 179, 731.

Feast, M., 1999. *Cepheids as Distance Indicators*. The Publications of the Astronomical Society of the Pacific, 111, 775.

Feldmeier, J. J., Ciardullo, R., & Jacoby, G. H., 1998. *Intracluster Planetary Nebulae in the Virgo Cluster. I. Initial Results*. The Astrophysical Journal, 503, 109.

Ferguson, H. C. & Binggeli, B., 1994. *Dwarf elliptical galaxies*. Astronomy & Astrophysics Reviews, 6, 67.

Ferguson, H. C. & Sandage, A., 1989. *The spatial distributions and intrinsic shapes of dwarf elliptical galaxies in the Virgo and Fornax Clusters*. The Astrophysical Journal Letters, 346, L53.

Ferguson, H. C., Tanvir, N. R., & von Hippel, T., 1998. *Detection of intergalactic red-giant-branch stars in the Virgo cluster*. Nature, 391, 461.

Ferrara, A. & Tolstoy, E., 2000. *The role of stellar feedback and dark matter in the evolution of dwarf galaxies*. Monthly Notices of the Royal Astronomical Society, 313, 291.

Ferrarese, L., Côté, P., Cuillandre, J.-C., Gwyn, S. D. J., Peng, E. W., MacArthur, L. A., Duc, P.-A., et al., 2012. *The Next Generation Virgo Cluster Survey (NGVS). I. Introduction to the Survey*. The Astrophysical Journal Supplement Series, 200, 4.

Ferrarese, L., Côté, P., Jordán, A., Peng, E. W., Blakeslee, J. P., Piatek, S., Mei, S., et al., 2006. *The ACS Virgo Cluster Survey. VI. Isophotal Analysis and the Structure of Early-Type Galaxies*. The Astrophysical Journal Supplement Series, 164, 334.

Ferrarese, L., Freedman, W. L., Hill, R. J., Saha, A., Madore, B. F., Kennicutt, R., Stetson, P. B., et al., 1996. *The Extragalactic Distance Scale Key Project. IV. The Discovery of Cepheids and a New Distance to M100 Using the Hubble Space Telescope*. The Astrophysical Journal, 464, 568.

Ferreras, I., Charlot, S., & Silk, J., 1999. *The Age and Metallicity Range of Early-Type Galaxies in Clusters*. The Astrophysical Journal, 521, 81.

Fields, B. D., 2011. *The Primordial Lithium Problem*. Annual Review of Nuclear and Particle Science, 61, 47.

Fouqué, P., Solanes, J. M., Sanchis, T., & Balkowski, C., 2001. *Structure, mass and distance of the Virgo cluster from a Tolman-Bondi model*. Astronomy & Astrophysics, 375, 770.

Francis, K. J., Drinkwater, M. J., Chilingarian, I. V., Bolt, A. M., & Firth, P., 2012. *The chemical composition of ultracompact dwarf galaxies in the Virgo and Fornax clusters*. Monthly Notices of the Royal Astronomical Society, 425, 325.

Frebel, A., Christlieb, N., Norris, J. E., Thom, C., Beers, T. C., & Rhee, J., 2007. *Discovery of HE 1523-0901, a Strongly r-Process-enhanced Metal-poor Star with Detected Uranium*. The Astrophysical Journal Letters, 660, L117.

Freedman, W. L., Madore, B. F., Gibson, B. K., Ferrarese, L., Kelson, D. D., Sakai, S., Mould, J. R., et al., 2001. *Final Results from the Hubble Space Telescope Key Project to Measure the Hubble Constant*. The Astrophysical Journal, 553, 47.

Freedman, W. L., Madore, B. F., Mould, J. R., Hill, R., Ferrarese, L., Kennicutt, R. C., Saha, A., et al., 1994. *Distance to the Virgo cluster galaxy M100 from Hubble Space Telescope observations of Cepheids*. Nature, 371, 757.

Friedman, A., 1922. *Über die Krümmung des Raumes*. Zeitschrift für Physik, 10, 377.

Fukugita, M., Okamura, S., & Yasuda, N., 1993. *Spatial distribution of spiral galaxies in the Virgo Cluster from the Tully-Fisher relation*. The Astrophysical Journal Letters, 412, L13.

Gallazzi, A., Charlot, S., Brinchmann, J., & White, S. D. M., 2006. *Ages and metallicities of early-type galaxies in the Sloan Digital Sky Survey: new insight into the physical origin of the colour-magnitude and the Mg_2 − σ_V relations*. Monthly Notices of the Royal Astronomical Society, 370, 1106.

Gamow, G., 1946. *Expanding Universe and the Origin of Elements*. Physical Review, 70, 572.

Gamow, G. & Teller, E., 1939. *The Expanding Universe and the Origin of the Great Nebulæ*. Nature, 143, 116.

Gavazzi, G., Boselli, A., Scodeggio, M., Pierini, D., & Belsole, E., 1999. *The 3D structure of the Virgo cluster from H-band Fundamental Plane and Tully-Fisher distance determinations*. Monthly Notices of the Royal Astronomical Society, 304, 595.

Gavazzi, G., Contursi, A., Carrasco, L., Boselli, A., Kennicutt, R., Scodeggio, M., & Jaffe, W., 1995. *The radio and optical structure of three peculiar galaxies in A 1367*. Astronomy & Astrophysics, 304, 325.

Gavazzi, G., Franzetti, P., Scodeggio, M., Boselli, A., & Pierini, D., 2000. *1.65 ÎŒm (H-band) surface photometry of galaxies. V. Profile decomposition of 1157 galaxies*. Astronomy & Astrophysics, 361, 863.

Gavazzi, G., Zibetti, S., Boselli, A., Franzetti, P., Scodeggio, M., & Martocchi, S., 2001. *1.65 ÎŒm (H-band) surface photometry of galaxies. VII. Dwarf galaxies in the Virgo Cluster*. Astronomy & Astrophysics, 372, 29.

Geha, M., Guhathakurta, P., & van der Marel, R. P., 2003. *Internal Dynamics, Structure, and Formation of Dwarf Elliptical Galaxies. II. Rotating versus Nonrotating Dwarfs*. The Astronomical Journal, 126, 1794.

Geller, M. J. & Huchra, J. P., 1989. *Mapping the universe*. Science, 246, 897.

Gerhard, O., Arnaboldi, M., Freeman, K. C., & Okamura, S., 2002. *Isolated Star Formation: A Compact H II Region in the Virgo Cluster*. The Astrophysical Journal Letters, 580, L121.

Gerhard, O. E. & Spergel, D. N., 1992. *Dwarf spheroidal galaxies and the mass of the neutrino*. The Astrophysical Journal Letters, 389, L9.

Gerssen, J. & Shapiro Griffin, K., 2012. *Disc heating agents across the Hubble sequence*. Monthly Notices of the Royal Astronomical Society, 423, 2726.

Giovanelli, R., Haynes, M. P., Kent, B. R., Perillat, P., Saintonge, A., Brosch, N., Catinella, B., et al., 2005. *The Arecibo Legacy Fast ALFA Survey. I. Science Goals, Survey Design, and Strategy*. The Astronomical Journal, 130, 2598.

Governato, F., Brook, C., Mayer, L., Brooks, A., Rhee, G., Wadsley, J., Jonsson, P., et al., 2010. *Bulgeless dwarf galaxies and dark matter cores from supernova-driven outflows*. Nature, 463, 203.

Governato, F., Zolotov, A., Pontzen, A., Christensen, C., Oh, S. H., Brooks, A. M., Quinn, T., et al., 2012. *Cuspy no more: how outflows affect the central dark matter and baryon distribution in Λ cold dark matter galaxies*. Monthly Notices of the Royal Astronomical Society, 422, 1231.

Graham, A. W., 2011. *A review of elliptical and disc galaxy structure, and modern scaling laws*. arXiv:1108.0997.

Graham, A. W., Driver, S. P., Petrosian, V., Conselice, C. J., Bershady, M. A., Crawford, S. M., & Goto, T., 2005. *Total Galaxy Magnitudes and Effective Radii from Petrosian Magnitudes and Radii*. The Astronomical Journal, 130, 1535.

Graham, A. W. & Guzmán, R., 2003. *HST Photometry of Dwarf Elliptical Galaxies in Coma, and an Explanation for the Alleged Structural Dichotomy between Dwarf and Bright Elliptical Galaxies*. The Astronomical Journal, 125, 2936.

Graham, A. W., Spitler, L. R., Forbes, D. A., Lisker, T., Moore, B., & Janz, J., 2012. *LEDA 074886: A Remarkable Rectangular-looking Galaxy*. The Astrophysical Journal, 750, 121.

Graham, A. W. & Worley, C. C., 2008. *Inclination- and dust-corrected galaxy parameters: bulge-to-disc ratios and size-luminosity relations*. Monthly Notices of the Royal Astronomical Society, 388, 1708.

Grant, N. I., Kuipers, J. A., & Phillipps, S., 2005. *Nucleated dwarf elliptical galaxies in the Virgo cluster*. Monthly Notices of the Royal Astronomical Society, 363, 1019.

Grebel, E. K., 2001. *Star Formation Histories of Nearby Dwarf Galaxies*. Astrophysics and Space Science, 277, 231.

Gunn, J. E., Carr, M., Rockosi, C., Sekiguchi, M., Berry, K., Elms, B., de Haas, E., et al., 1998. *The Sloan Digital Sky Survey Photometric Camera*. The Astronomical Journal, 116, 3040.

Gunn, J. E. & Gott, J. R. I., 1972. *On the Infall of Matter Into Clusters of Galaxies and Some Effects on Their Evolution*. The Astrophysical Journal, 176, 1.

Guo, Q., White, S., Boylan-Kolchin, M., de Lucia, G., Kauffmann, G., Lemson, G., Li, C., et al., 2011. *From dwarf spheroidals to cD galaxies: simulating the galaxy population in a ΛCDM cosmology*. Monthly Notices of the Royal Astronomical Society, 413, 101.

Guo, Q., White, S., Li, C., & Boylan-Kolchin, M., 2010. *How do galaxies populate dark matter haloes?* Monthly Notices of the Royal Astronomical Society, 404, 1111.

Guth, A. H., 1981. *Inflationary universe: A possible solution to the horizon and flatness problems*. Physical Review D, 23, 347.

Hanuschik, R. W., 2003. *A flux-calibrated, high-resolution atlas of optical sky emission from UVES*. Astronomy & Astrophysics, 407, 1157.

Harris, W. E., 1991. *Globular Cluster Systems in Galaxies Beyond the Local Group*. Annual Review of Astronomy & Astrophysics, 29, 543.

Haşegan, M., Jordán, A., Côté, P., Djorgovski, S. G., McLaughlin, D. E., Blakeslee, J. P., Mei, S., et al., 2005. *The ACS Virgo Cluster Survey. VII. Resolving the Connection between Globular Clusters and Ultracompact Dwarf Galaxies*. The Astrophysical Journal, 627, 203.

Hawking, S. W., 1974. *The anisotropy of the Universe at large times*. In *In: Confrontation of cosmological theories with observational data; Proceedings of the Symposium*. Cambridge University, Cambridge, England, 283–286.

Hernquist, L., 1992. *Structure of merger remnants. I - Bulgeless progenitors*. The Astrophysical Journal, 400, 460.

Hewett, P. C., Warren, S. J., Leggett, S. K., & Hodgkin, S. T., 2006. *The UKIRT Infrared Deep Sky Survey ZY JHK photometric system: passbands and synthetic colours*. Monthly Notices of the Royal Astronomical Society, 367, 454.

Hilker, M., Infante, L., Vieira, G., Kissler-Patig, M., & Richtler, T., 1999. *The central region of the Fornax cluster. II. Spectroscopy and radial velocities of member and background galaxies*. Astronomy & Astrophysics Supplement Series, 134, 75.

Hoyle, F., 1953. *On the Fragmentation of Gas Clouds Into Galaxies and Stars.* The Astrophysical Journal, 118, 513.

Hu, W. & Dodelson, S., 2002. *Cosmic Microwave Background Anisotropies*. Annual Review of Astronomy & Astrophysics, 40, 171.

Hubble, E., 1929. *A Relation between Distance and Radial Velocity among Extra-Galactic Nebulae.* In *Proceedings of the National Academy of Sciences of the United States of America*. 168–173.

Hubble, E. P., 1926. *Extragalactic nebulae.* The Astrophysical Journal, 64, 321.

Hubble, E. P., 1936. *Realm of the Nebulae*. Realm of the Nebulae.

Hunter, C., 1962. *The Instability of the Collapse of a Self-Gravitating Gas Cloud.* The Astrophysical Journal, 136, 594.

Ishak, M., 2007. *Remarks on the Formulation of the Cosmological Constant/Dark Energy Problems*. Foundations of Physics, 37, 1470.

Janz, J., Laurikainen, E., Lisker, T., Salo, H., Peletier, R. F., Niemi, S.-M., den Brok, M., et al., 2012. *Dissecting Early-type Dwarf Galaxies into Their Multiple Components*. The Astrophysical Journal Letters, 745, L24.

Janz, J. & Lisker, T., 2008. *The Sizes of Early-Type Galaxies*. The Astrophysical Journal Letters, 689, L25.

Janz, J. & Lisker, T., 2009a. *A continuum of structure and stellar content from Virgo cluster early-type dwarfs to giants?* Astronomische Nachrichten, 330, 948.

Janz, J. & Lisker, T., 2009b. *On the Color Magnitude Relation of Early-type Galaxies*. The Astrophysical Journal Letters, 696, L102.

Jarosik, N., Bennett, C. L., Dunkley, J., Gold, B., Greason, M. R., Halpern, M., Hill, R. S., et al., 2011. *Seven-year Wilkinson Microwave Anisotropy Probe (WMAP) Observations: Sky Maps, Systematic Errors, and Basic Results*. The Astrophysical Journal Supplement Series, 192, 14.

Jeans, J. H., 1902. *The Stability of a Spherical Nebula.* Philosophical Transactions of the Royal Society of London. Series A, Containing Papers of a Mathematical or Physical Character, 199, 1.

Jedrzejewski, R. I., 1987. *CCD surface photometry of elliptical galaxies. I - Observations, reduction and results*. Monthly Notices of the Royal Astronomical Society, 226, 747.

Jerjen, H. & Binggeli, B., 1997. *Are "Dwarf" Ellipticals Genuine Ellipticals?* The Nature of Elliptical Galaxies; 2nd Stromlo Symposium, 116, 239.

Jerjen, H., Binggeli, B., & Barazza, F. D., 2004. *Distances, Metallicities, and Ages of Dwarf Elliptical Galaxies in the Virgo Cluster from Surface Brightness Fluctuations*. The Astronomical Journal, 127, 771.

Jerjen, H., Kalnajs, A., & Binggeli, B., 2000. *IC3328: A "dwarf elliptical galaxy" with spiral structure*. Astronomy & Astrophysics, 358, 845.

Jerjen, H. & Tammann, G. A., 1997. *Studies of the Centaurus cluster. III. Luminosity functions of individual Hubble-types as compared to Virgo and Fornax.* The Astrophysical Journal, 321, 713.

Jones, J. B., Drinkwater, M. J., Jurek, R., Phillipps, S., Gregg, M. D., Bekki, K., Couch, W. J., et al., 2006. *Discovery of Ultracompact Dwarf Galaxies in the Virgo Cluster*. The Astronomical Journal, 131, 312.

Juneau, S., Glazebrook, K., Crampton, D., McCarthy, P. J., Savaglio, S., Abraham, R., Carlberg, R. G., et al., 2005. *Cosmic Star Formation History and Its Dependence on Galaxy Stellar Mass*. The Astrophysical Journal Letters, 619, L135.

Kaiser, N., Wilson, G., & Luppino, G. A., 2000. *Large-Scale Cosmic Shear Measurements*. arXiv:astro-ph/0003338.

Kalirai, J. S., 2012. *The age of the Milky Way inner halo.* Nature, 486, 90.

Karick, A. M., Drinkwater, M. J., & Gregg, M. D., 2003. *The surface brightness and colour-magnitude relations for Fornax cluster galaxies*. Monthly Notices of the Royal Astronomical Society, 344, 188.

Kelson, D. D., 2003. *Optimal Techniques in Two-dimensional Spectroscopy: Background Subtraction for the 21st Century*. Publications of the Astronomical Society of the Pacific, 115, 688.

Kereš, D., Katz, N., Davé, R., Fardal, M., & Weinberg, D. H., 2009. *Galaxies in a simulated ΛCDM universe - II. Observable properties and constraints on feedback.* Monthly Notices of the Royal Astronomical Society, 396, 2332.

King, I. R., 1966. *The structure of star clusters. III. Some simple dvriamical models.* The Astronomical Journal, 71, 64.

Klypin, A., Kravtsov, A. V., Valenzuela, O., & Prada, F., 1999. *Where Are the Missing Galactic Satellites?* The Astrophysical Journal, 522, 82.

Kodama, T. & Arimoto, N., 1997. *Origin of the colour-magnitude relation of elliptical galaxies.* Astronomy & Astrophysics, 320, 41.

Komatsu, E., Smith, K. M., Dunkley, J., Bennett, C. L., Gold, B., Hinshaw, G., Jarosik, N., et al., 2011. *Seven-year Wilkinson Microwave Anisotropy Probe (WMAP) Observations: Cosmological Interpretation*. The Astrophysical Journal Supplement Series, 192, 18.

Kormendy, J., 1985. *Families of ellipsoidal stellar systems and the formation of dwarf elliptical galaxies*. The Astrophysical Journal, 295, 73.

Kormendy, J. & Bender, R., 1994. *CFHT Photometry of Virgo Cluster Elliptical Galaxies*. Dwarf Galaxies, 49, 161.

Kormendy, J. & Bender, R., 2012. *A Revised Parallel-sequence Morphological Classification of Galaxies: Structure and Formation of So and Spheroidal Galaxies*. The Astrophysical Journal Supplement Series, 198, 2.

Kormendy, J., Drory, N., Bender, R., & Cornell, M. E., 2010. *Bulgeless Giant Galaxies Challenge Our Picture of Galaxy Formation by Hierarchical Clustering*. The Astrophysical Journal, 723, 54.

Kormendy, J., Fisher, D. B., Cornell, M. E., & Bender, R., 2009. *Structure and Formation of Elliptical and Spheroidal Galaxies*. The Astrophysical Journal Supplement Series, 182, 216.

Kormendy, J. & Kennicutt, R. C., Jr., 2004. *Secular evolution and the formation of pseudobulges in disk galaxies*. Annual Review of Astronomy & Astrophysics, 42, 603.

Kravtsov, A. V., Gnedin, O. Y., & Klypin, A. A., 2004. *The Tumultuous Lives of Galactic Dwarfs and the Missing Satellites Problem*. The Astrophysical Journal, 609, 482.

Kroupa, P., 2012. *The Dark Matter Crisis: Falsification of the Current Standard Model of Cosmology*. Publications of the Astronomical Society of Australia, 29, 395.

Kroupa, P., Famaey, B., de Boer, K. S., Dabringhausen, J., Pawlowski, M. S., Boily, C. M., Jerjen, H., et al., 2010. *Local-Group tests of dark-matter concordance cosmology*. Astronomy & Astrophysics, 523, A32.

Kuijken, K. & Dubinski, J., 1995. *Nearly Self-Consistent Disc / Bulge / Halo Models for Galaxies*. Monthly Notices of the Royal Astronomical Society, 277, 1341.

Larson, R. B., 1974. *Effects of supernovae on the early evolution of galaxies*. Monthly Notices of the Royal Astronomical Society, 169, 229.

Larson, R. B., Tinsley, B. M., & Caldwell, C. N., 1980. *The evolution of disk galaxies and the origin of So galaxies*. The Astrophysical Journal, 237, 692.

Lauer, T. R., Faber, S. M., Richstone, D., Gebhardt, K., Tremaine, S., Postman, M., Dressler, A., et al., 2007. *The Masses of Nuclear Black Holes in Luminous Elliptical Galaxies and Implications for the Space Density of the Most Massive Black Holes*. The Astrophysical Journal, 662, 808.

Laurikainen, E. & Salo, H., 2001. *BVRI imaging of M51-type interacting galaxy pairs - III. Analysis of the photometric parameters*. Monthly Notices of the Royal Astronomical Society, 324, 685.

Laurikainen, E., Salo, H., & Buta, R., 2005. *Multicomponent decompositions for a sample of So galaxies*. Monthly Notices of the Royal Astronomical Society, 362, 1319.

Laurikainen, E., Salo, H., Buta, R., & Knapen, J. H., 2011. *Near-infrared atlas of So-Sa galaxies (NIRSoS)*. Monthly Notices of the Royal Astronomical Society, 418, 1452.

Laurikainen, E., Salo, H., Buta, R., & Vasylyev, S., 2004. *Bar-induced perturbation strengths of the galaxies in the Ohio State University Bright Galaxy Survey - I*. Monthly Notices of the Royal Astronomical Society, 355, 1251.

Leavitt, H. S. & Pickering, E. C., 1912. *Periods of 25 Variable Stars in the Small Magellanic Cloud*. Harvard College Observatory Circular, 173, 1.

Lee, M. G., Park, H. S., & Hwang, H. S., 2010. *Detection of a Large-Scale Structure of Intracluster Globular Clusters in the Virgo Cluster*. Science, 328, 334.

Leinert, C., Bowyer, S., Haikala, L. K., Hanner, M. S., Hauser, M. G., Levasseur-Regourd, A. C., Mann, I., et al., 1998. *The 1997 reference of diffuse night sky brightness*. Astronomy & Astrophysics Supplement Series, 127, 1.

Lemaître, G., 1927. *Un Univers homogène de masse constante et de rayon croissant rendant compte de la vitesse radiale des nébuleuses extra-galactiques*. Annales de la Societe Scietifique de Bruxelles, 47, 49.

Lieder, S., Lisker, T., Hilker, M., Misgeld, I., & Durrell, P., 2012. *A deep view on the Virgo cluster core*. Astronomy & Astrophysics, 538, 69.

Lifshitz, E., 1946. *On the gravitational stability of the expanding universe*. J Phys(USSR), 10, 116.

Lin, D. N. C. & Faber, S. M., 1983. *Some implications of nonluminous matter in dwarf spheroidal galaxies*. The Astrophysical Journal Letters, 266, L21.

Lisker, T., 2009. *Early-type dwarf galaxies in clusters: A mixed bag with various origins?* Astronomische Nachrichten, 330, 1043.

Lisker, T., Glatt, K., Westera, P., & Grebel, E. K., 2006a. *Virgo Cluster Early-Type Dwarf Galaxies with the Sloan Digital Sky Survey. II. Early-Type Dwarfs with Central Star Formation*. The Astronomical Journal, 132, 2432.

Lisker, T., Grebel, E. K., & Binggeli, B., 2006b. *Virgo Cluster Early-Type Dwarf Galaxies with the Sloan Digital Sky Survey. I. On the Possible Disk Nature of Bright Early-Type Dwarfs*. The Astronomical Journal, 132, 497.

Lisker, T., Grebel, E. K., & Binggeli, B., 2008. *Virgo Cluster Early-Type Dwarf Galaxies with the Sloan Digital Sky Survey. Iv. The Color-Magnitude Relation*. The Astronomical Journal, 135, 380.

Lisker, T., Grebel, E. K., Binggeli, B., & Glatt, K., 2007. *Virgo Cluster Early-Type Dwarf Galaxies with the Sloan Digital Sky Survey. III. Subpopulations: Distributions, Shapes, Origins*. The Astrophysical Journal, 660, 1186.

Lisker, T. & Han, Z., 2008. *Stellar Age versus Mass of Early-Type Galaxies in the Virgo Cluster*. The Astrophysical Journal, 680, 1042.

Lisker, T., Janz, J., Hensler, G., Kim, S., Rey, S.-C., Weinmann, S., Mastropietro, C., et al., 2009. *The First Generation of Virgo Cluster Dwarf Elliptical Galaxies?* The Astrophysical Journal Letters, 706, L124.

Łokas, E. L., Kazantzidis, S., & Mayer, L., 2011. *Evolutionary Tracks of Tidally Stirred Disky Dwarf Galaxies*. The Astrophysical Journal, 739, 46.

Lord, S. D., 1992. *A new software tool for computing Earth's atmospheric transmission of near- and far-infrared radiation*. NASA Technical Memorandum 103957.

Lotz, J. M., Primack, J., & Madau, P., 2004. *A New Nonparametric Approach to Galaxy Morphological Classification*. The Astronomical Journal, 128, 163.

Lovell, M. R., Eke, V., Frenk, C. S., Gao, L., Jenkins, A., Theuns, T., Wang, J., et al., 2012. *The haloes of bright satellite galaxies in a warm dark matter universe*. Monthly Notices of the Royal Astronomical Society, 420, 2318.

Maihara, T., Iwamuro, F., Yamashita, T., Hall, D. N. B., Cowie, L. L., Tokunaga, A. T., & Pickles, A., 1993. *Observations of the OH airglow emission*. Astronomical Society of the Pacific, 105, 940.

Markevitch, M., Gonzalez, A. H., Clowe, D., Vikhlinin, A., Forman, W., Jones, C., Murray, S., et al., 2004. *Direct Constraints on the Dark Matter Self-Interaction Cross Section from the Merging Galaxy Cluster 1E 0657-56*. The Astrophysical Journal, 606, 819.

Martinez-Delgado, D., Romanowsky, A. J., Gabany, R. J., Annibali, F., Arnold, J. A., Fliri, J., Zibetti, S., et al., 2012. *Dwarfs Gobbling Dwarfs: A Stellar Tidal Stream around NGC 4449 and Hierarchical Galaxy Formation on Small Scales*. The Astrophysical Journal Letters, 748, L24.

Massey, R., Kitching, T., & Richard, J., 2010. *The dark matter of gravitational lensing*. Reports on Progress in Physics, 73, 6901.

Mastropietro, C., Moore, B., Mayer, L., Debattista, V. P., Piffaretti, R., & Stadel, J., 2005. *Morphological evolution of discs in clusters*. Monthly Notices of the Royal Astronomical Society, 364, 607.

Mateo, M. L., 1998. *Dwarf Galaxies of the Local Group*. Annual Review of Astronomy & Astrophysics, 36, 435.

Mather, J. C., Cheng, E. S., Eplee, R. E. J., Isaacman, R. B., Meyer, S. S., Shafer, R. A., Weiss, R., et al., 1990. *A preliminary measurement of the cosmic microwave background spectrum by the Cosmic Background Explorer (COBE) satellite*. The Astrophysical Journal Letters, 354, L37.

Mayer, L., Governato, F., Colpi, M., Moore, B., Quinn, T., Wadsley, J., Stadel, J., et al., 2001a. *The Metamorphosis of Tidally Stirred Dwarf Galaxies*. The Astrophysical Journal, 559, 754.

Mayer, L., Governato, F., Colpi, M., Moore, B., Quinn, T., Wadsley, J., Stadel, J., et al., 2001b. *Tidal Stirring and the Origin of Dwarf Spheroidals in the Local Group*. The Astrophysical Journal Letters, 547, L123.

McDonald, M., Courteau, S., Tully, R. B., & Roediger, J., 2011. *A survey of 286 Virgo cluster galaxies at optical griz and near-IR H band: surface brightness profiles and bulge-disc decompositions*. Monthly Notices of the Royal Astronomical Society, 414, 2055.

McLaughlin, D. E., 1999. *Evidence in Virgo for the Universal Dark Matter Halo*. The Astrophysical Journal Letters, 512, L9.

Mei, S., Blakeslee, J. P., Côté, P., Tonry, J. L., West, M. J., Ferrarese, L., Jordán, A., et al., 2007. *The ACS Virgo Cluster Survey. XIII. SBF Distance Catalog and the Three-dimensional Structure of the Virgo Cluster*. The Astrophysical Journal, 655, 144.

Meinel, I. A. B., 1950. *OH Emission Bands in the Spectrum of the Night Sky.* The Astrophysical Journal, 111, 555.

Méndez-Abreu, J., Sánchez-Janssen, R., & Aguerri, J. A. L., 2010. *Which Galaxies Host Bars and Disks? A Study of the Coma Cluster*. The Astrophysical Journal Letters, 711, L61.

Michielsen, D., Boselli, A., Conselice, C. J., Toloba, E., Whiley, I. M., Aragón-Salamanca, A., Balcells, M., et al., 2008. *The relation between stellar populations, structure and environment for dwarf elliptical galaxies from the MAGPOP-ITP*. Monthly Notices of the Royal Astronomical Society, 385, 1374.

Mieske, S., Hilker, M., & Infante, L., 2002. *Ultra compact objects in the Fornax cluster of galaxies: Globular clusters or dwarf galaxies?* Astronomy & Astrophysics, 383, 823.

Mieske, S., Hilker, M., & Infante, L., 2004. *Fornax compact object survey FCOS: On the nature of Ultra Compact Dwarf galaxies*. Astronomy & Astrophysics, 418, 445.

Mieske, S., Hilker, M., Infante, L., & Mendes de Oliveira, C., 2007. *The early-type dwarf galaxy population of the Fornax cluster*. Astronomy & Astrophysics, 463, 503.

Mihos, J. C., Harding, P., Feldmeier, J., & Morrison, H., 2005. *Diffuse Light in the Virgo Cluster*. The Astrophysical Journal Letters, 631, L41.

Miller, B. W., Lotz, J. M., Ferguson, H. C., Stiavelli, M., & Whitmore, B. C., 1998. *The Specific Globular Cluster Frequencies of Dwarf Elliptical Galaxiesfrom the Hubble Space Telescope*. The Astrophysical Journal Letters, 508, L133.

Minchin, R., Davies, J., Disney, M., Boyce, P., Garcia, D., Jordan, C., Kilborn, V., et al., 2005. *A Dark Hydrogen Cloud in the Virgo Cluster*. The Astrophysical Journal Letters, 622, L21.

Misgeld, I., Mieske, S., & Hilker, M., 2008. *The early-type dwarf galaxy population of the Hydra I cluster*. Astronomy & Astrophysics, 486, 697.

Misner, C. W., 1969. *Mixmaster Universe*. Physical Review Letters, 22, 1071.

Mo, H., van den Bosch, F., & White, S., 2010. *Galaxy Formation and Evolution*. Cambridge University Press.

Moore, B., Ghigna, S., Governato, F., Lake, G., Quinn, T., Stadel, J., & Tozzi, P., 1999a. *Dark Matter Substructure within Galactic Halos*. The Astrophysical Journal Letters, 524, L19.

Moore, B., katz, N., Lake, G., Dressler, A., & Oemler, A., 1996. *Galaxy harassment and the evolution of clusters of galaxies*. Nature, 379, 613.

Moore, B., Lake, G., & Katz, N., 1998. *Morphological Transformation from Galaxy Harassment*. The Astrophysical Journal, 495, 139.

Moore, B., Lake, G., Quinn, T., & Stadel, J., 1999b. *On the survival and destruction of spiral galaxies in clusters*. Monthly Notices of the Royal Astronomical Society, 304, 465.

Moss, C., 2006. *Enhanced mergers of galaxies in low-redshift clusters*. Monthly Notices of the Royal Astronomical Society, 373, 167.

Mukhanov, V., 2004. *Nucleosynthesis Without Computer*. International Journal of Theoretical Physics, 43, 669.

Naab, T., Johansson, P. H., & Ostriker, J. P., 2009. *Minor Mergers and the Size Evolution of Elliptical Galaxies*. The Astrophysical Journal Letters, 699, L178.

Nagashima, M., Yahagi, H., Enoki, M., Yoshii, Y., & Gouda, N., 2005. *Numerical Galaxy Catalog. I. A Semianalytic Model of Galaxy Formation with N-Body Simulations*. The Astrophysical Journal, 634, 26.

Navarro, J. F., Frenk, C. S., & White, S. D. M., 1997. *A Universal Density Profile from Hierarchical Clustering*. The Astrophysical Journal, 490, 493.

Noordermeer, E. & van der Hulst, J. M., 2007. *The stellar mass distribution in early-type disc galaxies: surface photometry and bulge?disc decompositions*. Monthly Notices of the Royal Astronomical Society, 376, 1480.

Norberg, P., Baugh, C. M., Hawkins, E., Maddox, S., Madgwick, D., Lahav, O., Cole, S., et al., 2002. *The 2dF Galaxy Redshift Survey: the dependence of galaxy clustering on luminosity and spectral type*. Monthly Notices of the Royal Astronomical Society, 332, 827.

Oh, K. S. & Lin, D. N. C., 2000. *Nucleation of Dwarf Galaxies in the Virgo Cluster*. The Astrophysical Journal, 543, 620.

Oh, S.-H., Brook, C., Governato, F., Brinks, E., Mayer, L., de Blok, W. J. G., Brooks, A., et al., 2011. *The Central Slope of Dark Matter Cores in Dwarf Galaxies: Simulations versus THINGS*. The Astronomical Journal, 142, 24.

Okazaki, T. & Taniguchi, Y., 2000. *Dwarf Galaxy Formation Induced by Galaxy Interactions*. The Astrophysical Journal, 543, 149.

Oke, J. B. & Gunn, J. E., 1983. *Secondary standard stars for absolute spectrophotometry*. The Astrophysical Journal, 266, 713.

Ostriker, J. P., Peebles, P. J. E., & Yahil, A., 1974. *The size and mass of galaxies, and the mass of the universe*. The Astrophysical Journal Letters, 193, L1.

Papaderos, P., Izotov, Y. I., Thuan, T. X., Noeske, K. G., Fricke, K. J., Guseva, N. G., & Green, R. F., 2002. *The blue compact dwarf galaxy I Zw 18: A comparative study of its low-surface-brightness component*. Astronomy & Astrophysics, 393, 461.

Papaderos, P., Loose, H.-H., Fricke, K. J., & Thuan, T. X., 1996. *Optical structure and star formation in blue compact dwarf galaxies. II. Relations between photometric components and evolutionary implications*. Astronomy & Astrophysics, 314, 59.

Parry, O. H., Eke, V. R., Frenk, C. S., & Okamoto, T., 2012. *The baryons in the Milky Way satellites*. Monthly Notices of the Royal Astronomical Society, 419, 3304.

Pasquali, A., van den Bosch, F. C., & Rix, H.-W., 2007. *The Isophotal Structure of Early-Type Galaxies in the SDSS: Dependence on Active Galactic Nucleus Activity and Environment*. The Astrophysical Journal, 664, 738.

Paudel, S., Lisker, T., & Janz, J., 2010a. *Nuclei of Early-type Dwarf Galaxies: Are They Progenitors of Ultracompact Dwarf Galaxies?* The Astrophysical Journal Letters, 724, L64.

Paudel, S., Lisker, T., & Kuntschner, H., 2011. *Nuclei of early-type dwarf galaxies: insights from stellar populations*. Monthly Notices of the Royal Astronomical Society, 413, 1764.

Paudel, S., Lisker, T., Kuntschner, H., Grebel, E. K., & Glatt, K., 2010b. *Stellar populations of Virgo cluster early-type dwarf galaxies with and without discs: a dichotomy in age?* Monthly Notices of the Royal Astronomical Society, 405, 800.

Pedraz, S., Gorgas, J., Cardiel, N., Sánchez-Blázquez, P., & Guzmán, R., 2002. *Evidence of fast rotation in dwarf elliptical galaxies*. The Astrophysical Journal Letters, 332, L59.

Peebles, P. J. E. & Dicke, R. H., 1968. *Origin of the Globular Star Clusters*. The Astrophysical Journal, 154, 891.

Peng, C. Y., Ho, L. C., Impey, C. D., & Rix, H.-W., 2010. *Detailed Decomposition of Galaxy Images. II. Beyond Axisymmetric Models*. The Astronomical Journal, 139, 2097.

Peng, E. W., Jordán, A., Côté, P., Blakeslee, J. P., Ferrarese, L., Mei, S., West, M. J., et al., 2006. *The ACS Virgo Cluster Survey. IX. The Color Distributions of Globular Cluster Systems in Early-Type Galaxies*. The Astrophysical Journal, 639, 95.

Penny, S. J., Conselice, C. J., de Rijcke, S., & Held, E. V., 2009. *Hubble Space Telescope survey of the Perseus Cluster - I. The structure and dark matter content of cluster dwarf spheroidals*. Monthly Notices of the Royal Astronomical Society, 393, 1054.

Penzias, A. A. & Wilson, R. W., 1965. *A Measurement of Excess Antenna Temperature at 4080 Mc/s.* The Astrophysical Journal, 142, 419.

Percival, W. J., Reid, B. A., Eisenstein, D. J., Bahcall, N. A., Budavari, T., Frieman, J. A., Fukugita, M., et al., 2010. *Baryon acoustic oscillations in the Sloan Digital Sky Survey Data Release 7 galaxy sample*. Monthly Notices of the Royal Astronomical Society, 401, 2148.

Perlmutter, S., Aldering, G., Goldhaber, G., Knop, R. A., Nugent, P., Castro, P. G., Deustua, S., et al., 1999. *Measurements of Ω and Λ from 42 High-Redshift Supernovae*. The Astrophysical Journal, 517, 565.

Petrosian, V., 1976. *Surface brightness and evolution of galaxies*. The Astrophysical Journal Letters, 209, L1.

Phillipps, S., Drinkwater, M. J., Gregg, M. D., & Jones, J. B., 2001. *Ultracompact Dwarf Galaxies in the Fornax Cluster*. The Astrophysical Journal, 560, 201.

Pier, J. R., Munn, J. A., Hindsley, R. B., Hennessy, G. S., Kent, S. M., Lupton, R. H., & Ivezić, Ž., 2003. *Astrometric Calibration of the Sloan Digital Sky Survey*. The Astronomical Journal, 125, 1559.

Planck Collaboration, Ade, P. A. R., Aghanim, N., Arnaud, M., Ashdown, M., Aumont, J., Baccigalupi, C., et al., 2011. *Planckearly results. I. The Planckmission*. Astronomy & Astrophysics, 536, A1.

Pospelov, M. & Pradler, J., 2010. *Big Bang Nucleosynthesis as a Probe of New Physics*. Annual Review of Nuclear and Particle Science, 60, 539.

Press, W. H. & Schechter, P., 1974. *Formation of Galaxies and Clusters of Galaxies by Self-Similar Gravitational Condensation*. The Astrophysical Journal, 187, 425.

Proctor, R. N. & Sansom, A. E., 2002. *A comparison of stellar populations in galaxy spheroids across a wide range of Hubble types*. Monthly Notices of the Royal Astronomical Society, 333, 517.

Riess, A. G., Filippenko, A. V., Challis, P., Clocchiatti, A., Diercks, A., Garnavich, P. M., Gilliland, R. L., et al., 1998. *Observational Evidence from Supernovae for an Accelerating Universe and a Cosmological Constant*. The Astronomical Journal, 116, 1009.

Robertson, H. P., 1935. *Kinematics and World-Structure.* The Astrophysical Journal, 82, 284.

Roediger, E., 2009. *Ram pressure stripping of disk galaxies in galaxy clusters*. Astronomische Nachrichten, 330, 888.

Rousselot, P., Lidman, C., Cuby, J. G., Moreels, G., & Monnet, G., 2000. *Night-sky spectral atlas of OH emission lines in the near-infrared*. Astronomy & Astrophysics, 354, 1134.

Rubin, V. C., Thonnard, N., & Ford, W. K. J., 1980. *Rotational properties of 21 SC galaxies with a large range of luminosities and radii, from NGC 4605 /R = 4kpc/ to UGC 2885 /R = 122 kpc/*. The Astrophysical Journal, 238, 471.

Ruiz, L. O., Falceta-Gonçalves, D., Lanfranchi, G. A., & Caproni, A., 2012. *The mass loss process in dwarf galaxies from 3D hydrodynamical simulations: the role of dark matter and starbursts*. arXiv:1211.4068.

Ryś, A., Falcón-Barroso, J., & van de Ven, G., 2012. *Virgo Cluster and field dwarf ellipticals in 3D: I. On the variety of stellar kinematic and line-strength properties*. arXiv:1210.3591, 1210, 3591.

Sandage, A., 2005. *The Classification of Galaxies: Early History and Ongoing Developments*. Annual Review of Astronomy & Astrophysics, 43, 581.

Sandage, A. & Binggeli, B., 1984. *Studies of the Virgo cluster. III - A classification system and an illustrated atlas of Virgo cluster dwarf galaxies*. The Astronomical Journal, 89, 919.

Sandage, A., Binggeli, B., & Tammann, G. A., 1985. *Studies of the Virgo Cluster - Part Five - Luminosity Functions of Virgo Cluster Galaxies*. The Astronomical Journal, 90, 1759.

Sandage, A. & Visvanathan, N., 1978a. *Color-absolute magnitude relation for E and So galaxies. III - Fully corrected photometry for 405 galaxies: Comparison of color distributions for E and So field and cluster galaxies*. The Astrophysical Journal, 225, 742.

Sandage, A. & Visvanathan, N., 1978b. *The color-absolute magnitude relation for E and So galaxies. II - New colors, magnitudes, and types for 405 galaxies*. The Astrophysical Journal, 223, 707.

Scannapieco, C., White, S. D. M., Springel, V., & Tissera, P. B., 2011. *Formation history, structure and dynamics of discs and spheroids in simulated Milky Way mass galaxies*. Monthly Notices of the Royal Astronomical Society, 417, 154.

Schindler, S., Binggeli, B., & Böhringer, H., 1999. *Morphology of the Virgo cluster: Gas versus galaxies*. Astronomy & Astrophysics, 343, 420.

Schlegel, D. J., Finkbeiner, D. P., & Davis, M., 1998. *Maps of Dust Infrared Emission for Use in Estimation of Reddening and Cosmic Microwave Background Radiation Foregrounds*. The Astrophysical Journal, 500, 525.

Searle, L. & Zinn, R., 1978. *Compositions of halo clusters and the formation of the galactic halo*. The Astrophysical Journal, 225, 357.

Secker, J., Harris, W. E., & Plummer, J. D., 1997. *Dwarf Galaxies in the Coma Cluster. II. Photometry and Analysis*. Publications of the Astronomical Society of the Pacific, 109, 1377.

Shapiro, K. L., Gerssen, J., & van der Marel, R. P., 2003. *Observational Constraints on Disk Heating as a Function of Hubble Type*. The Astronomical Journal, 126, 2707.

Shlosman, I., Begelman, M. C., & Frank, J., 1990. *The fuelling of active galactic nuclei*. Nature, 345, 679.

Shlosman, I., Frank, J., & Begelman, M. C., 1989. *Bars within bars - A mechanism for fuelling active galactic nuclei*. Nature, 338, 45.

Silk, J., 1967. *Fluctuations in the Primordial Fireball*. Nature, 215, 1155.

Silk, J., 1968. *Cosmic Black-Body Radiation and Galaxy Formation*. The Astrophysical Journal, 151, 459.

Simien, F. & Prugniel, P., 2002. *Kinematical data on early-type galaxies. VI.* Astronomy & Astrophysics, 384, 371.

Smith, J. A., Tucker, D. L., Kent, S., Richmond, M. W., Fukugita, M., Ichikawa, T., Ichikawa, S.-I., et al., 2002. *The u′g′r′i′z′ Standard-Star System*. The Astronomical Journal, 123, 2121.

Smith, R., Davies, J. I., & Nelson, A. H., 2010. *How effective is harassment on infalling late-type dwarfs?* Monthly Notices of the Royal Astronomical Society, 405, 1723.

Smith, R., Fellhauer, M., & Assmann, P., 2012. *Ram pressure drag - the effects of ram pressure on dark matter and stellar disc dynamics.* Monthly Notices of the Royal Astronomical Society, 420, 1990.

Smith Castelli, A. V., Bassino, L. P., Richtler, T., Cellone, S. A., Aruta, C., & Infante, L., 2008. *Galaxy populations in the Antlia cluster - I. Photometric properties of early-type galaxies.* Monthly Notices of the Royal Astronomical Society, 386, 2311.

Smoot, G. F., Bennett, C. L., Kogut, A., Wright, E. L., Aymon, J., Boggess, N. W., Cheng, E. S., et al., 1992. *Structure in the COBE differential microwave radiometer first-year maps.* The Astrophysical Journal Letters, 396, L1.

Soderblom, D. R., 2010. *The Ages of Stars.* Annual Review of Astronomy & Astrophysics, 48, 581.

Somerville, R. S. & Primack, J. R., 1999. *Semi-analytic modelling of galaxy formation: the local Universe.* Monthly Notices of the Royal Astronomical Society, 310, 1087.

Spergel, D. N., Verde, L., Peiris, H. V., Komatsu, E., Nolta, M. R., Bennett, C. L., Halpern, M., et al., 2003. *First-Year Wilkinson Microwave Anisotropy Probe (WMAP) Observations: Determination of Cosmological Parameters.* The Astrophysical Journal Supplement Series, 148, 175.

Springel, V., 2005. *The cosmological simulation code GADGET-2.* Monthly Notices of the Royal Astronomical Society, 364, 1105.

Springel, V., White, S. D. M., Jenkins, A., Frenk, C. S., Yoshida, N., Gao, L., Navarro, J., et al., 2005. *Simulations of the formation, evolution and clustering of galaxies and quasars.* The Astrophysical Journal Supplement Series, 435, 629.

Stoughton, C., Lupton, R. H., Bernardi, M., Blanton, M. R., Burles, S., Castander, F. J., Connolly, A. J., et al., 2002. *Sloan Digital Sky Survey: Early Data Release.* The Astronomical Journal, 123, 485.

Strauss, M. A., Weinberg, D. H., Lupton, R. H., Narayanan, V. K., Annis, J., Bernardi, M., Blanton, M., et al., 2002. *Spectroscopic Target Selection in the Sloan Digital Sky Survey: The Main Galaxy Sample.* The Astronomical Journal, 124, 1810.

Strigari, L. E., Bullock, J. S., Kaplinghat, M., Simon, J. D., Geha, M., Willman, B., & Walker, M. G., 2008a. *A common mass scale for satellite galaxies of the Milky Way.* Nature, 454, 1096.

Strigari, L. E., Koushiappas, S. M., Bullock, J. S., Kaplinghat, M., Simon, J. D., Geha, M., & Willman, B., 2008b. *The Most Dark-Matter-dominated Galaxies: Predicted Gamma-Ray Signals from the Faintest Milky Way Dwarfs.* The Astrophysical Journal, 678, 614.

Teerikorpi, P., 1984. *Malmquist bias in a relation of the form $M = AP + B$.* Astronomy & Astrophysics, 141, 407.

Tegmark, M., 1996. *The Angular Power Spectrum of the Four-Year COBE Data.* The Astrophysical Journal Letters, 464, L35.

Teyssier, R., Pontzen, A., Dubois, Y., & Read, J., 2012. *Cusp-core transformations in dwarf galaxies: observational predictions.* arXiv:1206.4895, 1206, 4895.

Thomas, D., Maraston, C., & Bender, R., 2003. *Stellar population models of Lick indices with variable element abundance ratios*. Monthly Notices of the Royal Astronomical Society, 339, 897.

Thornley, M. D., Schreiber, N. M. F., Lutz, D., Genzel, R., Spoon, H. W. W., Kunze, D., & Sternberg, A., 2000. *Massive Star Formation and Evolution in Starburst Galaxies: Mid-infrared Spectroscopy with the ISOShort Wavelength Spectrometer*. The Astrophysical Journal, 539, 641.

Thuan, T. X., Alimi, J.-M., Gott, J. R. I., & Schneider, S. E., 1991. *Northern dwarf and low surface brightness galaxies. IV - The large-scale space distribution*. The Astrophysical Journal, 370, 25.

Tollerud, E. J., Bullock, J. S., Strigari, L. E., & Willman, B., 2008. *Hundreds of Milky Way Satellites? Luminosity Bias in the Satellite Luminosity Function*. The Astrophysical Journal, 688, 277.

Toloba, E., Boselli, A., Cenarro, A. J., Peletier, R. F., Gorgas, J., Gil de Paz, A., & Muñoz-Mateos, J. C., 2011. *Formation and evolution of dwarf early-type galaxies in the Virgo cluster*. Astronomy & Astrophysics, 526, A114.

Toloba, E., Boselli, A., Gorgas, J., Peletier, R. F., Cenarro, A. J., Gadotti, D. A., Gil de Paz, A., et al., 2009. *Kinematic Properties as Probes of the Evolution of Dwarf Galaxies in the Virgo Cluster*. The Astrophysical Journal Letters, 707, L17.

Toloba, E., Boselli, A., Peletier, R. F., Falcón-Barroso, J., van de Ven, G., & Gorgas, J., 2012. *Formation and evolution of dwarf early-type galaxies in the Virgo cluster. II. Kinematic scaling relations*. Astronomy & Astrophysics, 548, 78.

Tolstoy, E., Hill, V., & Tosi, M., 2009. *Star-Formation Histories, Abundances, and Kinematics of Dwarf Galaxies in the Local Group*. Annual Review of Astronomy & Astrophysics, 47, 371.

Tonnesen, S., Bryan, G. L., & van Gorkom, J. H., 2007. *Environmentally Driven Evolution of Simulated Cluster Galaxies*. The Astrophysical Journal, 671, 1434.

Tonry, J. L., Dressler, A., Blakeslee, J. P., Ajhar, E. A., Fletcher, A. B., Luppino, G. A., Metzger, M. R., et al., 2001. *The SBF Survey of Galaxy Distances. IV. SBF Magnitudes, Colors, and Distances*. The Astrophysical Journal, 546, 681.

Toomre, A., 1964. *On the gravitational stability of a disk of stars*. The Astrophysical Journal, 139, 1217.

Toomre, A. & Toomre, J., 1972. *Galactic Bridges and Tails*. The Astrophysical Journal, 178, 623.

Tully, R. B. & Fisher, J. R., 1977. *A new method of determining distances to galaxies*. Astronomy & Astrophysics, 54, 661.

Urban, O., Werner, N., Simionescu, A., Allen, S. W., & Böhringer, H., 2011. *X-ray spectroscopy of the Virgo Cluster out to the virial radius*. Monthly Notices of the Royal Astronomical Society, 414, 2101.

Vader, J. P., 1986. *Metal-enhanced galactic winds. I.* The Astrophysical Journal, 305, 669.

van den Bergh, S., 1976. *A new classification system for galaxies*. The Astrophysical Journal, 206, 883.

van Dokkum, P. G., 2001. *Cosmic-Ray Rejection by Laplacian Edge Detection*. The Publications of the Astronomical Society of the Pacific, 113, 1420.

van Gorkom, J. H., 2004. *Interaction of Galaxies with the Intracluster Medium*. Clusters of Galaxies: Probes of Cosmological Structure and Galaxy Evolution, 305.

van Zee, L., Skillman, E. D., & Haynes, M. P., 2004. *Rotationally Supported Virgo Cluster Dwarf Elliptical Galaxies: Stripped Dwarf Irregular Galaxies?* The Astronomical Journal, 128, 121.

Visvanathan, N. & Sandage, A., 1977. *The color-absolute magnitude relation for E and So galaxies. I - Calibration and tests for universality using Virgo and eight other nearby clusters*. The Astrophysical Journal, 216, 214.

Voit, G., 2005. *Tracing cosmic evolution with clusters of galaxies*. Reviews of Modern Physics, 77, 207.

Vollmer, B., Cayatte, V., Balkowski, C., & Duschl, W. J., 2001. *Ram Pressure Stripping and Galaxy Orbits: The Case of the Virgo Cluster*. The Astrophysical Journal, 561, 708.

Walker, A. G., 1935. *On Riemanntan spaces with spherical symmetry about a line, and the conditions for isotropy in genj relativity*. The Quarterly Journal of Mathematics, 6, 81.

Walsh, D., Carswell, R. F., & Weymann, R. J., 1979. *0957 + 561 A, B: twin quasistellar objects or gravitational lens?* Nature, 279, 381.

Wang, Y., Yang, X., Mo, H. J., & van den Bosch, F. C., 2007. *The Cross-Correlation between Galaxies of Different Luminosities and Colors*. The Astrophysical Journal, 664, 608.

Weinmann, S. M., Lisker, T., Guo, Q., Meyer, H. T., & Janz, J., 2011. *Dwarf galaxy populations in present-day galaxy clusters - I. Abundances and red fractions*. Monthly Notices of the Royal Astronomical Society, 416, 1197.

White, S. D. M., 1978. *Simulations of merging galaxies*. Reviews of Modern Physics, 184, 185.

White, S. D. M., 1979. *Further simulations of merging galaxies*. Monthly Notices of the Royal Astronomical Society, 189, 831.

White, S. D. M., Davis, M., & Frenk, C. S., 1984. *The size of clusters in a neutrino-dominated universe*. Monthly Notices of the Royal Astronomical Society, 209, 27P.

Wirth, A. & Gallagher, J. S. I., 1984. *The families of elliptical-like galaxies*. The Astrophysical Journal, 282, 85.

Wittman, D. M., Tyson, J. A., Kirkman, D., Dell'Antonio, I., & Bernstein, G., 2000. *Detection of weak gravitational lensing distortions of distant galaxies by cosmic dark matter at large scales*. Nature, 405, 143.

Worthey, G., Faber, S. M., Gonzalez, J. J., & Burstein, D., 1994. *Old stellar populations. 5: Absorption feature indices for the complete LICK/IDS sample of stars*. The Astrophysical Journal Supplement Series, 94, 687.

Yoshii, Y. & Arimoto, N., 1987. *Spheroidal systems as a one-parameter family of mass at their birth*. Astronomy & Astrophysics, 188, 13.

Young, C. K. & Currie, M. J., 1995. *Distances to 64 Virgo dwarf-elliptical galaxies and the depth in their spatial distribution*. Monthly Notices of the Royal Astronomical Society, 273, 1141.

Zel'dovich, Y. B., 1970. *Gravitational instability: An approximate theory for large density perturbations.* Astronomy & Astrophysics, 5, 84.

Zel'dovich, Y. B., 1972. *A hypothesis, unifying the structure and the entropy of the Universe.* Monthly Notices of the Royal Astronomical Society, 160, 1P.

Zwicky, F., 1933. *Die Rotverschiebung von extragalaktischen Nebeln.* Helvetica Physica Acta, 6, 110.

Zwicky, F., 1937. *On the Masses of Nebulae and of Clusters of Nebulae.* The Astrophysical Journal, 86, 217.

Official acknowledgments

Based on observations collected at the European Organisation for Astronomical Research in the Southern Hemisphere, Chile, under programme IDs 064.N-0288, 078.B-0178, 085.B-0919, and 085.B-0971.

Based on observations made with the Italian TNG operated on the island of La Palma by the Fundación Galileo Galilei of the INAF (Istituto Nazionale di Astrofisica) at the Spanish Observatorio del Roque de los Muchachos of the Instituto de Astrofisica de Canarias.

Based on observations made with the Nordic Optical Telescope, operated on the island of La Palma jointly by Denmark, Finland, Iceland, Norway, and Sweden, in the Spanish Observatorio del Roque de los Muchachos of the Instituto de Astrofisica de Canarias.

Funding for SDSS-III has been provided by the Alfred P. Sloan Foundation, the Participating Institutions, the National Science Foundation, and the U.S. Department of Energy Office of Science. The SDSS-III web site is http://www.sdss3.org/. SDSS-III is managed by the Astrophysical Research Consortium for the Participating Institutions of the SDSS-III Collaboration including the University of Arizona, the Brazilian Participation Group, Brookhaven National Laboratory, University of Cambridge, Carnegie Mellon University, University of Florida, the French Participation Group, the German Participation Group, Harvard University, the Instituto de Astrofisica de Canarias, the Michigan State/Notre Dame/JINA Participation Group, Johns Hopkins University, Lawrence Berkeley National Laboratory, Max Planck Institute for Astrophysics, Max Planck Institute for Extraterrestrial Physics, New Mexico State University, New York University, Ohio State University, Pennsylvania State University, University of Portsmouth, Princeton University, the Spanish Participation Group, University of Tokyo, University of Utah, Vanderbilt University, University of Virginia, University of Washington, and Yale University.

This publication makes use of data products from the Two Micron All Sky Survey, which is a joint project of the University of Massachusetts and the Infrared Processing and Analysis Center/California Institute of Technology, funded by the National Aeronautics and Space Administration and the National Science Foundation.

This work is based in part on data obtained as part of the UKIRT Infrared Deep Sky Survey.

This research has made use of the NASA/IPAC extragalactic database (NED) which is operated by the Jet Propulsion Laboratory, California Institute of Technology, under contract with the National Aeronautics and Space Administration.

SQL data bases containing the full galaxy data for the semi-analytic model of Guo et al. (2010) at all redshifts and for both the Millennium and Millennium-II simulations are publicly released at http://www.mpa-garching.mpg.de/millennium. The Millenium site was created as part of the activities of the German Astrophysical Virtual Observatory.

IRAF is distributed by the National Optical Astronomy Observatory, which is operated by the Association of Universities for Research in Astronomy (AURA) under cooperative agreement with the National Science Foundation.

This thesis has made use of GADGET2 (Springel, 2005), GALFIT (Peng et al., 2010), and SExtractor (Bertin & Arnouts, 1996).

This research has made use of NASA's Astrophysics Data System.